

**Feasibility Analysis of Novel Maglev Electrical  
Discharge Machine (MEDM)**

**BY**

**Mangal Singh Sisodiya**

**(Admission No:2016DR1084)**



**INDIAN INSTITUTE OF TECHNOLOGY  
(INDIAN SCHOOL OF MINES) DHANBAD (INDIA)**

**For award of the degree of**

**DOCTOR OF PHILOSOPHY**

**February 2024**

**INDIAN INSTITUTE OF TECHNOLOGY (INDIAN SCHOOL OF MINES) DHANBAD****CERTIFICATE FROM THE SUPERVISOR(S)**  
**(To be submitted at the time of Thesis Submission)**

This is to certify that the thesis entitled “**Feasibility Analysis of Novel Maglev Electrical Discharge Machine (MEDM)**” being submitted to the Indian Institute of Technology (Indian School of Mines), Dhanbad by Mr Mangal Singh Sisodiya\_, Admission No\_\_\_2016DR1084\_\_\_, for the award of Doctor of Philosophy (Ph.D.) Degree is a bonafide work carried out by him/her, in the Department of \_\_\_Mechanical Engineering\_\_\_, IIT (ISM), Dhanbad, under my/our supervision and guidance. The thesis has fulfilled all the requirements as per the regulations of this Institute and, in my/our opinion, has reached the standard needed for submission. The results embodied in this thesis have not been submitted to any other university or institute for the award of any degree or diploma.

*Vivek Bajpai* \_\_\_\_\_  
Signature of Supervisor (s)

Name: Dr. Vivek Bajpai

Date: \_\_\_28/02/2024\_\_\_

**INDIAN INSTITUTE OF TECHNOLOGY (INDIAN SCHOOL OF MINES) DHANBAD****CERTIFICATE REGARDING ENGLISH CHECKING**  
**(To be submitted at the time of Thesis Submission)**

This is to certify that the thesis entitled “**Feasibility Analysis of Novel Maglev Electrical Discharge Machine (MEDM)**” being submitted to the Indian Institute of Technology (Indian School of Mines), Dhanbad by Mr. Mangal Singh Sisodiya, Admission No\_\_2016DR1084\_\_\_\_, for the award of Doctor of Philosophy (Ph.D.) Degree has been thoroughly checked for quality of English and logical sequencing of topics.

It is hereby certified that the standard of English is good, and that grammar and typos have been thoroughly checked.

It is now worthy for evaluation by the panel of examiners.

\_\_\_\_\_  
Signature of Supervisor (s)

Name: Dr. Vivek Bajpai\_\_\_\_\_

Date: \_\_\_\_28/02/2024\_\_\_\_\_

\_\_\_\_\_  
Signature of Scholar

Name: \_\_Mangal Singh Sisodiya\_

Date: \_\_\_\_\_28/02/2024\_\_



Form No: PH11

**INDIAN INSTITUTE OF TECHNOLOGY (INDIAN SCHOOL OF MINES) DHANBAD**

**CERTIFICATE FOR CLASSIFIED DATA**  
(To be submitted at the time of Thesis Submission)

This is to certify that the thesis entitled “**Feasibility Analysis of Novel Maglev Electrical Discharge Machine (MEDM)**” is being submitted to the Indian Institute of Technology (Indian School of Mines), Dhanbad by Mr. Mangal Singh Sisodiya for the award of Doctor of Philosophy (Ph.D) Degree in Mechanical Engineering does not contain any classified information. This work is original and yet not been submitted to any institution or university for the award of any degree.

*Vinod Bysai*

\_\_\_\_\_  
Signature of Supervisor (s)

*Mangal Singh*

\_\_\_\_\_  
Signature of Scholar



Form No: PH10

## INDIAN INSTITUTE OF TECHNOLOGY (INDIAN SCHOOL OF MINES) DHANBAD

### **COPYRIGHT AND CONSENT FORM**

**(To be submitted at the time of Thesis Submission)**

To ensure uniformity of treatment among all contributors, other forms may not be substituted for this form, nor may any wording of the form be changed. This form is intended for original material submitted to the IIT (ISM), Dhanbad, and must accompany any such material to be published by the ISM. Please read the form carefully and keep a copy for your files.

**TITLE OF THESIS:** “Feasibility Analysis of Novel Maglev Electrical Discharge Machine (MEDM)”.

**AUTHOR'S NAME & ADDRESS:** Mangal Singh Sisodiya, Mechanical Engineering

### **COPYRIGHT TRANSFER**

1. The undersigned hereby assigns to Indian Institute of Technology (Indian School of Mines), Dhanbad all rights under copyright that may exist in and to: (a) the above Work, including any revised or expanded derivative works submitted to the ISM by the undersigned based on the work; and (b) any associated written or multimedia components or other enhancements accompanying the work.

### **CONSENT AND RELEASE**

2. In the event the undersigned makes a presentation based upon the work at a conference hosted or sponsored in whole or in part by the IIT (ISM) Dhanbad, the undersigned, in consideration for his/her participation in the conference, hereby grants the ISM the unlimited, worldwide, irrevocable permission to use, distribute, publish, license, exhibit, record, digitize, broadcast, reproduce and archive; in any format or medium, whether now known or hereafter developed: (a) his/her presentation and comments at the conference; (b) any written materials or multimedia files used in connection with his/her presentation; and (c) any recorded interviews of him/her (collectively, the "Presentation"). The permission granted includes the transcription and reproduction of the Presentation for inclusion in products sold or distributed by IIT(ISM) Dhanbad and live or recorded broadcast of the Presentation during or after the conference.
3. In connection with the permission granted in Section 2, the undersigned hereby grants IIT (ISM) Dhanbad the unlimited, worldwide, irrevocable right to use his/her name, picture, likeness, voice and biographical information as part of the advertisement, distribution and sale of products incorporating the Work or Presentation, and releases IIT (ISM) Dhanbad from any claim based on right of privacy or publicity.
4. The undersigned hereby warrants that the Work and Presentation (collectively, the "Materials") are original and that he/she is the author of the Materials. To the extent the Materials incorporate text passages, figures, data or other material from the works of others, the undersigned has obtained any necessary permissions. Where necessary, the undersigned has obtained all third party permissions and consents to grant the license above and has provided copies of such permissions and consents to IIT (ISM) Dhanbad.

### **GENERAL TERMS**

- \* The undersigned represents that he/she has the power and authority to make and execute this assignment.
- \* The undersigned agrees to indemnify and hold harmless the IIT (ISM) Dhanbad from any damage or expense that may arise in the event of a breach of any of the warranties set forth above.
- \* In the event the above work is not accepted and published by the IIT (ISM) Dhanbad or is withdrawn by the author(s) before acceptance by the IIT(ISM) Dhanbad, the foregoing copyright transfer shall become null and void and all materials embodying the Work submitted to the IIT(ISM) Dhanbad will be destroyed.
- \* For jointly authored Works, all joint authors should sign, or one of the authors should sign as authorized agent for the others.

Signature of the Author

## DEDICATION

Dedicated to my beloved parents

**Shri. Gopal Singh Sisodiya,**

and

**Late Smt. Shayama Sisodiya**

## ACKNOWLEDGMENTS

I am grateful to all the people who provided me with their colossal support during my doctoral study. I wish to express my sincere thanks and deep sense of gratitude to my thesis advisor **Dr. Vivek Bajpai** for introducing me to this exciting topic. I would also like to thank him for his valuable guidance, encouragement, and freedom they gave me throughout the course of my work. His constant energy and immense enthusiasm for research have always motivated me. I experienced both ups and downs, good and bad times, in my life during the stay at IIT (ISM), Dhanbad and away from the institute. He was always there for me to support and encourage. I am thankful to him for the excellent research facilities provided by him and also his willingness to spare his precious time for research discussions and clarifying my doubts. I acknowledge the constant encouragement and advice he has given me, not only towards research but also for personal life.

I am extremely thankful to the members of my Doctoral Scrutiny Committee, start with Chairperson **Prof.(Dr) Pawan Kumar Singh**, Members **Prof. (Dr) SK Singh** and **Prof. (DR) SK Gupta** for their constant encouragement and support.

I also thank **Prof. Rajiv Shekhar**, Director, IIT (ISM), Dhanbad, for providing the necessary infrastructure and facilities for the research work during the period of study. I express my sincere thanks to Head of department **Prof.(Dr) Somnath Chattopadhyaya**, Faculty Members **Prof.(Dr) Amit Rai Dixit**, **(Dr) ML Chandrawanshi**, **Dr. Deepak Mandal**, **(Dr) Suman Saha** , all

of them have always been very kind and cooperative with me. I would also like to thank all of the **faculties** and **staff** members in the Department of Mechanical Engineering at IIT (ISM) who worked directly with me during this study and indirectly to support me during the preparation of the thesis. I individually thank all of my lab mates **Dr. Deepak Kumar, Dr. Shashank Shukla, Dr. Mohan Kumar, Dr. Rachit Ranjan, Dr. Ankit Jain, Dr. Ravi Shankar Rai, Dr. Arnab Das, Mr. Rajesh Sahoo, Mr. Prince Anand, Ms. Abhipsa Kar** and **Mr. Dhiraj Bajpai** for their help and support during my research period. This dissertation would have been impossible without the support of my family.

I express my deepest gratitude to my family for their love and support throughout my life. I am indebted to my, father, **Shri Gopal Singh Sisodiya** , my mother **Lt. Smt. Shayama Sisodiya**, and my wife **Smt. Abhiruchi Sisodiya** for their care and love. I don't have the right words to express how much they love and support me during this tenure. I also express love to my two daughters, **Ms. Mishika Sisodiya, Ms. Kavisha Sisodiya** as well as my son **Mr. Ranvijay Singh Sisodiya**. Further, I extend my thanks to **Dr. Kapil Nagwanshi** for helping me with the thesis documentation work and **Dr. Ritu Singh** for editing the entire document. Last but not least, I thank the almighty God for being with me all the time. May your name be honored and glorified always.

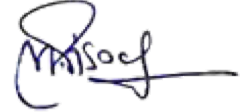
**Funding support:**

The most of Machines and other equipment which are used in this research work are supported by Department of Science and Technology (DST). Mechanical En-



gineering Project (DST(SERB)/533/2017-18/File No. ECR/2016/001956). In-  
dia under project number DST(SERB)/533/2017- 18/Mechanical Engineering  
(File No. ECR/2016/001956).

Place: IIT (ISM), Dhanbad  
Date: 23-02-2024



(Mangal Singh Sisodiya)

# TABLE OF CONTENTS

<b>Abstract</b>	<b>xi</b>
<b>Chapter 1 INTRODUCTION</b>	<b>1</b>
1.1 Background . . . . .	1
1.2 Evolution of EDM . . . . .	4
1.3 Electrical Discharge Machine . . . . .	6
1.3.1 Mechanism of material removal in EDM . . . . .	6
1.3.2 EDM Hardware . . . . .	7
1.3.3 Control Parameters . . . . .	9
1.3.4 Process Responses . . . . .	11
1.4 Problem Definition . . . . .	12
1.5 Objectives of the present work . . . . .	13
1.6 Organization of the report . . . . .	15
<b>Chapter 2 LITERATURE REVIEW</b>	<b>17</b>
2.1 Servo mechanism . . . . .	17
2.2 Control Unit . . . . .	23
2.3 Power Supply . . . . .	28
2.4 Dielectric Medium . . . . .	32
2.5 Summary . . . . .	33
<b>Chapter 3 DESCRIPTION OF MAGLEV EDM</b>	<b>37</b>
3.1 Introduction . . . . .	37
3.2 Working principle and development of MEDM . . . . .	37
3.2.1 Construction and working of self-servo bipolar linear . . . . .	38
3.3 Summary . . . . .	47
<b>Chapter 4 FEASIBILITY ANALYSIS ON CPTI WORK MATERIAL</b>	<b>49</b>
4.1 Introduction . . . . .	49
4.2 Experimental Methodology . . . . .	50
4.3 Observations . . . . .	51
4.3.1 Discharge voltage-current characteristics . . . . .	51
4.3.2 Material removal rate (MRR) . . . . .	56
4.3.3 Specific energy in EDM . . . . .	59
4.3.4 Surface morphology and surface roughness . . . . .	60
4.4 Summary . . . . .	65
<b>Chapter 5 FEASIBILITY ANALYSIS ON TITANIUM ALLOY WORK MATERIAL</b>	<b>66</b>
5.1 Introduction . . . . .	66
5.2 Experimental method . . . . .	66
5.2.1 Discharge waveform . . . . .	67
5.2.2 Predictive modeling . . . . .	70
5.3 Results and discussion . . . . .	74
5.3.1 Model validation and prediction . . . . .	74

5.3.2	Characterization of surface morphology . . . . .	77
5.3.3	Evaluation of the specific Energy . . . . .	81
5.3.4	Summary . . . . .	85
<b>Chapter 6</b>	<b>FEASIBILITY ANALYSIS ON INCONEL 625 WORK MATERIAL</b>	<b>87</b>
6.1	Introduction . . . . .	87
6.2	Materials and Methods . . . . .	88
6.2.1	Workpiece and tool material . . . . .	88
6.2.2	Experimental Procedure . . . . .	88
6.3	Results and Discussions . . . . .	90
6.3.1	Morphological characterization of the machined surface through FESEM . . . . .	90
6.3.2	Material migration and diffusion analysis through EDX . . . . .	92
6.3.3	Material migration and diffusion analysis through EDX . . . . .	93
6.3.4	Discharge characteristic curve analysis . . . . .	94
6.3.5	Surface integrity (SI) analysis . . . . .	96
6.3.6	Specific energy consumption (common performance index) analysis . . . . .	98
6.3.7	Material removal rate (MRR) and tool wear rate (TWR) analysis . . . . .	100
6.4	Summary . . . . .	102
<b>Chapter 7</b>	<b>FEASIBILITY ANALYSIS ON NIMONIC ALLOY WORK MATERIAL</b>	<b>104</b>
7.1	Introduction . . . . .	104
7.2	Materials and Methods . . . . .	104
7.2.1	Workpiece and tool material . . . . .	104
7.2.2	Experimental Procedure . . . . .	106
7.3	Results and Discussions . . . . .	107
7.3.1	Discharge stability monitoring through V-I curve . . . . .	107
7.3.2	MRR and Specific energy consumption (SE) analysis . . . . .	110
7.3.3	Surface roughness (SR) and tool wear analysis . . . . .	113
7.3.4	Surface topography analysis by FESEM . . . . .	115
7.3.5	Bidirectional material migration and diffusion analysis through EDX . . . . .	116
7.4	Summary . . . . .	118
<b>Chapter 8</b>	<b>CONCLUSION AND FUTURE SCOPE</b>	<b>119</b>
8.1	Conclusion . . . . .	119
8.2	Future Scope . . . . .	121

## LIST OF FIGURES

1.1	Material Removal Mechanism . . . . .	7
1.2	Schematic arrangement of EDM . . . . .	8
1.3	Voltage and current graph of conventional EDM process . . . . .	10
2.1	EDM Servo mechanism . . . . .	18
2.2	RC Power generator . . . . .	30
2.3	Transistor type power generator [1] . . . . .	31
3.1	Working Principle of MEDM . . . . .	39
3.2	True scale working prototype of Maglev EDM; magnified view of machining zone . . . . .	41
3.3	Mechanics of servo stabilized maglev EDM system . . . . .	41
3.4	Schematic showing the basic principle of working of maglev EDM system with actual arrangement of peripheral components . . . . .	44
3.5	The current pictorial view of the maglev EDM . . . . .	47
4.1	The five different possible EDM conditions . . . . .	52
4.2	Illustration of the discharge waveform of conventional EDM . . . . .	54
4.3	(a) Voltage and current characteristics showing stable and uniform discharge; (b) detailed pulse characteristics. . . . .	56
4.4	Comparison of the material removal rate between maglev EDM and the literature . . . . .	57
4.5	Comparison of the specific energy between the maglev EDM and the literature . . . . .	60
4.6	Optical microscope and profilometer images of surface morphology . . . . .	62
4.7	Comparison of the surface roughness . . . . .	64
5.1	Discharge waveform of maglev EDM process (a) Single-pulse; (b) Multi-pulses . . . . .	67
5.2	Positioning response of maglev EDM in terms of time displacement curve . . . . .	69
5.3	Experimental vs. Predicted result during different EDM process (a) MRR; (b) Average surface roughness . . . . .	75
5.4	Surface morphology during maglev EDM (a) 3D profile map of whole texture; (b) 3D profile map of machined surface . . . . .	78
5.5	Surface morphology during maglev EDM (a) 2D profile of whole dimple (b) 2D profile with 20 $\mu\text{m}$ scale of maglev EDM taken from microscope (c) 2D profile with 3 $\mu\text{m}$ scale of maglev EDM taken from FESEM . . . . .	79
5.6	Roughness values observed on machined surface during maglev EDM by Optical profilometer . . . . .	80

5.7	Specific energy comparison of different experimental setup . . .	82
6.1	Surface topography/morphology analysis of machined workpiece parts through FESEM . . . . .	91
6.2	The re-solidified layer (recast layer) near the interface region of the machined surface . . . . .	91
6.3	(a) Chemical characterization (b) material migration, and elemental diffusion analysis through EDX spectrum . . . . .	93
6.4	(a) Surface morphology of the eroded tool part (confined tool wear with their spark position) (b) material migration and diffusion within the tool eroded part . . . . .	94
6.5	Real time voltage and current waveform at the time scale of (a) 100ms and (b) 10ms . . . . .	95
6.6	(a) 3D plot for area surface roughness for the scanned area (b) 2D surface roughness plot (c) variation of linear surface integrity parameters (Ra, Rq, and Rz) over three different slices . . . . .	98
6.7	Comparative analysis of specific energy consumption (SEC) with the existing literature . . . . .	100
6.8	Average material removal rate (MRR) and tool wear rate (TWR)	101
7.1	Real-time voltage-current waveforms (as measured) of maglev EDM at (a) 100ms and (b) 10ms time scale . . . . .	107
7.2	Real time pulse characteristics (as measured in DSO) and machining stability testing in conventional EDM through voltage current waveforms . . . . .	109
7.3	Variation in MRR with respect to discharge power in (a) Maglev EDM (deviation from average MRR) (b) conventional EDM . . . . .	111
7.4	Comparative analysis of specific energy consumption (SEC) rate at varying range of discharge power (a) Maglev EDM (b) conventional EDM and in the reported literature . . . . .	112
7.5	(a) 3D plot for surface roughness variation and crater geometry (b) area surface roughness and their variation (c) variation of linear surface integrity parameters (Ra, Rq, and Rz) . . . . .	114
7.6	Surface morphology/topography analysis of machined workpiece parts through FESEM in two iterations at the same location . . . . .	116
7.7	(a) Chemical characterization (b) material migration, and elemental diffusion analysis (c) machined copper tool electrode surface (inset: localized tool erosion with their spark location) (d) bidirectional material transfer in EDX spectra after machining on the tool surface . . . . .	117

## LIST OF TABLES

5.1	Dimensions of parameters applied on dimensional analysis . . .	71
5.2	Parameters and their values applied to develop mathematical model	74
6.1	Chemical constituents (% weight) and mechanical properties of Inconel 625 workpiece . . . . .	88
6.2	Thermo mechanical property of tool electrode (Copper) material	88
6.3	The measured gap voltage, gap current and duty factor in four iterations during processing of Inconel 625 . . . . .	89
7.1	Chemical constituents (%weight) of Nimonic C-263 workpiece(under Mass Density= $8.36 \text{ g/cm}^3$ and Melting Point $1300 - 1355^\circ\text{C}$ ) .	105
7.2	Thermo-physical property of tool electrode (Copper) material .	105
7.3	Measured voltage and current signal in four iterations (IT1-IT4) via digital storage oscilloscope during machining on maglev EDM	106
7.4	Parameter setting for machining of Nimonic alloy (C-263) on conventional EDM . . . . .	106

<b>ABBREVIATION</b>	<b>DESCRIPTION</b>
EDM	Electrical Discharge Machining
MRR	Material Removal Rate
SR	Surface Roughness
TWR	Tool Wear Rate
SE	Specific Energy
A/D	Analog to Digital
VI	Voltage Current
FESEM	Field Emission Scanning Electron Microscopy
EDX	Electron diffraction X-ray spectroscopy
DOF	Degree Of Freedom
SMPS	Switched Mode Power Supply
RC	Resistance Capacitance
FET	Field Effect Transistor
DC	Direct Current
AC	Alternative Current
R	Resistance
C	Capacitance
PID	Proportional-Integral-Derivative
CNC	Computer Numerical Control

<b>ABBREVIATION</b>	<b>DESCRIPTION</b>
FE	Finite-Element
PM	Permanent Magnet
Frs	Force Restoration
Fem	Repelling Force
EM	Electromagnet
$\theta$	Inter-electrode gap
m1 & m2	Magnetic pole strength
Xm	Operating distance
Kf	Magnetic force constant
Kg	Magnetic force constant
DIP	Digital Image Processing
amp	Ampere
IEG	Inter Electrode Gap
HAZ	Heat-Affected Zone
T(on)	Machine on time
T(off)	Machine off time
Vd	Discharge voltage
Id	Discharge current
Df	Duty factor
$\alpha$	Thermal diffusivity
Ds	Dielectric strength
$\sigma$	Tool electrical conductivity



<b>ABBREVIATION</b>	<b>DESCRIPTION</b>
3D	Three Dimensional
Rq	Root mean Square Roughness
Rsk	Skewness
Rku	Kurtosis
$\lambda$	Thermal Conductivity
$\theta$	Melting Point
CpTi	Commercially available pure titanium
SEC	Specific Energy Consumption
$\theta$	Diameter
DSO	Digital Storage Oscilloscope
$\mu$ -EDM	Micro EDM
Sa	Arithmetic mean height
Sq	Root mean square roughness
Sz	Maximum height
SCD	Surface Crack Density
Ra	Average surface roughness

## ABSTRACT

Electric discharge machining (EDM) is widely used in industries for machining hard metals. A number of manufacturers worldwide are producing EDMs, and this is a well-established commercial product. The EDM works on the principle of maintaining electrode gaps (between tool and workpiece) for producing an electrical discharge, which converts into high-temperature plasma. This discharge is reasonable for the erosion of the workpiece (positive polarity). The servo mechanism and the power supply are the key components of an EDM machine. Although few micro-EDMs use capacitor-type power supplies, they are very less popular due to their low efficiency. A servo mechanism is used to control the gap between electrodes for stable discharge. The response time of the servo mechanism is much lower than the discharge time; therefore, the pulse power supply helps in avoiding the short-circuit condition. The irregularities on the contact surfaces of the workpiece and the tool and debris particles flowing with the dielectric are the major reasons for the short-circuit condition. The literature review shows that even with the best servo mechanism and by adjusting the process parameters of the power supply, such as pulse width, duty cycle, discharge voltage, and discharge current, achieving a uniform discharge is difficult. Most of the voltage-current plots have shown that the ionisation and the short circuit are taking up a significant fraction of the on-time. Which ultimately reduces the efficiency of the process and lowers MRR with slower machining speeds. Apart

from the technical deficiency, the complex circuit of the pulse power supply and the servo mechanism make it costly. The above two issues with the existing commercial EDMs have been addressed in the present work. A self-servo bipolar linear actuator has been developed to maintain the inter-electrode gap. The developed actuator is highly responsive and currently works with a DC power source. The servo mechanism and the power supply (straight DC) are simple in design and much lower in cost than the existing EDM. The servo mechanism is based on a magnetic levitation balance to ensure the set discharge voltage. The developed technology needs a feasibility analysis with a range of materials. Therefore, the objective of the proposed work is to analyse the feasibility of the maglev EDM. IIT (ISM) Dhanbad and Varnica Precision Pvt Ltd. jointly developed the prototype and provided it for the feasibility analysis. The first prototype has performed well and was machined on pure Ti, Ti6Al4V, Inconel 625, and nimonic alloys. Cylindrical brass and copper were used as tool materials, with deionized water as a dielectric medium. An open circuit voltage of 12 V with a current of 2 amps was set in the power supply with a discharge voltage of 6-7.5 V and a discharge current of 500 mA to 1.5 A. Specific energy consumption (SEC), material removal rate (MRR), tool wear rate (TWR), average surface roughness (Ra), and voltage-current characteristics were analysed. Moreover, mathematical modelling of the plasma, material removal rate, and surface roughness have been developed. The process responses were compared with the available literature, and a few experiments have been performed on the existing EDM. It has been noted that the performance of the recently created maglev EDM is comparable

to that of traditional EDMs. However, it's expected that more advancements in maglev EDM technology will allow it to outperform the current EDM and possibly simplify maintenance.

# CHAPTER 1

## INTRODUCTION

### 1.1 Background

Electrical discharge machining (EDM) is a popular unconventional machining process. It allows the machining of high-strength and wear-resistant materials such as titanium and nickel-based alloys. These materials have proven to be either impossible or economically unproductive to process using conventional machining methods. Nevertheless, the exceptional qualities of these materials motivate engineers to employ them in cutting-edge industries like aerospace, medicine, and electronics. It has been reported that these materials are tough to cut due to their low thermal conductivity and strong strength. The EDM is the most suitable machining method to process these materials. The primary advantage of EDM is that it is a non-contact approach. Consequently, no contact force, tension, or vibration components are present during the machining process[2]. In EDM, material removal is based on the thermal impact of electrical discharges in a micro-confined gap (spark gap) under a dielectric circulation medium [3]. In recent years, the method has gained the ability to produce complex 3D geometry, shapes, and structures with enhanced surface integrity and stability[4]. Ideally, EDM is a favourable machining technique to process hard materials, but practically, the dependency on various electrical and non-electrical process parameters makes the process stochastic[5]. Hence, the process characteristics are

still dubious, which can be easily observed on a voltage-current plot due to uneven discharge. Subsequently, EDM shows undesirable responses like uneven material removal rate (MRR), high tool wear, generation of a recast layer, poor surface finish, and improper flushing of debris[6]. In EDM, machining speed and accuracy are the critical issues that are limited by the probability of normal discharge. Normal discharge is essential because it ensures good machining stability and the surface finish of the machined parts. A suitable servo control mechanism responded well to ensure the occurrence of normal discharge because it restored the initial gap in the repeated cycle [7]. In conventional EDM, a geared-based or lead-screw-based servo control system is typically used for gap control. Due to mass inertia and backlash, the dynamic response of these servo control systems is sluggish[8]. In addition, the servo system's delayed response is what causes arcing and short-circuiting phenomena. This reduces efficiency, productivity, and speed in terms of machining. Inadequate flushing and a sluggish positioning response may also result in secondary discharge[9]. It is well known that EDM takes place in a narrow gap between two electrodes. The inter-electrode gap, also known as the spark gap, is controlled using a servo control mechanism. This spark gap plays a crucial role and is responsible for effective machining in terms of higher MRR and lower surface roughness (SR) with a minimum tool wear rate (TWR). The concentration of eroded material particles in the narrow gap increases the chance of ineffective discharge energy, hence diminishing EDM's effectiveness. Considering the above, the function of the servo control mechanism is vital. Therefore, the optimisation of servo mechanisms or tool feeding technol-

ogy is essential. The conventional servo controller uses motors and ball screws, which decreases the capability of EDMs due to their slower reaction. Utilising magnetic actuators, scientists have tried to enhance the precise electrode gap. It is reported that every pulse is essential for accelerating machines by keeping the proper electrode gap; the typical servo system is incapable of regulating the correct gap[10]. In the present work, an analysis of the existing feed mechanism was carried out, and to execute the toned-gap condition, a technology employing the maglev theory was analyzed. The proposed technology is referred to as maglev EDM. In the past, Zhang used the maglev actuator and successfully incorporated it into an existing EDM to enhance its performance. The suggested maglev EDM is distinct from the original maglev actuator. The proposed method does not require an EDM machine, and the second significant characteristic of the system is its superior control. The Maglev EDM is an adaptive system and may thus employ a DC power supply instead of an RC or pulsed power supply. A series of experiments were conducted to confirm the results and viability of the technology. The experimental results demonstrate that Maglev EDM outperforms the existing EDM technology. The analysis of MRR, specific energy, and surface roughness (SR) revealed the possibilities of the innovative Maglev EDM. In the forthcoming chapters, thorough explanations and comparisons will be presented. The report starts with the primary knowledge of EDM and highlights the little history needed to understand the EDM process. Later, in subsequent chapters, the feasibility of the proposed technology for machining hard-to-cut metals is compared with the reported results and presented.

## 1.2 Evolution of EDM

The inception of the electrical discharge machine (EDM) was reported in 1770. The uncontrolled eroding effect of the electric spark was discovered at that time. Later in 1943, Russian scientists B.R. and N.I. Lazarenko noticed that electric current wears valuable metals. The present electric discharge machining was created by the couple using the current's inverse action to control material erosion[11] in a systematic manner. The couple also analysed spark frequency and spacing to optimise EDM. In addition, the first EDM drilling apparatus employing an intense control spark of current was created at this time. In the 1950s, electrical discharge machining (EDM) entered its pioneering phase, bringing technology from the laboratory to industrial applications. Russia and its socialist allies dominated the evolution of EDM for a considerable length of time. Resistance capacitance (RC) was the type of power supply that the Lazarenkos used. However, the charging of condensers to provide discharge energy was halted for an extended period of time, and ionization in the electrode gap was thoroughly observed by researchers[12][13]. Numerous studies have been conducted to differentiate between an arc and a spark. As a result, research concluded that sparks might provide a more distinct and superior surface finish than arcs, which degrade the surface finish due to the unregulated flow of power[14]. As a result, many more circuits were created to aid in the development of power supplies. During the same time, the general circuitry changed from the R.C. circuit to other RCL circuits, which increased the machining speed and efficiency as a result of an increase in the discharge rate. The Americans also discovered a variety of circuits



for generating power discharge and enhancing the capabilities of controllers. The United States and the United Kingdom developed several cutting-edge technologies, particularly for improved discharge on and off management. A number of businesses produced EDM technology at the same time, including ELOX, which dominated the market at the time. However, the other producers of machine tools were also attempting to establish their products on the market. A business named Agie created and manufactured the first sinking EDM in 1954, which attracted manufacturing researchers due to its novelty. The same business subsequently invented the CNC wire-cut EDM in 1969[15]. The late 1960s and early 1970s were groundbreaking years for the development of EDM technology. Specifically, the three major technological and scientific breakthroughs improved performance. The first invention was the planar transistor in 1959, and the second formed the foundation for integrated circuit technology. Following this advancement, the static pulse generator became a reality. Subsequently, with the assistance of integrated circuits, the third evolution of digital equipment, similar to the first computer machine, enhanced the control and programming of the servo control system. In 1971, the first microprocessor was invented to aid in the numerical control and programming of servo systems. However, socialist countries could not benefit from such inventions, so Mitsubishi, Fanuc, Sodick, and Seibu Denki took over the market. AGIE and CHARMILLES' first static pulse generator reduced open-circuit voltage and gap control for efficient discharge to achieve a high machining rate, wear resistance, and precision. After 1980, CNC improved the efficiency of self-control machining and quality.

### **1.3 Electrical Discharge Machine**

Electrical discharge machining (EDM) is a technique for machining electrically conductive materials using controlled sparks. The procedure involves the gradual melting of the work material via application of thermal energy with high-frequency sparks between the cathode (tool) and the anode (workpiece), in the presence of a dielectric fluid [16].

#### **1.3.1 Mechanism of material removal in EDM**

EDM is based on a thermoelectric model in which electrical energy is turned into heat energy through a series of small electrical discharges between two electrodes. Once the potential difference is applied to the electrodes, the cathode acts as a tool and the anode as a workpiece [17]. A suitable dielectric medium occupies the narrow, confined gap between the electrodes and immerses the electrodes into it. Because of the potential difference, the cathode emits electrons. These expelled electrons from the cathode rush towards the anode and collide with the dielectric fluid that is in their way. Such collisions split the molecules of the dielectric medium into electrons and positive ions. The formation of a narrow column of ionized dielectric fluid molecules between the electrodes creates an electrical path. This electrical path, or plasma channel, has a very low electrical resistance, allowing a large number of electrons to pass through it. This phenomenon significantly increases the temperature as a result of the striking and kinetic energy on the work surface. Due to this, the electrode and workpiece both melt and evaporate, leaving a crater on the surface of the workpiece. When the pulse is switched off, the plasma channel breaks down, and circulating dielectric

fluid flushes away machined material in the form of microscopic debris from the inter-electrode gap. The material removal mechanism is shown in Fig1.1

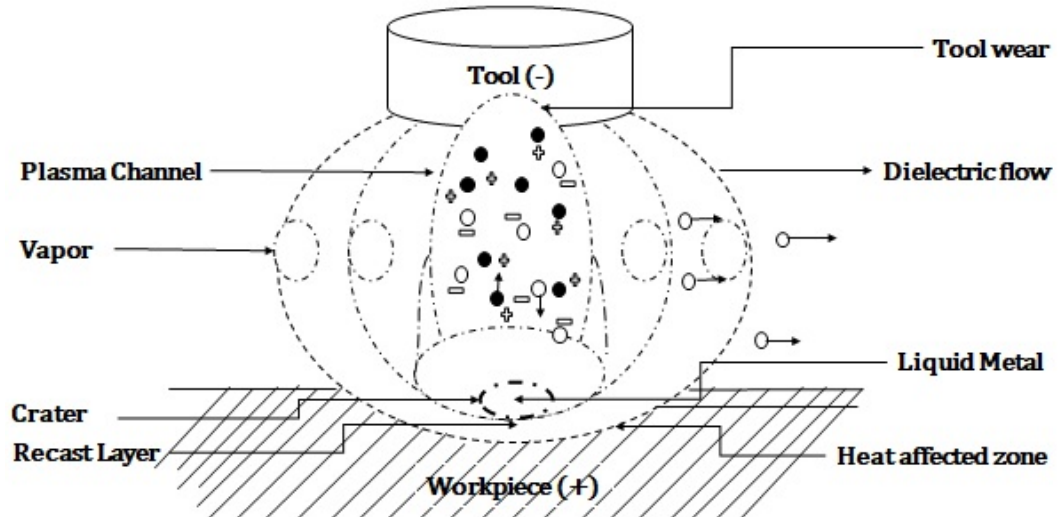


Figure 1.1: Material Removal Mechanism

### 1.3.2 EDM Hardware

**Servo Mechanism:** In EDM, the servo mechanism is very important because it predicts the spark gap and makes the mechanical changes that are needed to keep the gap constant. The most significant module in a servo control system is the microcontroller, which transmits the digital control signal, converts analogue signals to digital signals using an A/D module, and drives the motor using a pulse width modulation (PWM) module [18]. It controls the optimal gap between the electrodes as well as avoids physical contact between the electrodes, which results in arcing, short circuits, or a worthless open circuit[19]. Additionally, the servo mechanism includes a servo motor and a lead screw [20]. This mechanism is commonly referred to as a servo controlled feed mechanism[21]. The servo control can be run using different algorithms or rules, such as predict-

ing the gap distance and offsetting the tool position, the ignition delay time, the average gap voltage, the average delay time, etc[22]. It evident that the proper functioning of the servo controller mechanism ensures efficient EDM.

**Power Supply:** Electrical discharge machine (EDM) requires controlled high-frequency energy sources. In general, the EDM power supply is made up of an electrical circuit that produces a power pulse and a control device that regulates the amount of energy in each pulse. A variety of power supply unit solutions have been created to date, ranging from simple resistance-capacitance RC power supplies, which are still in use today, to complicated resonant power supply units[23]. By selecting the appropriate power source and pulse generator for the application, excellent material removal rate (MRR) results can be obtained. The schematic arrangement of the important hardware and elements is presented in Fig1.2

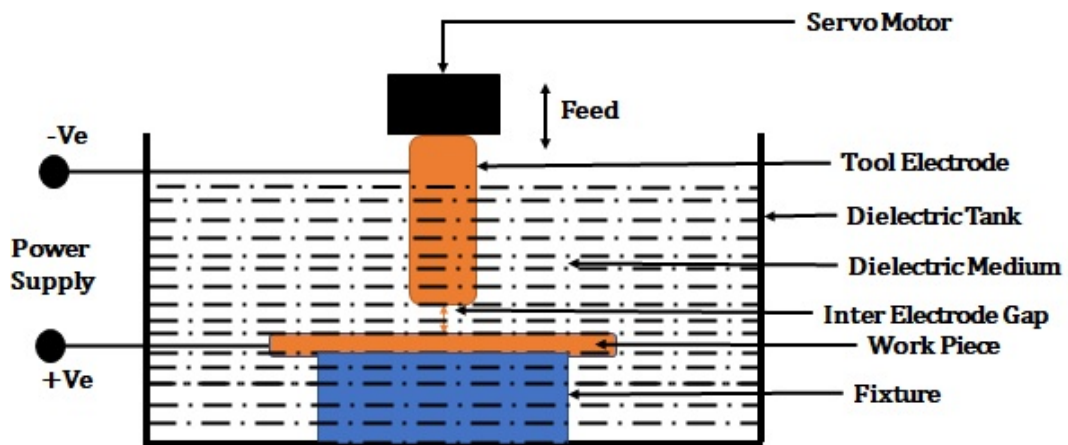


Figure 1.2: Schematic arrangement of EDM

**Dielectric :** The dielectric fluid is a form of isolation that flows between the electrode gap and permits the requisite spark whenever it is necessary by ionizing.

It is mandatory that dielectric medium must initially function as an insulator and then transform into a conductor by reducing its dielectric strength when it attains the required voltage for the spark. During the deionization process, the dielectric medium should regain its strength. Usually, kerosene, distilled water, or an oil are used as dielectric medium that can be ionized. The other job of dielectric medium is to protect metals from heat stress and oxidation and to make sure that chip debris is flushed away properly[24]. For efficient machining, the right selection of a suitable dielectric medium is necessary; numerous characteristics, including dielectric strength, viscosity, colour, and odour, influence the selection of a suitable dielectric medium.

### 1.3.3 Control Parameters

**Voltage and Current plot:** In the EDM process, the temperature difference between the tool and workpiece is mostly a consequence of the power source and narrow gap distance between the electrodes. Consequently, the performance of EDM is predicated primarily on these essential aspects. The influencing parameters in EDM can be classified in two ways: electrical parameters such as discharge current, discharge voltage, and pulse on and off duration, and non-electrical characteristics including electrode gap and dielectric medium [25]. The researcher analyzed every component of EDM and determined that these influencing parameters were accountable for the efficiency of the machining process. In conventional EDM, each process parameter is meticulously regulated, and pulse length is kept by power regulation devices. As depicted in Fig1.3, every energy pulse can be divided into three distinct zones: ionization, discharge, and short

circuit.

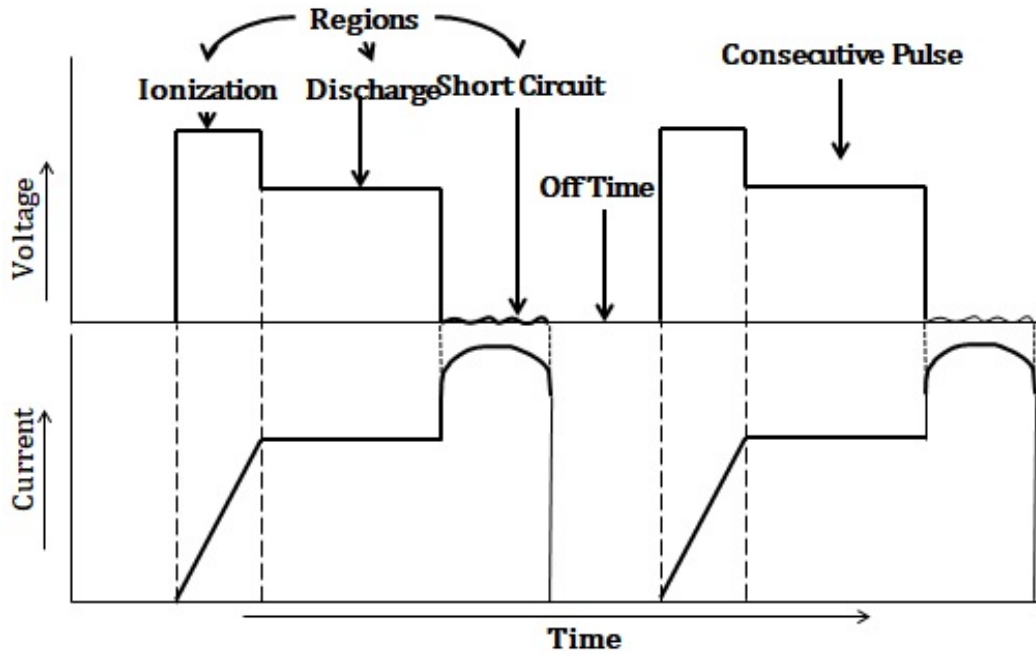


Figure 1.3: Voltage and current graph of conventional EDM process

During the machining process, first the dielectric fluid is ionized, which increases the discharge energy, and then a spark is produced in the second discharge zone to remove the material. The third possible zone may be undesirable (a short circuit) and must be avoided in the machine by briefly disconnecting the power supply and then re-establishing a stable spark. The occurrence of short-circuiting is detrimental to the quality of the EDM surface.

**Pulse on/off time:** It is refer the time interval during which the spark occurs between the tool electrode and the workpiece once the breakdown voltage of the dielectric is reached, causing its ionization. Whereas the Pulse off time refers the interval between consecutive sparks during which no current is supplied

to the electrodes and deionization of the dielectric occurs.

**Gap Voltage, Peak Current and Duty Cycle:** The gap voltage or also known as discharge voltage is the average potential difference between the tool and workpiece. It determines the sparking energy during the spark. The Peak Current is another crucial element that affects machining rate and surface roughness. It is the amount of energy that can be measured by the flow of electrons during discharge machining. whereas the duty cycle is the ratio of pulse on time to the total cycle time (sum of pulse on time and pulse off time).

#### 1.3.4 Process Responses

**Material removal rate:** The Material removal rate (MRR) is calculated by the volume of the material removed or the weight difference of workpiece before and after EDM operation. It is observed that the material removal rate increases significantly with the increase in peak current [26]. The MRR is given by the following Eq. 1.1[27]. It increases with supplied energy in the form of either peak current or gap voltage

$$MRR = \frac{w_b - w_a}{T} \quad (1.1)$$

where  $w_b$  and  $w_a$  are the workpiece weights before and after machining, respectively, and  $T$  is the machine time.

**Tool Wear Rate:** The tool wear rate (TWR) is the weight difference between the tool before and after the machining, divided by the machining time. The TWR is given in microgram per minute. It is expressed by the following Eq.

1.2[27].

$$TWR = \frac{T_b - T_a}{T} \quad (1.2)$$

$T_b$  and  $T_a$  are the weights of the cutting tool before and after machining, respectively, and  $T$  is the machine time.

**Specific Energy:** The specific energy consumption (SEC) is defined as the amount of discharge energy required to remove a single unit of volume or mass. In actuality, it is the power to material removal rate ratio, usually expressed in  $J/\mu g$ . It express by the following Eq. 1.3

$$SE = \frac{DischargePower}{Materialremovalrate} \quad (1.3)$$

**Surface morphology:** The surface roughness (SR) in EDM is also one of the important process outputs. Ideally, each electrical pulse forms a crater on the work surface and the eroded material moves with dielectric flow, but the small amount of material eventually re-solidifies and forms undesirable peaks on work surface and hamper the quality of surface. It is observed that surface roughness increased when the pulse-on time and open-circuit voltage were increased. Surface roughness is affected by pulse time and open-circuit voltage due to higher discharge energy [28]. The surface roughness is measured in  $\mu m$  and is considered a performance indicator in EDM.

#### 1.4 Problem Definition

After a comprehensive study of the literature survey, the following gaps have been identified: In existing EDM, generally, a geared-based or lead screw-based



servo mechanism is utilised to maintain the inter-electrode gap. The dynamic response of this type of servo control system is slow due to mass inertia and backlash problem[8]. The slow response of the servo system further causes arcing and short-circuiting phenomena. This reduces the machining efficiency, productivity, and speed of the process. Further, the condition of secondary discharge may occur due to improper flushing and slow positioning response[29]. Additionally, inconsistent discharge is another open issue in EDM. The traditional power supply, especially the RC pulse generator type, does not ensure an efficient spark condition; a functional delay affects the machining rate and surface quality; and additional thermal damage occurs on the work surface due to a lack of dielectric strength recovery[30]. Hence, the issues associated with existing EDM tool-feeding servo mechanisms and power supply difficulties are the focus of this investigation. The list of open issues is as follows:

1. Slow response of the conventional servo Mechanism,
2. Inconsistent discharge energy,
3. Issues of arcing and short-circuiting ,
4. Complexity of power supply.

### **1.5 Objectives of the present work**

The issues addressed in Section 1.4 have been tried to resolve by the invention of the maglev EDM. It is a self-servo bipolar linear actuator that needs a pure DC power supply for EDM. Similar to any other new technology, it needs a feasibility test with various workpieces (electrically conductive materials) similar to the existing EDM process. Therefore, the objective of the present work

is to experimentally test the **Feasibility of Maglev EDM with difficult-to-machine materials**. During the feasibility analysis, the experimental data available in the literature was used for the performance evaluation. The performance evaluation was done by comparing the specific energy (SE) of material removal in the reported works with the specific energy measured in the maglev EDM. Apart from the specific energy, surface roughness, material removal rate, tool wear rate, and voltage-current characteristics have been compared with the available literature for the performance evaluation.

Additionally, mathematical models of material removal rate and surface roughness have been developed. A detailed analysis of the machined surface has been performed for any material migration and diffusion detected through energy dispersion X-ray (EDX). Surface morphology has been studied in detail using field emission scanning electron microscopy (FESEM). Focusing on the aim of the work, multiple hard metals have been machined, and machining performance has been evaluated with the help of available literature. In this study, the following materials have been used to assess the feasibility of EDM in presence of deionized water as a dielectric medium:

#### **WorkPiece Material**

1. Commercial available Pure titanium
2. Titanium alloy (Ti6Al4V)
3. Inconel 625
4. Nimonic alloy

## **Tool Material**

1. Brass
2. Copper

### **1.6 Organization of the report**

The entire report is organized into eight chapters. Chapter 1 introduces the basics of electrical discharge machines and the technological research gap. This chapter includes the background and motivation behind the current work. A literature review on the evolution of EDM and the work reported by the investigators are presented in Chapter 2 with their various essential aspects. The literature review has been separated into different sections, component-wise, such as servo controllers, power supplies, etc. At the end of Chapter 2, a summary of the relevant work is given. Chapter 3 includes the development and description of the Maglev EDM (MEDM) in various sections. The chapter includes pictorial and schematic views of the MEDM, which helps to understand the working principles and design of present technology. The next chapter is based on the feasibility analysis of MEDM through a series of experiments and resultant discussions on commercially pure titanium as the work material. This chapter analyses the working capabilities of MEDM using the different process parameters. The chapter compares the output response of MEDM with the reported work and provides a conclusive statement. Chapter 5 examines the feasibility of MEDM through experiments on the work material, titanium alloy, and discussions of process outputs. The chapter compares the response output of MEDM with work carried

out on the same material in the past. At the end of the chapter, the summary of the work is represented. Chapter 6 focuses on the feasibility test through experimentation and discusses Inconel 625 work materials. Similar to the previous chapter, the response output of MEDM and reported work concerning the same work material are provided here. In Chapter 7, the feasibility of the MEDM is analysed by performing experiments on another work material, Nimonic Alloy. The response output of the MEDM is observed and compared using the graphs and 3D views. At the end of the chapter, the work is summarised point-wise. Chapter 8 presents the key conclusions of the entire work carried out to justify the feasibility of the Maglev EDM (MEDM). The concise report of the present work explains the performance and feasibility of Maglev EDM; the process output response has been presented through pictorial views appropriately, wherever required. The findings of this study demonstrate that the maglev EDM outperforms conventional EDM in terms of performance.

## CHAPTER 2

### LITERATURE REVIEW

The current chapter highlights the significant aspects of EDM that researchers have previously developed. The chapter is organised from the earliest stages of EDM development to the most advanced facilities currently available. The investigators faced several issues and challenges while exploring the EDM. Many of them have been fixed with technological advancements, while many are still unsettled and open to further research, requiring pioneering work for robust EDM technology.

The entire chapter is divided into sections that discuss technological advances in EDM components, such as the servo mechanism, controller units, and power supply system. From the subject's perspective, the functioning and development of these three elements are significant. Consequently, the present chapter focuses on the primary problems and issues with the current servo mechanism, power supply system, and inconsistent discharge.

#### **2.1 Servo mechanism**

The overall performance of EDM in terms of material removal rate (MRR), tool wear rate (TWR), and surface roughness (SR) has received considerable attention for many years[31][32]. In EDM, metal is removed from the workpiece and very little from the tool as a result of tool wear. This leads to a gap between

tools and work. To maintain spark voltage, avoid short circuits, and keep the electrodes (tool and work) the appropriate distance apart, a tool feed mechanism is needed. In conventional EDM, a servo mechanism is used to maintain the gap. It is a mechanical system comprised of a servo motor and a lead screw that operates with the aid of feedback signals. The typical servo controller is shown in Fig2.1

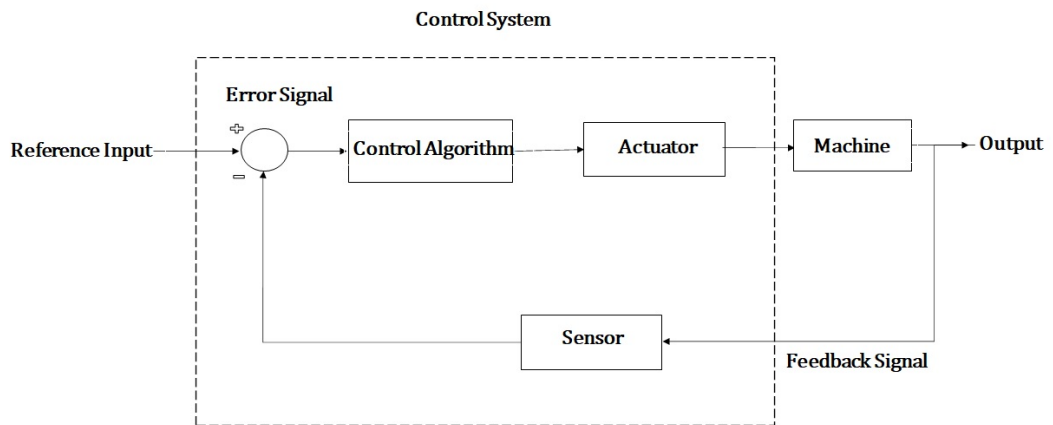


Figure 2.1: EDM Servo mechanism

The principle of the servo mechanism is based on error-sensing feedback and acts as a self-acting device to keep the right distance between electrodes. It comprises electronic and mechanical components to regulate the electrode's mobility. The EDM process is conducted in a limited space (typically measured in microns). Due to the formation of a bridge over the plasma channel between the electrodes, the buildup of eroded material particles in a confined area increases the chance of undesirable conditions. The formation of such unwanted connections between electrodes results in short circuiting and arcing, which decreases the efficiency of the machine. Consequently, it has been determined that an instantaneous response of the drive mechanism to elevate the tool electrode without inertia

delays is needed. In the early stages of EDM development, conventional servo mechanisms were used. For instance, when the distance between the electrodes is high, the voltage across the electrodes is typically considered an open circuit and has the greatest magnitude of voltage. In addition, this state defines the absence of load or the absence of material erosion during open-circuit voltage. In circumstances where the distance between the electrodes is narrow, debris may become lodged between the electrodes, resulting in a short circuit. As a result, in a short circuit, the voltage across the gap reaches zero magnitude.

This has been explored in prior studies that, the Z-axis servo drive system is used to maintain the proper inter-electrode gap based on the spark state. With the advancement in the field, electro-hydraulic drive systems replaced electric motors due to the hysteresis and low responsiveness of the existing mechanism[33]. The majority of the previous studies have shown that the appropriate positional stability influences the entire machining process. The servo control system ensures proper and rapid positioning of the tool electrode for efficient discharge. The literature review shows that with advancements in the field, sophisticated servo control systems were used to control the range with transistorised variable speed controllers and more accurate digital positioning encoders. Several studies found that by reducing the typical servo control system's response time and backlash error, the researchers optimised the positioning system. EDM stability and precision were improved by different methods. This has been discussed by a great number of authors in the literature that due to servo controller issues such

as backlash error, stack inertia, and delayed response, the researchers used piezoelectric ceramic actuators to drive a linear motor. The piezoelectric actuator was investigated for high-frequency response. These controllers had better transient response and tracking than the previous controller due to their ceramic material's unique properties[34]. In the literature, it was reported that piezoelectric logic offered the remarkable advantages of superior resolution, faster response, and high rigidity. The usual constraint with the piezoelectric controller was its limited stroke, and the need to realise a higher degree of freedom was noted. Further, it was observed that such a system is necessary to reduce friction and delay response without physical contact. Subsequently, a new concept based on the magnetic bearing was successfully established [35]. Eventually, the issues of friction and inertia were rectified using magnetic bearings. This advanced technology had the ability to provide a wide band width, precise actuation with many degrees of freedom, and a large stroke that allowed for proper electrode placement. A significant amount of magnetic bearing research was conducted for the high-speed and contact-free spindle, and as a result, a maglev wide-bandwidth, highly precise, longer stroke 5 DOF positioning system was developed[36]. The entire research was carried out in phases. In the first step, the actuator was designed and manufactured, and in the second phase, the local feedback enhanced the positioning precision, bandwidth, and other characteristics.

The newly developed actuator was small enough to be installed on a standard, electrically powered machine. Parallel to the magnetic bearings system,



research was carried out, and the invention of a micro inchworm-style feed mechanism was developed[37]. The analysis revealed that the piezoelectric properties had very low strain, which is less than 0.02 mm, and a maximum thrust force of roughly 30 N, with a little accuracy. Later, to accommodate a large stroke and larger force, the piezoelectric linear inchworm actuator was discovered. These actuators were more smart or adaptive than the previous ones[38]. To realise the optimum gap between electrodes and sufficient stroke length, the research was continued globally. The other group of researchers was working on a linear electrostrictive motor with significantly increased thrust capacity, high positioning responsiveness, and enhanced tracking precision[39]. An innovative linear electrostrictive motor with electromagnetic clamping was designed to significantly overcome the feeding mechanism concerns.

In addition to these solutions, the voice coil and piezoelectric components also realised high response and direction on the Z-axis exclusively. These solutions had the same drawbacks. To add electrode rotation or automatic electrode retraction, the drive weight was limited to a few grammes. Subsequently, it was difficult to attain a few microns of length and high-speed responsiveness in all three directions (X, Y, and Z). Consequently, the investigators developed two theories or modules, one of which was a local actuator for microholes and the other for extremely precise microdie cutting. These two prototype local actuator modules were 10 times more efficient than typical electrode servo systems[40]. Later, again, another set of researchers worked on the piezoelectric material and

evaluated it. They reported the same issue, which was a restricted stroke of the actuator. This difficulty was overcome by adopting the inchworm principle to get the large stroke[41]. A novel linear piezomotor with great positional resolution, stiffness, and output force has been designed. By substituting point-to-point contact with a surface, the developed system was able to reduce the number of mechanical elements and interfaces. The performance of the piezo motor was spectacular. It displayed a positional resolution of 5 nm, a stiffness of 90 N/m, and an output force of 200 N.

Previous studies have shown that, despite the physical properties of the material, like the piezo effect, the researchers focused on the magnetic properties of the material to get the suitable placement and strokes of the electrode. Further field research led to the discovery of a new method that legalised the maglev effect. In consequence, the maglev actuators demonstrated a positioning stroke bandwidth of greater than 100 Hz and positioning strokes of 2 mm in the thrust direction. The maglev actuator could create stability even in discharge situations and boost the machining rate by 21.8% [42]. Due to the magnetic local actuator's (MLA) exact control, the right distance between the electrodes was attainable. The study also discovered that the MLA increased machining speed by 20–40% compared to EDM without the MLA. The only major difficulty with the Maglev local actuator concerned the power supply brushes. When the current supply to the electrode's power brushes hits the levitated shaft, friction is created between the shaft and brushes. This friction causes a disruption in the spindle shaft's

motion, which decreases the efficiency of the action. The researchers overcame this issue by creating an additional novel 5-DOF Maglev local actuator. The novel MLA overcame every worry raised by the prior controller. In this actuator, the discharge current was supplied via a soft, excitable wire, allowing the levitated shaft to move freely and unimpeded[43]. With bandwidths of up to 200 Hz in the 5-DOF directions, the MLA was able to accommodate positioning resolutions of sub-micron and several microradians. The work presented demonstrates that the system accomplished a stroke of 2 mm in the thrust direction, 180 metres in the radial direction, and 3.6 radians in the tilt direction. Recently, more advanced types of feeding systems are in trend, like in the recent past, a 6-DOF maglev levitated parallel actuated dual-stage system with positioning in x-y plane motion was developed[44]. Later, the six-axis industrial robot (IR) technique was used and investigated in EDM. The IR techniques were not suitable due to the high vibrations. However, the use of novel WEDM and IR as servos was discovered to improve results.

## **2.2 Control Unit**

EDM, like other non-traditional machining processes, employs automatic control components. Depending on the machining circumstances, these automated components receive instructions or signals to carry out the procedure. It is evident from prior research that the mechanism of machining is complex and unpredictable due to its dependence on various input parameters[33]. Even an experienced operator can't control the suitable spark state manually because the pulse frequency is higher and the spark conditions change. Scientists have,

however, come up with a number of ways to control the gap or spark condition. EDM normally uses automated control servomechanisms as mentioned in the previous section. The servo mechanism consists of a control unit. This control unit functions as an adaptive system and uses error sensor feedback to compare the machine's output response with input. In addition, based on the state error signal, the condition is evaluated, and the servo control mechanism receives the necessary inputs. It was observed that this system eliminated the arcing and resulted 50% boost in process productivity[45].

Later, the researchers employed a neural-network methodology to implement online monitoring and control measures. It was significantly superior to the old system; the new control system could respond promptly to spark-gap conditions. This method was built on a feed-forward neural network that monitors the amount of voltage and current in the gap between the electrodes via supplied signals [46]. A group of researchers further explored the neural network approach so that optimal parameters could be applied to the EDM in order to improve its performance. According to the findings of the tests, the neural network method produces more accurate forecasts for the various EDM states[47]. Subsequently, researchers investigated the adaptive control system and determined that the process model and control parameters were the most challenging. This issue was resolved by a self-regulating system that checks the gap conditions of the real-time process [48]. After optimising the first adaptive control optimisation system (ACOS), the researcher created another advanced system. The

latest system might detect problems early on and fix them to save energy and time[33][49]. The researchers tuned controlling factors to maximise material removal with little tool wear. Several more characteristics can be improved during the process, according to online optimisation. Nevertheless, researchers discovered that the ACO system can handle the automated adjustment based on the conditions, although there is room for improvement. Due to the volatile nature of the EDM process, researchers discovered that exact control over the spark gap is challenging. In response, a new system based on fuzzy logic was developed[50]. Fuzzy logic is typically based on qualitative logic and relevant data pertaining to a certain condition. The EDM is a type of nonlinear multi-variable process, and researchers have found the fuzzy system to be effective in such processes. The system allowed the EDM machine to vary the effective distance between the electrodes. Researchers examined the capability of quick reaction and the compactness of fuzzy logic[51][52][53]. Fuzzy logic-based EDM with a piezoelectric stage provides stable machining due to a normal, efficient discharge. Without fuzzy logic and the piezoelectric stage, discharge was uneven, affecting machined surfaces[54]. The fuzzy logic-based controller avoids short-circuiting and smooths EDM by responding quickly and accurately to normal discharge. All gap control methods were based on the expected servo reference voltage and could not self-regulate. The novel self-tuning regulator with proportional-integral (PI) feedback used electrode gap feedback signals. Researchers used a PI controller to improve EDM placement[55]. In motion control, inertia and path friction are important[56]. Since the entire EDM process is based on different process factors and

variables that greatly affect the process, a PI controller was advantageous[57][58].

For the majority of EDMs, the proportional-integral-derivative (PID) method was developed. The feedback signals adjust the servo controller using specified mathematical models[59]. This system assigns parameters based on EDM process attributes[60]. PID controllers increased the efficiency of sinking EDM processes by 30%[61]. A powerful microcomputer adjusts the servo driving signals instead of the reference voltage. The EDM self-turning controller and P.I. controller worked best together. Despite numerous adaptive control servo systems, flushing was still lacking, especially in the deep-hole EDM process. A self-turning integrated controller for EDM solved the flushing problem. This controller removes trash from deep-hole EDM operations using tool withdrawal[62].

This novel method measured the cumulative time ratio of the gap, usual spark, temporary arcs, dangerous arcing, and short-circuiting with 0.2 or 1 ms resolution. The transient arcing parameter predicts arcing, and employing its time ratio in the control system process boosts machining productivity by 20%. Even with tough flushes, the integrated EDM controller stabilises machining and eliminates arcing during EDM sinking. Another upgraded adaptive control system was created to control gap situations using EDM monitor data[63]. This proposed system used the gap condition. EDM is highly dynamic and stochastic, making online adjustment to increase reliable, efficient spark discharge difficult for any controller[64]. All control systems could execute certain functions to make the EDM more efficient. Still, the procedure included flaws, including unattended

flushing. Another study group developed a more complex technique to fix the poor flushing. This sophisticated system comprised a model reference, an adaptive control system, and new servo interface technology that could solve the most practical problem of poor flushing conditions during machining. This model reference system could observe each discharge state and optimise the servo voltage as needed. Feedback and error signals are used for online optimisation to improve flushing[65]. This new servo control circuit had a servo reference voltage in a wide range to get a higher time ratio than normal sparks and avoid interference due to changes in the duty cycle. As a result, the overall productivity of the innovative servo control unit turned out to be about 40% higher than the previous controller[45]. Lately, a new adaptive control with the well-known fuzzy controller that uses energy consumption and short-circuit ratio as control inputs has been proposed[66]. Despite the novel method, energy consumption is computed from pulse-on time, discharge voltage, and peak current as a frequency function. Isolating discharge signal noise first determines each pulse's ignition delay duration. Hence, stability and fast servo cutting are obtained. Over time, an extensive literature has developed on control units. With the advancement in the field, a unique pulse servo control was made by figuring out the four most important gap voltage waveform states: open circuit, normal spark, arcing, and short circuit[67]. They adjusted the pulse interval in real-time using an anomalous spark ratio. The control approach regulates each pulse's pulse delay in real time according to the discriminated gap states. It was observed that despite being done under constant workpiece thickness, the discrimination system with changing

pulse interval can achieve stable machining even in unanticipated disturbances of varying workpiece thickness. With the high contouring precision that EDM needs, an indirect adaptive servo control was made[68]. To fix the nonlinear friction and cogging effects of servos, the output relationships of the auto-regressive moving average model and the neural network-based compensation were combined. A group of researchers used vibration activation on the workpiece and adaptive servo feed-rate control in an RC pulse generator to increase flushing, MRR, and SR [69]. Discharge frequency, voltage, and current inputs. Feed-rate and discharge frequency evaluate workpiece thickness and calculate the adjusted feed-rate. Hence, the servo feed rate achieved 2.5 times EDM speeds without vibration. Recently , an advanced adaptive neuro-fuzzy inference system (ANFIS) for servo control was created[70]. It is intended for wire EDM and improves prediction of gap voltages and wire breakages. The control uses pulse on time, pulse off time, mean gap voltage fluctuation, and wire feed rate. The method worked well with wire deterioration during high-intensity gap voltage machining.

### **2.3 Power Supply**

EDM requires high-frequency power like other unconventional machining methods. The pulse power generator produces controlled energy for sparking in EDM. The pulse power generator has an effect on the MRR and the surface finish quality[71][72]. Two sub-components make up the EDM power generator: the power supply and the pulse generator[71].The power supply may be either linear or switching mode power supply (SMPS). The SMPS type of power supply is commonly used in EDM due to its low cost, greater MRR, and superior surface



finish[73]. A pulse generator with two types of relaxation or resistance capacitance (RC) and a transistor pulse generator constitutes the other component of the power generator unit. Fig 2.2 depicts the fundamental construction of an RC power generator.

Prior research suggests that initially, RC pulse generators were used; however, charging condensers to provide discharge energy took a long time, and researchers carefully investigated ionization in the electrode gap[74]. Due to the charging and discharging phenomenon in RC-type circuits, it is difficult to keep the voltage at a consistent level[75]. RC-type pulse power supplies' restrictions are overcome by transistor-type power supplies' higher discharge frequency. Due to the circuit delay, it helps trigger the pulse quickly. By switching off the circuit for an ultra-short time, the delay prevents abnormal discharges like arcing and short-circuiting, leads enhancing material removal[7]. Due to its increased capabilities, massive current handling capacity, and quick reaction, the transistor is replacing the RC-type pulse generator[4]. The pictorial view of a transistor power generator is shown in Fig2.3. It has been found that the transistor-resistor and transistor-inductor pulse power supplies are capable of meeting the conditions for a self-sustaining spark discharge after the gap has been broken. This capability continues until the end of the discharge, at which point the gap voltage needs to be maintained above the threshold value[76]. Due to their high discharge energy and material removal rate, transistor pulse generators are used in conventional EDM[77][78][79]. Pulse duration and discharge current can be

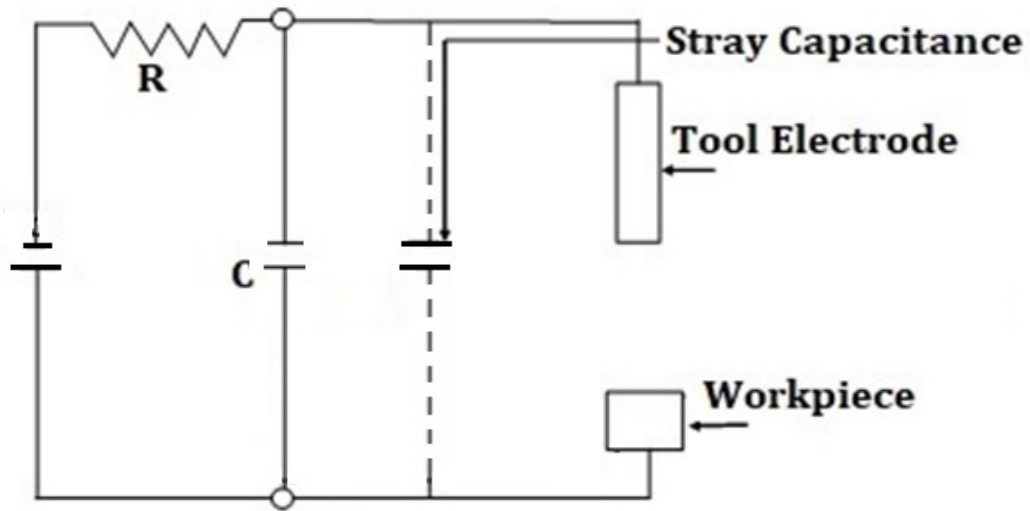


Figure 2.2: RC Power generator  
[19]

adjusted in transistor pulse generators. To reduce gap current in EDM, simple RC power generators or transistor generators with a resistor are used. The transistor's key output voltage may vary due to the direct current power source's design[80]. The results indicate that the selection of an EDM generator is influenced by the desired machining outputs. With a larger peak current and longer discharge period, a transistor-type generator produces more energy and consider for the higher MRR[81]. The notable benefits of transistor-based pulse generators include the ability to set pulse shape and broad ranges of peak current and pulse width[82]. This enables diverse methods for managing servo speed via pulse discrimination[83]. There are two distinct types of transistor pulse generators, iso frequency and iso-energy, whereas current WEDM machines provide operator selection to operate under both regimes[84]. Iso-frequency is a constant pulse frequency and matches transistor train generators[85]. This pulse gener-

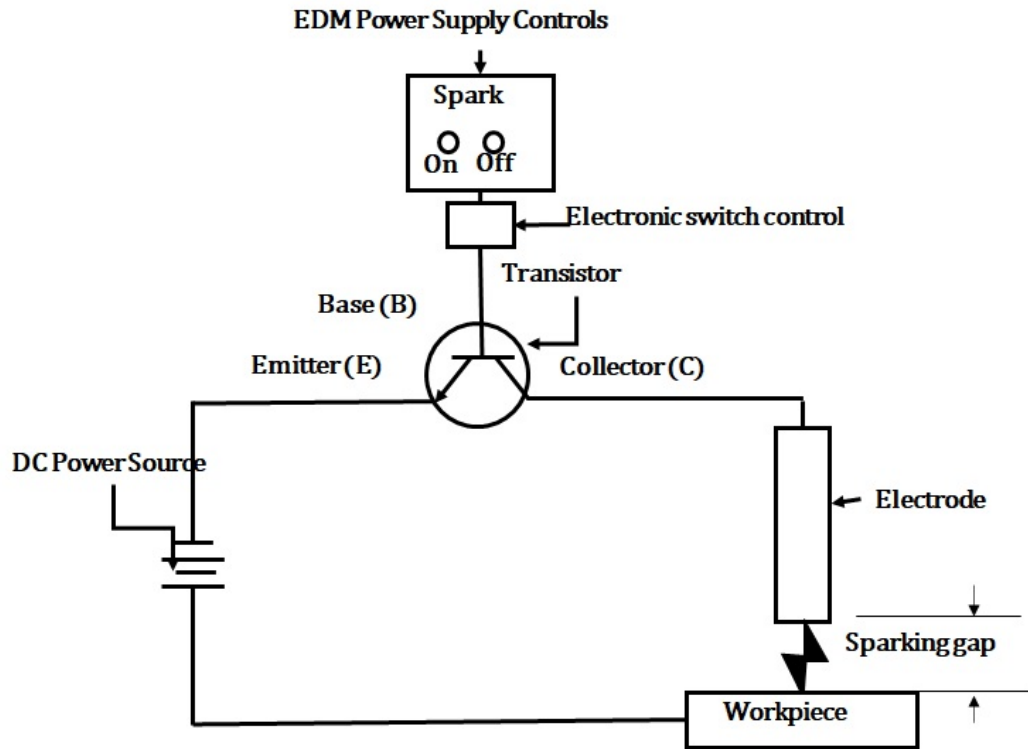


Figure 2.3: Transistor type power generator [1]

ator is better for applications with high MRR[86] or high insulation and high voltage, such as polycrystalline diamond machining with oil dielectric fluid[87]. Whereas, the iso-energy pulse generator, also called isopulse[86], gives out the same amount of energy with each pulse and makes triangle-shaped waves with equal slopes[88]. The iso-energy generator was made to reduce the random discharge process so that SR and MRR would be better than with regular transistor pulse generators[85].

It was discovered after some time that iso-energy generators provide a more stable process, which is advantageous for control techniques due to less arc and short-circuits, improved flushing conditions, and a uniform MRR[89]. On the other hand RC generators function by storing electric field energy in a capacitor.

The parallel capacitor located across the machining gap regulates the discharge energy[90]. Once fully charged, the capacitor discharge is discharged without a switch and is guided only by the gap distance[91]. It was observed that RC pulse generators have a lower discharge energy distribution than transistor pulse generators[92], resulting in smoother SR and mirror-like surfaces with SR up to 0.2  $\mu\text{m}$  Ra[93]. However, the RC pulse generator may be carefully tuned to produce less energy with a shorter discharge period. Therefore, the RC pulse generator produces pulses for micro-EDM to form extremely fine micro structures[94]. Consequently the power supply choice, depends on the type of application. Micro-EDM with low material removal may use the RC pulse generator. The transistor pulse generator is used for high material removal. Recent research has resulted in the development of a novel and hybrid strategy. In this method, rough cuts are executed using the relaxation-type pulse, and the trim cut makes successful use of the isoenergetic-type pulse[95]. However, resistance reduction is a problem for transistor power. Its widespread use is limited by internal resistance-induced ripple and attenuation (noise) in the intended signal. Because it's free of disturbance and attenuation, pure DC power may help the spark gap discharge energy (noise). Researchers used a DC power source directly to perform EDM and produced a considerably greater material removal rate than standard power supplies[96].

## 2.4 Dielectric Medium

In addition to the above components, the flushing system is also an important component of EDM. In actuality, the dielectric medium keeps the debris or eroded

material away from the machining zone. In most of the applications, deionized water, kerosene, and hydrocarbon oil are commonly used as working mediums in EDM[97][98]. The kind of dielectric medium, pressure and flow velocity further affects the machining response in terms of MRR, surface roughness and tool wear rate[99]. It is reported that kerosene can be used as a dielectric medium when processing titanium to get a good surface finish. But the TiC that forms during EDM of titanium alloy slows down the rate of material removal and makes it hard to remove debris. Deionized water may speed up the rate of material removal by making it easy for titanium alloys to oxidise. This process of oxidation and decomposition of the medium creates heat to improve the MRR[100]. Further, to improve the MRR, the combination of water and kerosene can also be employed. For example, a research group found in an experiment that 60% of MRR can be enhanced by combining dielectric media with distilled water[101]. According to the literature, oxygen decomposition from hydrogen forms bubbles across the electrode gap, which creates pressure differences inside and outside of the bubble. The pressure difference and dielectric pressure segregate the debris equally in the electrode gap. The proper distribution of debris leads to sufficient instant discharge energy for the improved surface finish [102][103][104].

## **2.5 Summary**

Numerous cutting-edge approaches have been implemented to improve positioning response and machining precision. Important innovations such as a pivot-bearing-supported actuator arm without friction, a vibrating tool electrode for enhanced flushing, and a magnetic field have been implemented. It is reported

that the following works represent important steps forward in the areas of EDM positioning response and machining accuracy. A piezoelectric actuator technique was added as major advancement to improve tool electrode placement[34]. Later the piezoelectric actuator realized limited use due to the lack of sufficient degree of freedom (DOF) and quick stroke retraction. Such limitations of the piezoelectric actuator were addressed by developing the magnetic bearing levitation technique. The new approach employed the magnetic force, which was able to provide contact-free motion under the effect of the magnetic field. It was observed that magnetic levitation can be considered a solution to overcome the limitations of piezoelectric actuators like DOF and limited stroke [105]. Later, taking into account the magnetic field effect, the researchers developed a magnetic actuator based on the maglev lucidity. The developed maglev actuator outperformed in terms of wide bandwidth and millimeter stroke for more accurate positioning in 5 DOF. This actuator was used as an additional attachment in the micro EDM, the performance improved [41][57]. A PID (proportional-integral-derivative) controller was utilized to regulate the electrode tip of the tool at a very low vibration magnitude (approximately 2 mm).The same study group enhanced the work and found a high material removal rate with a stable discharge using a 5-DOF local actuator arm [43][9]. Although successful magnetic levitation was reported with the RC power supply, it was an addition to the existing EDM machine.The other group made machining faster and more accurate by combining a high-speed maglev actuator arm with EDM. The maglev actuator arm boosted the rate of machining by 434.2% in comparison to traditional EDM[106].

Lately, a revolutionary maglev transportation platform was made to allow for high-precision, high-speed linear motion over a large distance. In the levitation subsystem, the moving platform was constructed by six sets of electromagnets. By using the finite-element (FE) method to study the magnetic coupling of electromagnets, the best way to place electromagnets in space was found [107]. A maglev-levitated lens-driven actuator was designed and manufactured to realize the maglev effect in laser machining first. The goal of actuator was to reduce assist gas consumption and increase machining rates in laser machining, particularly for high aspect ratio holes. The actuator was capable of driving the lens to achieve real-time control of the relative displacement between the lens axis and the assist gas jet nozzle axis[108]. To quickly maintain the appropriate electrode gap and obtain radial vibration for debris removal, a 3 DOF precise magnetic/piezoelectric hybrid drive actuator was used to regulate the tool electrode in the thrust direction. The positioning performance of the actuator is then tested through experimentation using a controller that includes local current feedback for the electromagnets[109].

In micro EDM, a magnetic levitation device with a hollow spindle and PID algorithm is proposed to reduce the complexity of the machine tool and utilize a large electrode. The incremental PID method achieves 150Hz axial (Z) response frequency and 5 micrometer and 2 micrometer radial and axial position precision, respectively. In the reported work, micro-EDM was accomplished with a magnetic suspension spindle with a 1.3 mm stroke [9]. The maglev actuators have been

employed in many other applications like micro-gravity vibration isolation systems in space station for the ideal experimentation conditions. In accordance with the Lorentz force theory, a maglev actuator was designed and constructed [110]. In recent past a 6-DOF maglev levitated parallel actuated dual-stage system with coarse-to-fine positioning in x-y plane motion was developed. This two-stage motion system was made up of a 6-DOF maglev primary stage and a 2-DOF planar motion flexure-based secondary stage. This design reduced the levitated platform's weight and dimensions, enhancing its dynamics using the maglev effect[44]. It was observed that the use of magnetic field assistance generates the Lorentz and Ampere forces increase plasma channel stability, current density, and consequently material removal efficiency [111]. Due to the convenience of contact-less forces, magnetic field-aided methods have recently demonstrated considerable potential and superiority for upgrading the machining process and its performance [112]. In line with the present subject matter, the effect of the magnetic field was employed by the researchers to improve the machining characteristics like MRR and Surface quality. Prior research and development either incorporated magnets as an integrated part of the servomechanism or as an accessory to enhance the machining characteristics. None of these used magnets as a self-actuating mechanism. In present technology, the magnetic circuit is created and structured so that the electrode gap is governed by the current flowing into the electric magnet. It is an adaptive system, and can use a DC power source for EDM instead of an RC or pulsed power supply.



## CHAPTER 3

### DESCRIPTION OF MAGLEV EDM

#### 3.1 Introduction

In the previous chapter, the significant difficulties associated with conventional EDM were discussed. The challenges inspire development of a dependable engineering system that guarantees the correct translation of the cutting tool. The recommended technology replaces the standard tool feed mechanism, i.e., the servo controller, with a this technique. The proposed method is based on the Maglev principle and employs bipolar fixed and movable magnets. This new approach regulates the movement of tool electrode towards the workpiece by applying a voltage differential across the space between electrodes.

However, according to the available literature, magnets have been employed as servo controller attachments in tool feeding systems. Magnets are employed to prevent physical contact and friction between mechanical components of the servo system. But the present technology works without a servo controller and has never been used for tool translation. Additionally, a DC supply replaces the pulse power supply. The current investigation shows that the new method is feasible and provides improved output response.

#### 3.2 Working principle and development of MEDM

A maglev EDM is a technology to erode material by the exact same process as classical EDM does. The novelty of proposed system is its inter-electrode

gap control mechanism. In present technology a self-servo bipolar linear actuator (SSBLA) has been developed to perform the task of controlling the inter-electrode gap at the desired value of gap voltage. The SSBLA is the key component of the maglev EDM.

### **3.2.1 Construction and working of self-servo bipolar linear**

#### **Mechanical components**

It consists of three major mechanical components arranged logically as shown in fig 3.1 .

- Electromagnet stationery (EMS);
- Permanent magnet moving (PMM);
- Permanent magnet stationary (PMS).

The EMS is connected to a DC power supply to apply a vertical downward force due to the repulsive force ( $F_{EMS}$ ) between two magnets, viz., the EMS and PMM. The PMM can move in a vertical direction on a slide and contain the tool electrode. The movement of the tool and PMM assembly governs the inter-electrode gap for the discharge process. The PMS, a permanent stationary magnet, is fixed to provide floating force ( $F_{PMS}$ ) to the moving assembly.

All three magnets are aligned in a vertical line so that the PMM can float over the PMS with influence of the repulsive balance force  $F_{EMS}$  and  $F_{PMS}$ . The self-weight of moving assembly is supporting the repulsive force between PMM and EMS. Thus, in equilibrium condition  $F_{PMS} = F_{EMS} + \text{Weight of the assembly of PMM and tool.}$

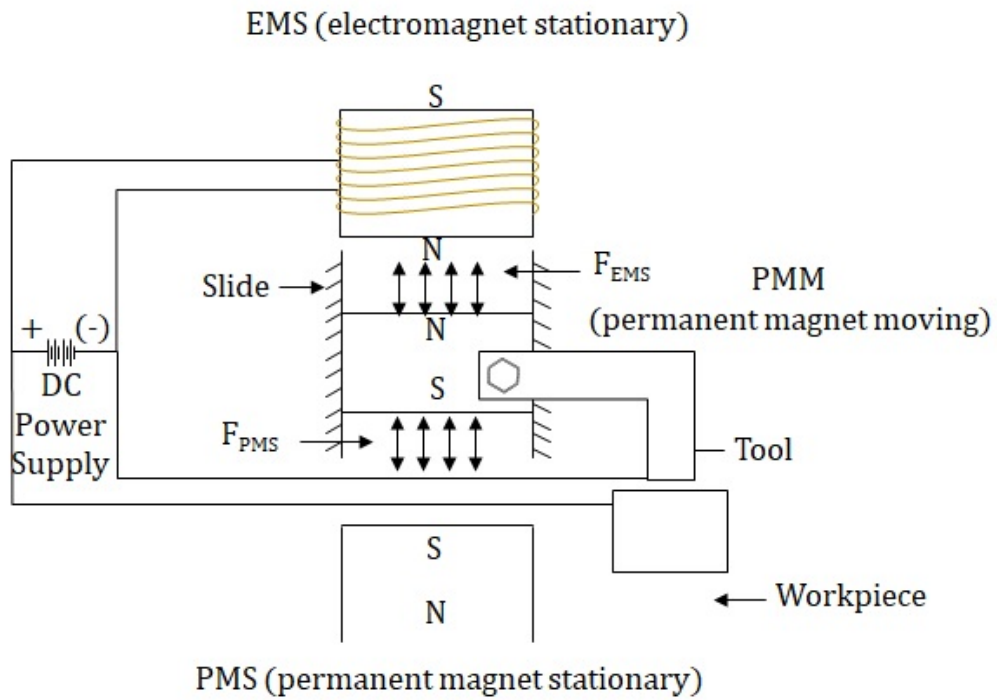


Figure 3.1: Working Principle of MEDM

### Electrical components and connections

A DC power source is connected with the EMS to push the PMM downward to maintain the system in equilibrium. The DC power supply is connected with the tool (-) and workpiece (+) in a parallel electrical connection. The potential difference between the electrode and EMS is in parallel; therefore, both voltages are the same.

### The function of the SSBPLA

Initially, the system is in equilibrium, and the DC power source is at full applied voltage ( open circuit ), with a small amount of current (about 200–300 mA) passing through the EMS. For EDM process to start, the workpiece is mov-

ing upward, i.e., closer to the workpiece, with the help of a manual linear stage. Once the inter-electrode gap reaches the threshold value of the gap, ionization and discharge start between the electrodes. The voltage between the electrodes drops, and the reduction in this voltage results in a reduction in the voltage at the terminals of the EMS. Hence, it reduces its repulsive force. The reduction in  $F_{EMS}$  will allow PMM and tool assembly to move away from the workpiece, and as a result, the discharge process will stop. The gap voltage will increase and may reach to the open circuit voltage. This increase in the voltage increases the  $F_{EMS}$  and the tool will move towards the workpiece. Further movement of the workpiece towards tool will result in lowering the discharge voltage with an increase in discharge current. Thus, tool motion between equilibrium conditions will cause electrical discharge during motion. The aim of the mechanism is to reach an equilibrium condition at a discharge voltage, and here continuous discharge will be happening between the electrodes.

A true-scale working prototype was developed and is shown in Fig3.2 with an enlarged view of the machining zone. As mentioned that the proposed technology is based on the concept of magnetic levitation. Here, two magnetic repulsive forces ( $F_{EMS}$  &  $F_{PMS}$ ) are balanced using two sets of magnets. One is an electromagnet (which acts as a bipolar linear motor), while the other two are permanent magnets. A pure DC power source is connected to the electromagnet to energize it. Further, the same DC power supply is connected in parallel to the tool and workpiece in straight polarity as shown in Fig3.3. A pivot-bearing supported

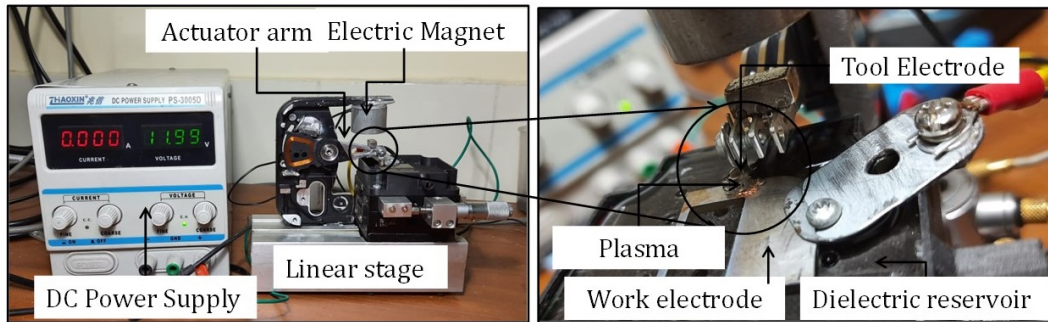


Figure 3.2: True scale working prototype of Maglev EDM; magnified view of machining zone

actuator arm is used to hold the tool electrode along with a movable permanent magnet (PMM). An electromagnet Stationary (EMS) is fixed just above this movable permanent magnet (PMM) to facilitate the strong electromagnetic repelling force ( $F_{EMS}$ ).

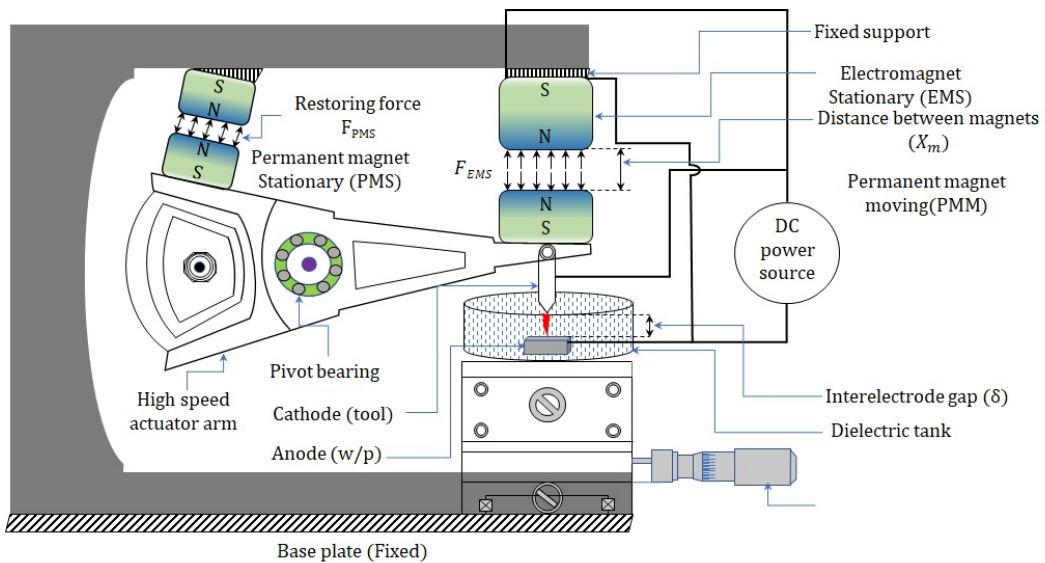


Figure 3.3: Mechanics of servo stabilized maglev EDM system

Another permanent magnet stationary (PMS) is kept below this movable permanent magnet (PMM), which keeps the tool electrode away from the work-piece and offers the second magnetic repulsive force called force restoration ( $F_{PMS}$ ). The complete arrangement develops two parallel electrical loops with the same poten-

tial as per the Kirchhoff voltage law. One loop is in between the electromagnet (bipolar linear motor) and permanent movable magnet (EMS & PMM), while another loop is in between the movable permanent magnet and permanent magnet stationary (PMM & PMS).

### **General specification of magnets are used**

- Rectangular bar magnet
- Width: 1 cm
- Height: 3 cm
- Power/Strength: Depends on the electric current I in wire.
- SI unit N. Tesla-1

The mechanism is set in such a way that the magnetic repulsive force ( $F_{EMS}$ ) moves down the tool towards workpiece, which reduces the electrode gap. The electrode gap decreases the voltage potential of the power supply and thus the magnitude of magnetic repelling force ( $F_{EMS}$ ). A situation where the magnetic repulsive force and restoring force will be equal, i.e., ( $F_{EMS}$ ) = ( $F_{PMS}$ ). This is the state of equilibrium at which the tool will oscillate to maintain the proper gap. Fig3.4 depicts servo-stabilized gap control mechanism as well as the variation of different magnetic forces. Curve 1 depicts the no-load voltage state (open circuit voltage). Curve 2 depicts the electromagnetic repulsive force ( $F_{EMS}$ ) that acts between the electromagnet (EMS) and permanent magnet moving (PMM),

pushing the tool electrode towards the workpiece. The restoring force operating between permanent magnet moving (PMM) and permanent magnet stationary (PMS) is shown in curve 3. The process begins at the far left of the graph (point A), where the inter-electrode gap is significantly large and the applied voltage potential is equal to the electrode's no-load condition. The horizontal axis in Fig3.4 shows the inter-electrode gap. The electrical resistance (R) between the electrodes reduces with the gap distance. Therefore, the horizontal axis represents the inter-electrode gap along with the electrical resistance. At the extreme left, the gap and the resistance are maximum and reducing towards right direction. At the extreme right the gap between the electrodes is zero with zero resistance i.e., short circuit condition. The electromagnet is at its maximum magnetic strength in this position. The tool begins to move towards the workpiece due to the high strength of magnetic repulsive force ( $F_{EMS}$ ), and the distance between electromagnet stationary (EMS) and permanent magnet moving (PMM) begins to increase. The inter-electrode gap  $\delta$  between the tool electrode and the workpiece will be reduced as the distance between them increases. The electromagnet's magnetic field intensity will be decreasing in nature from point A to point B when the voltage drops owing to ionization. As the magnetic repulsive force reduced rapidly (point B onward), the restoring force (curve 3) will be increased simultaneously. The inter-electrode will reach point C after a certain tool movement. This is the point at which the electromagnetic repulsive force and the restoring force are equal. To keep the electrode's gap constant, the tool starts oscillating around the equilibrium point (target point C). The discharge continues

at this moment because the channel is entirely ionized. The tool should ideally stay there for a few microseconds at this point, however, due to mass inertia, it sometimes goes forward. The restoring force ( $F_{PMS}$ ) becomes stronger than the electromagnetic repulsive force ( $F_{PMS}$ ) as the tool travels forward, and the tool retracts. An acceptable inter-electrode spacing has been maintained for smooth and continuous discharge based on the above concept. The magnetic repulsive

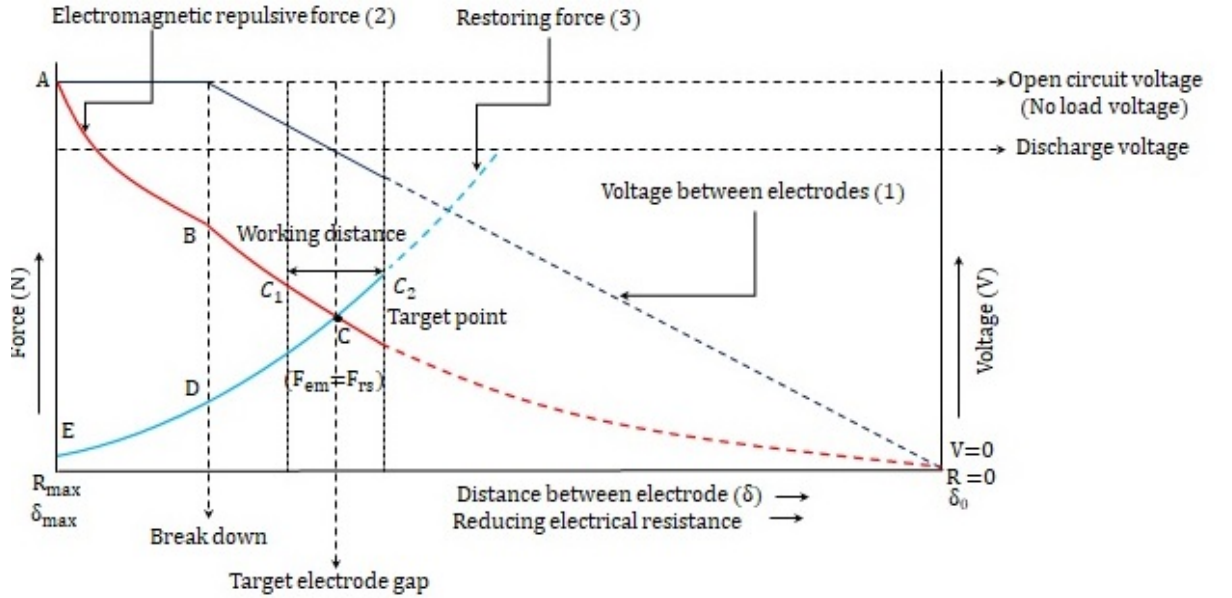


Figure 3.4: Schematic showing the basic principle of working of maglev EDM system with actual arrangement of peripheral components

force acting between the two magnets with pole strength  $m_1$  and  $m_2$  and distance  $x_m$  is illustrated in equation (3.1)

$$F_{EMS} = k_f \frac{m_1 \times m_2}{x_m^2} \quad (3.1)$$

Equation indicates the nature of magnetic force significantly depends on the magnetic pole strength and the operating distance. As voltage is not varying during the open circuit condition before breakdown hence, there is no change



in magnetic poles strength. This means magnetic pole strength is constant and it forms a straight line (see curve 1) before the breakdown point. But after breakdown, the voltage decreases continuously hence magnetic pole strength is also decreasing. This will form a straight with decreasing slope (see curve 1 after breakdown). Later on, it is observed in equation (3.2) that the magnetic repulsive force is also changing due to the variation in the distance in square terms. Hence, it will form a parabolic curve up to the breakdown point. After the breakdown point, the distance is still continuously changing in the square term ( $1/x_m^2$ ) (see curve 2) due to the voltage drop, hence it will again form a parabolic curve. As the magnitude of the electromagnetic repulsive force decreased, the magnitude of the restoring force will be increasing in nature (see curve 3). A situation will come where both magnetic repulsive forces will be balanced ( $F_{EMS} = F_{PMS}$ ). This is the equilibrium point (target point C) in the curve about which tool will oscillate to maintain the suitable gap and machining will occur. The magnetic repulsive force ( $F_{EMS}$ ) experienced by the magnets (EMS & PMM) is given by [113]. Similarly, the restoring force ( $F_{PMS}$ ) between permanent magnet moving (PMM) and permanent magnet stationary (PM2) [113] is given in equation (3.2)

$$F_{PMS} = k_g \frac{m_2 \times m_3}{x_g^2} \quad (3.2)$$

where  $m_2$  and  $m_3$  are the magnetic pole strength of, permanent magnets moving (PMM), and permanent magnets stationary (PM2) respectively. In above two equations  $X_m$  is the operating distance between the EMS and PMS while  $X_g$  is the operating distance between PMM and PMS.  $K_f$  and  $K_g$  are the magnetic

force constants. The voltage is applied across the electrodes in parallel to the electric magnet, in Fig3.4. In a parallel circuit the voltage between parallel ports is equal. As the electrode gap reduces (left to write in X axis of fig3.4) the gap voltage decreases and hence the voltage applied to the electric magnet reduces. The reduction in the voltage of the electric magnet reduces its strength. The following equation (3.3) shows the general magnetic strength.

$$B = \frac{\mu \times V}{2 \times \pi r R} \quad (3.3)$$

Here, magnetic field (B) is directly proportional to Voltage (V),  $\mu$  is permeability of free space, r is the distance of separation, R is electrical resistance of the coil. Equation (3.1) presents the significance of magnetic pole strength with respect to distance. In present technology, the inter-electrode voltage regulates the magnetic pole strength, and consequently, the gap between electrodes is adjusted by repelling and attracting forces.

This technology presented a unique gap control system based on magnetic levitation to improve machining productivity and servo response frequency. In the proposed technology, fluctuation of 1mm is observed by high speed camera. The motion was based on the magnetic force balance therefore, it is considered as analog motion. The vertical motion resolution of the system was 100 micrometers.

In addition, a unique actuator arm technology is used to firmly lift the tool and precisely position it for effective discharge. The tool electrode's quick oscillation enhanced the gap condition by effectively flushing debris particles from the

machining zone [140]. The positional response was assessed using digital image processing (DIP) and the time displacement curve. The time transient voltage-current curve (V-I curve) was used to test the machining speed and stability. The current state, pictorial view of the maglev EDM is shown in Fig 3.5 with the enlarge view of the tool and work electrodes. The improvement in the design is

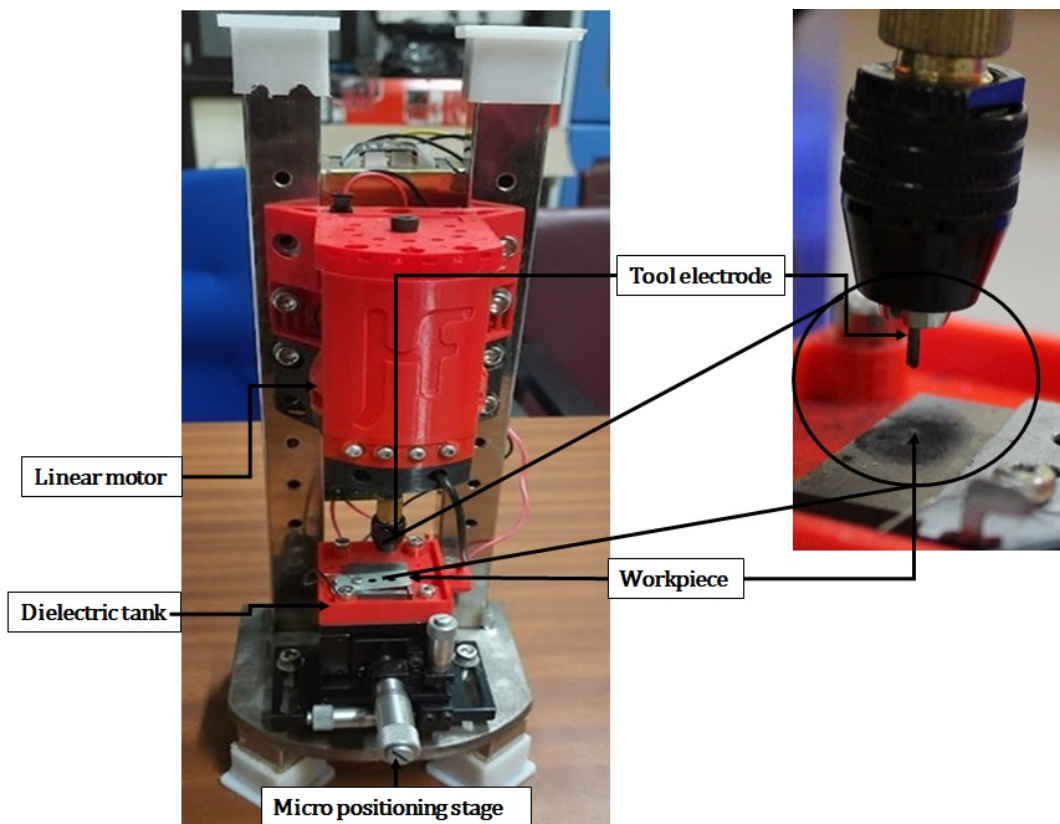


Figure 3.5: The current pictorial view of the maglev EDM

ongoing process. Hence, maglev EDM in its refined form will be available soon for industrial applications.

### 3.3 Summary

The present chapter explains the construction and working principles of the Maglev EDM (MEDM). Fig 3.1 shows the principle and construction details

of the MEDM. Fig3.2 shows the prototype of the currently developed MEDM. Whereas Fig3.4 outlines the logic of the actual process and movement of the tool electrodes with respect to the applied voltage. In the later section of the chapter, specific components and a pictorial view of the MEDM were presented.

## CHAPTER 4

### FEASIBILITY ANALYSIS ON CPTI WORK MATERIAL

(List of publications1)

#### 4.1 Introduction

The present chapter deals with the feasibility analysis of the proposed Maglev EDM (MEDM) through a series of experiments. The chapter explores one of the objectives of the present work, which is to perform a feasibility check on hard-to-cut metals. The hard-to-cut material, commercially available pure titanium alloys, is chosen as a workpiece because it exhibits machining difficulty. The feasibility of developing EDM is the prime concern, so such difficult-to-cut material is utilized as work material. The present chapter includes the experimentation details, the result, and the discussion in the same order. The result and discussion sections briefly discuss the effect of various typical process parameters on machining. Finally, the output responses like material removal rate, surface roughness, and specific energy are computed and compared with the reported work. The conclusive summary of the entire experimentation is summarized at the end of the chapter. The summary of the work proclaims that the Maglev EDM is superior to the conventional EDM in terms of better output response.

## 4.2 Experimental Methodology

The experiments were performed on commercially pure titanium (CPTI). A small plate with a thickness of 3 mm. It was a raw sample and polishing was not performed. The average area surface roughness of the raw sample was 2-3 micrometers (measured on non-contact profilometer zygo NV9000). CPTI is the most commonly used material for making non-structural applications, such as water channels, ducts, and pipes, owing to its high strength at elevated temperatures, corrosive resistance, and good formability. A brass tool electrode with a 2 mm diameter was used with deionized water as a dielectric medium. Both electrodes were connected to a direct current (DC) power supply, so the cutting tool and workpiece acted as the cathode and anode, respectively. The work applies a 12 V open-circuit voltage and a 2-amp peak current through the DC power supply. A digital oscilloscope (Tektronix, TDS2012C, 2-channel, 100 MHz bandwidth) using a differential type voltage (TPP0201, Tektronix) and current probe (65A-Hantek), BNC type, was used to assess the waveforms of the discharge voltage and current. In four different experiments, the workpiece material was eroded into the shape of a circular pocket with a 2 mm diameter.

The experiments were repeated three times to estimate the experimental errors. A digital weighing pan (Mettler Toledo) with a minimum count of  $10\mu g$  was used to measure the weight of the workpiece before and after machining. In this work, the distance between the electrodes and the movement of the tool electrode were carefully kept at a play distance to get the most energy out of the

discharge. The play distance has a finite value and does hamper the discharge, as described by the V-I characteristics in the following sections. By putting mini/micro dampers on the tool, the play distance was expected to be cut down.

### **4.3 Observations**

The experiments were conducted systemically, and all the observations were noted carefully. The following sections discuss the explanation and science behind the occurrences of all response outputs. The entire process itself adequately explained and validated the EDM. In the process, metal was removed from the harder work-piece (CP-TI) without any physical contact with the tool (brass), which is a comparatively soft material. In order to illustrate the procedure, the voltage-current plot of Maglev EDM was described and contrasted with the die sink EDM machine currently in use. In addition, the material removal rate was analyzed and compared with the existing literature. The specific energy of the machining is a measure of proficiency. Low specific energy shows high machining efficiency. The specific energy of the machining was calculated for the maglev EDM and compared with the existing literature, which showed that the specific energy is minimum in maglev EDM for CPTI. The other critical response in EDM process is surface roughness. The following sections provide insights into the capabilities and proficiency of the Maglev EDM.

#### **4.3.1 Discharge voltage-current characteristics**

The discharge voltage and current characteristics play a crucial role in forming the required appropriate spark between the electrodes. The discharge energy

of EDM process can be given by the following eq. 4.1 as the product of current, voltage and pulse time. Mathematically,

$$DischargeEnergy = V \times I \times T \quad (4.1)$$

Where: V= Voltage (Volt) , I = Current (Ampere) and T= time ( $\mu$ s).

In general, during EDM, there can be five different types/conditions of pulses, as shown in figure 4.1. These all are based on the input process variables. In the first type, open voltage is the condition where the voltage is maximum, and the current is minimum. This circumstance is an ideal condition in which there is no removal of work material. The following condition is that spark or normal spark conditions have sufficient capability to perform proper machining that utilizes high current amplitudes between electrodes.

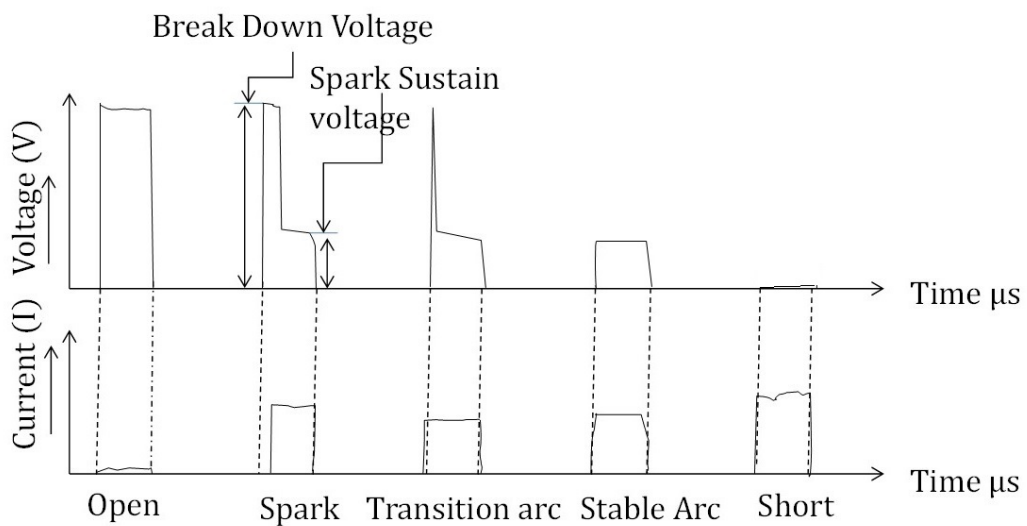


Figure 4.1: The five different possible EDM conditions [114]

The usual spark provides the proper delay for the breakdown and recovery



of the dielectric strength of the liquid medium for the next pulse. The transition arc or stable arc is a common phenomenon except that the stable arc has no high-frequency component as in a transition arc. However, the stable arc differs from the normal discharge and has a weak high frequency signal compared to normal discharge. In the last possible phenomenon, short-circuiting is the state where the gap voltage is almost zero, and the current amplitude is the highest. Short-circuiting occurs for various reasons, such as debris that are formed between electrode gaps, shallow electrode gaps, or physical contact of electrodes[114]. Short-circuiting affects the process stability and leads to a lower MRR with a poor machined surface. Further investigation of the voltage-current waveform found that arcing is another harmful phenomenon for the quality of the surface in EDM and micro EDM. The arcing results from the uncontrolled thermal energy transformation during the process. Arcing is the successful discharge of current before attaining the open-circuit voltage, which results in repetitive discharge at the same location[115]. During arcing, the current flows in the same plasma without recharging the capacitor and recovering the dielectric strength of the previous discharge[116]. Experiments were carried out on a standard die sink EDM to explain the conditions above. (SPARKONIX ZNC/ENC35). Fig 4.2 shows the voltage-current characteristics recorded during conventional EDM. The plot shows arcing, short circuit, ionization, and normal discharge during conventional EDM.

In the study of waveforms, it is observed that an ignition delay occurs as the

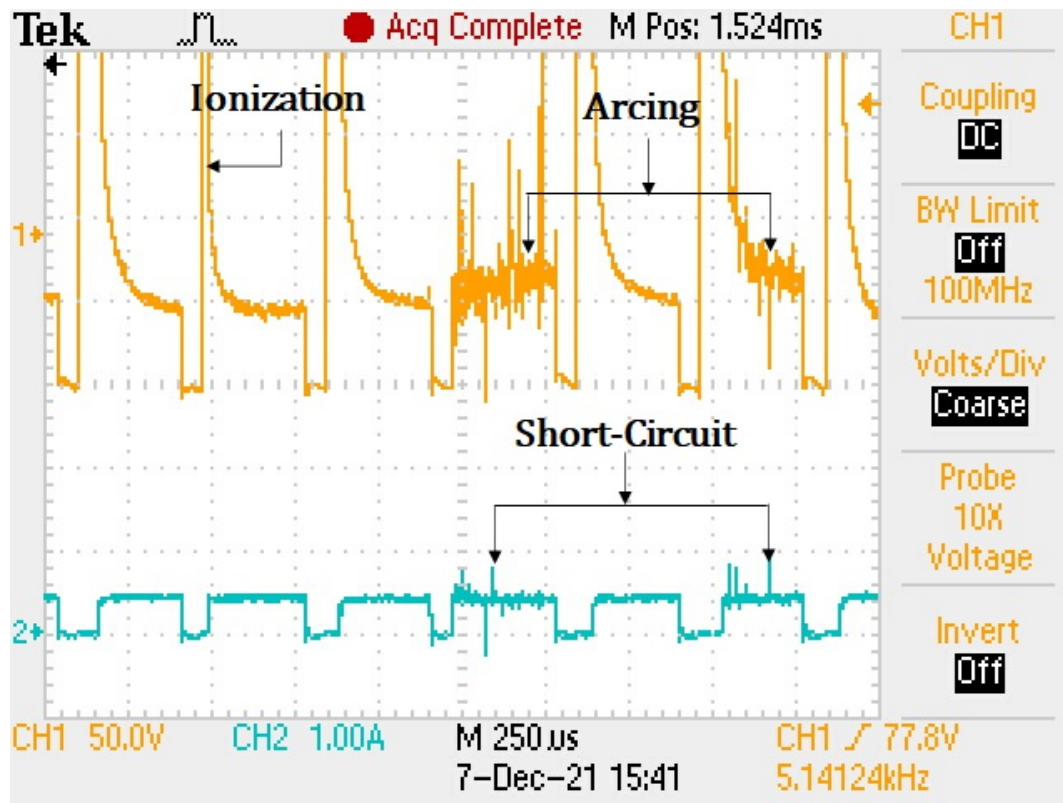


Figure 4.2: Illustration of the discharge waveform of conventional EDM

voltage is applied between the electrodes, and the dielectric does not break down immediately, which results in a slight static time lag. Therefore, the researcher investigated the spreading of the ignition delay and determined that discharge occurred after the activation time[117]. The discharge interval must be long enough to generate and recover suitable plasma and dielectric strength respectively, to achieve a stable spark. However, it has been reported that an interval that is too long leads to a low MRR. Hence, the precise control of electrode movement is the most essential, especially in micro EDM. In addition to the discharge interval, the plugging of debris in the electrode gap, the electrode geometry, and inappropriate input parameters affect the machining about arcing and short-circuiting (which is the most undesirable). Therefore, steady discharge energy is the prime require-

ment for micro EDMs. Hence, the attention and consideration of voltage-current wave-forms are the most important in the process.

In the present work, a digital storage oscilloscope (DSO) was used to observe the waveform of the discharge voltage and current. Fig4.3 a and b illustrate the discharge voltage and current wave-forms of the Maglev EDM. The waveforms clearly express that the discharge is stable throughout the process. Since the power supply is a pure DC power source, the  $T_{(off)}$  time is zero in the waveform. Fig4.3 a shows multiple pulses, which show a uniform discharge after each retraction of the tool. Fig 4.3 b shows two pulses in detail. No short circuit is shown in the waveform, which is nearly impossible in conventional EDM. Instead, an almost stable discharge with a negligible arcing at a few places is shown. The proper discharge without short-circuiting ensures a higher MRR in Maglev EDM. No ionization time is visible in the plot due to zero time in the process. This finding again supports a high energy supply and less non-productive time and enhances the MRR. Over all, the Maglev EDM proceeds continuously without any abruption, as occurred in conventional EDM, indicating the Maglev EDM's proficiency. The proposed MEDM is fabricated out of an invention of "Self-servo bipolar linear motor" This can be used in micro-EDM and macro EDM by varying it power. In some cases, it is used for nano EDM also [118].

Further, the EDM process is governed by either discharge voltage or discharge current. In The present work discharge voltage is set at pre-defined value. The interelectrode gap changes to attain the value of the set discharge voltage

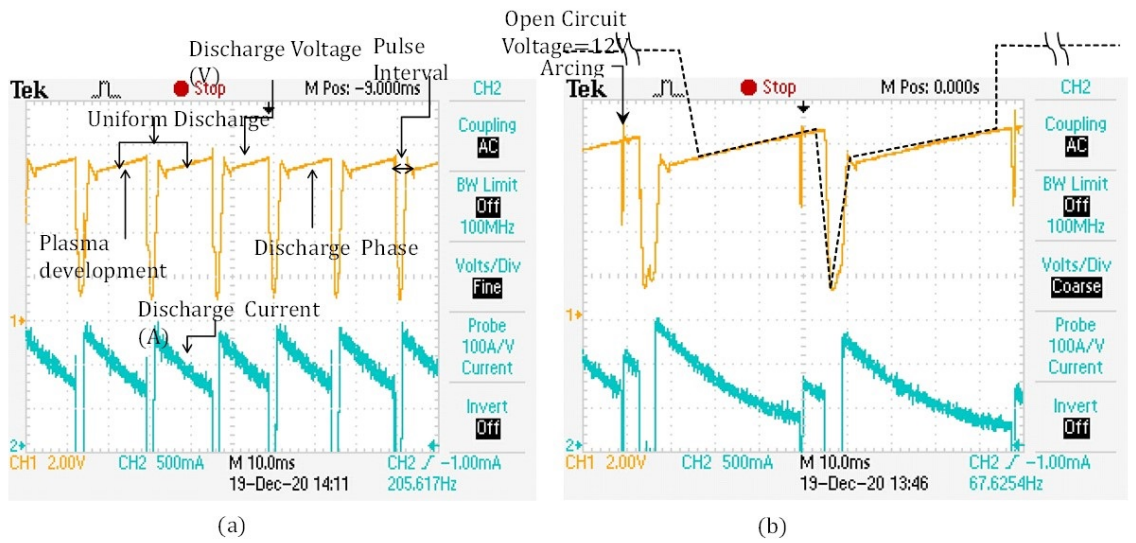


Figure 4.3: (a) Voltage and current characteristics showing stable and uniform discharge; (b) detailed pulse characteristics.

based on the dielectric material. Therefore, the target is discharging voltage and not the gap between the electrodes. Manual linear stages have been used in the current work and the workpiece is kept stationary. Since the EDM is a very low-MR process, a stationary workpiece is sufficient to characterise the process. Moreover, it is planned to use a motorised stage. However, it is not in the scope of the present work.

#### 4.3.2 Material removal rate (MRR)

The MRR and TWR are the most significant factors in the machining process that affect the manufacturing firms' productivity over time. The MRR is the weight difference of the workpiece before and after machining, divided by the machining time presented by Equation 1.1. Similarly, TWR is the difference in the weight of the tool before and after machining and divided by the machining time presented by Equation 1.2. The MRR is the key component to be considered

from the economic point of view of any machining operation. In the field of EDM, especially in the machining of hard to cut materials, MRR is always a prime concern for researchers.

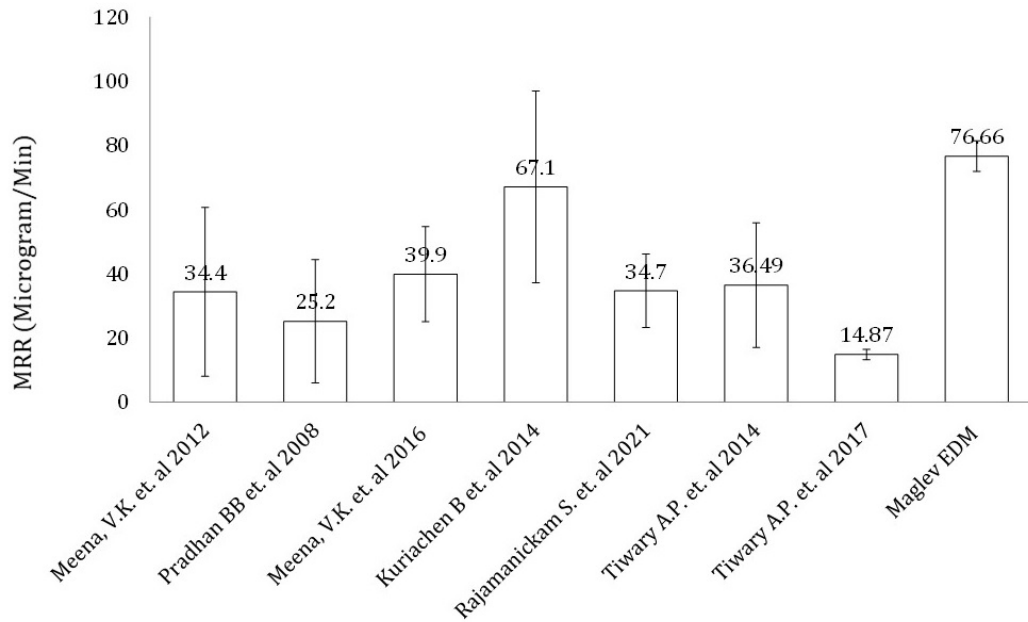


Figure 4.4: Comparison of the material removal rate between maglev EDM and the literature

Research continues to optimize this machining response from inspection to the present era. As per figure 4.4, many researchers have suggested that the tools and techniques enhance EDM from time to time. For example, the study by Meena et al. [119] calculated the MRR at an average of  $34.4 \text{ microgram}/\text{min}$  and concluded that the voltage is the most influential parameter among all of the parameters. The MRR observed by Pradhan et al. [120] was  $25.2 \text{ microgram}/\text{min}$ . They produced micro holes in titanium alloy and observed that the pulse on time is the most significant factor in MRR and that the peak current mainly affects the TWR in micro EDM. They attributed the peak current to a higher MRR

and high tool wear because of the monotonic increase in the high energy density. Later, Meena et al. confirmed that the current is the most promising factor among all of the parameters of micro EDM for higher MRR. They observed the MRR in the average range of 39.9microgram/min while machining commercially pure titanium. The MRR measured by Kuriachen et al.[121] was in the average range of 67.1microgram/min during the multi-response optimization technique. They used multi-objective particle swarm optimization and considered that the gap voltage influences the MRR in micro EDMs. Rajamanickam et al.[122] calculated the MRR in the average range of 34.7microgram/min. They used tap water as a dielectric medium with and without additives to compare conductive and nonconductive additives.

Tiwary et al.[123] observed the MRR in the 36.49microgram/min and concluded that the pulse on time, the peak current, and the gap voltage affect the range of MRR. During maglev EDM, the average measured material removal rate is 76.6microgram/min, which is significantly higher than that of other conventional EDMs for a similar range of discharge energy. In the current work, the maximum TWR was observed at 8.5microgram/min, the minimum TWR was noted at 2microgram/min, and the average TWR was found to be 10% of the MRR in Maglev EDM. The accumulation of eroded material on the tool electrode and the absence of pressure flushing are the most significant causes of the tool wear rate variation. The above results demonstrated the higher performance of Maglev EDM due to the availability of continuous discharge energy

with an external pulse of time compared to conventional EDM. In the current work, the values of MRR and TWR are observed in natural flushing, which can be additionally enhanced by employing a forced flushing system. Fig4.4 shows the Comparison of MRR attained by conventional EDM and Maglev EDM. The MRR is higher, showing the capability of Maglev EDM over other conventional EDM systems. The Maglev EDM shows a higher MRR because of the superior inter-electrode gap (IEG) control, which almost wholly removes harmful effects such as short-circuiting and arcing.

### 4.3.3 Specific energy in EDM

In the previous section, a higher MRR was achieved in Maglev EDMs as compared to the literature; however, a higher MRR could be due to the high energy supply. The comparison could be fairer if specific energy could be compared with the available literature. It could be helpful to explore a wide range of literature with different input process parameters. The specific energy is required to remove the unit amount of material from the workpiece. It is denoted by SE and refers to EDM as in other machining processes. Specific energy is another factor crucial to defining the machining productivity of any manufacturing firm. In EDM, the SE is defined by Equation 4.2

$$SE = \frac{DischargePower}{MRR} \quad (4.2)$$

Furthermore, here the discharge power can be evaluated in EDM as a product of the discharge voltage, current, and duty factor. During the Maglev EDM, the maximum MRR was achieved at approximately 82microgram/min, and the SE

ranged from approximately 30.76 to 35.21 J/g in three repetitions.

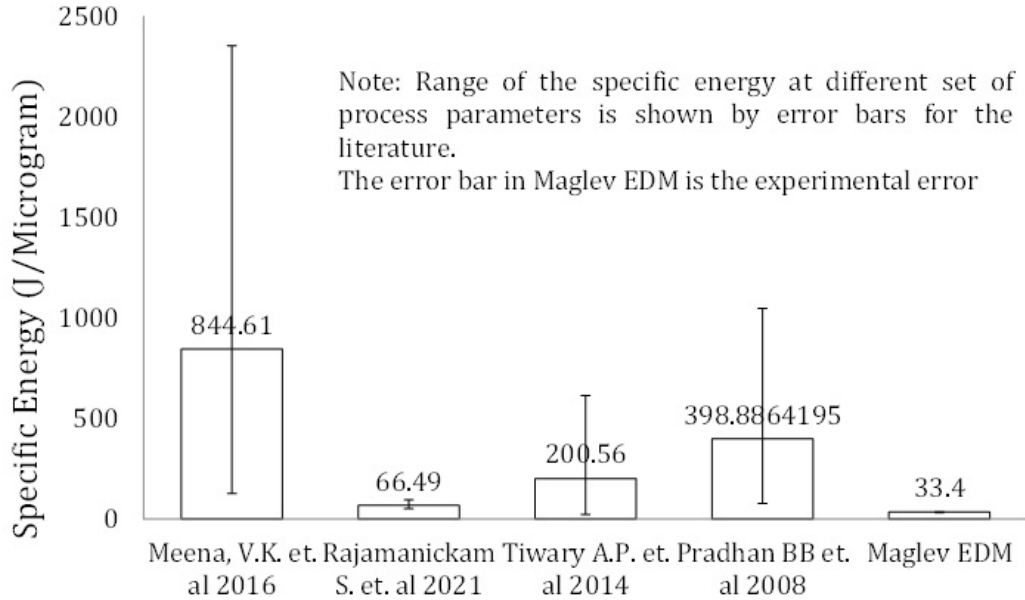


Figure 4.5: Comparison of the specific energy between the maglev EDM and the literature

This finding indicates that the current Maglev EDM utilizes low energy to erode the substantial material, which demonstrates the proficiency of the current Maglev EDM over conventional EDM. A proper IEG produces efficient specific energy (SE) by utilizing each power pulse during spark generation. The specific energy of past reported work with Maglev EDM has been studied and presented in figure 4.5. From the comparison plot, the specific energy is found to be lowest in the Maglev EDM for the same range of MRRs compared to the literature.

#### 4.3.4 Surface morphology and surface roughness

The quality of any machined surface can be demonstrated by the arbitrary range of craters and hills formed during the machining process. In EDM, the discrete discharge pulses are responsible for the quality of the surface. The ma-



ching parameters significantly affect surface roughness, resulting in overlapping craters and hills. The surface quality in engineering applications is an important constraint, such as in the mould and die manufacturing industries[124]. The recast layer is one of the downsides of EDM and is a prime issue to be considered in the enhancement of surface quality[125]. The recast layer is one of the downsides of EDM and is a prime issue to be considered in the enhancement of surface quality [87]. The recast layer was developed by the lack of appropriate elimination of melted material and re-solidification, similar to quenching phenomena [126]. Therefore, the recast layer is closely associated with the pulse duration. The long pulse duration can reduce the thickness of the recast layer to a great extent.

Furthermore, the recast layer's thickness depends on the dielectric type, as a study reported that kerosene dielectric form a thinner layer compared to other dielectric media[127]. The long pulse releases more energy to enhance the effect of the dielectric force and reduce the thickness of the layer further[128]. In addition, it has been seen that the surface roughness values of the machined component are increased at higher currents and during longer pulse duration[129]. Since the discharge energy is associated with the melting and vaporization of the work-piece material, with high discharge energy, larger craters are produced on the work surface, which deteriorates the quality of the surface [130][131][132]. In addition, in some instances, the process is further prolonged undesirably since the movement of the electrode tool toward the work-piece and the extended movement of the

tool result in short circuits during machining. This short circuit and arcing intensify the discharge energy at a high level, and high energy deteriorates the surface quality through uneven erosion of the work material and tool[14]. In the present Maglev EDM, the material is removed from the workpiece in circular cavities, as shown in figure 4.6. Under the recast layer, the heat penetration is prolonged on the machining surface, and a heated zone is formed, called a heat-affected zone (HAZ). Here, the surface morphology was detected by Zygo new view 9000 3D optical profilometer and an OLYMPUS BX51 M optical microscope. From the obtained images, the presence of the HAZ is evident, as shown in figure 4.6.

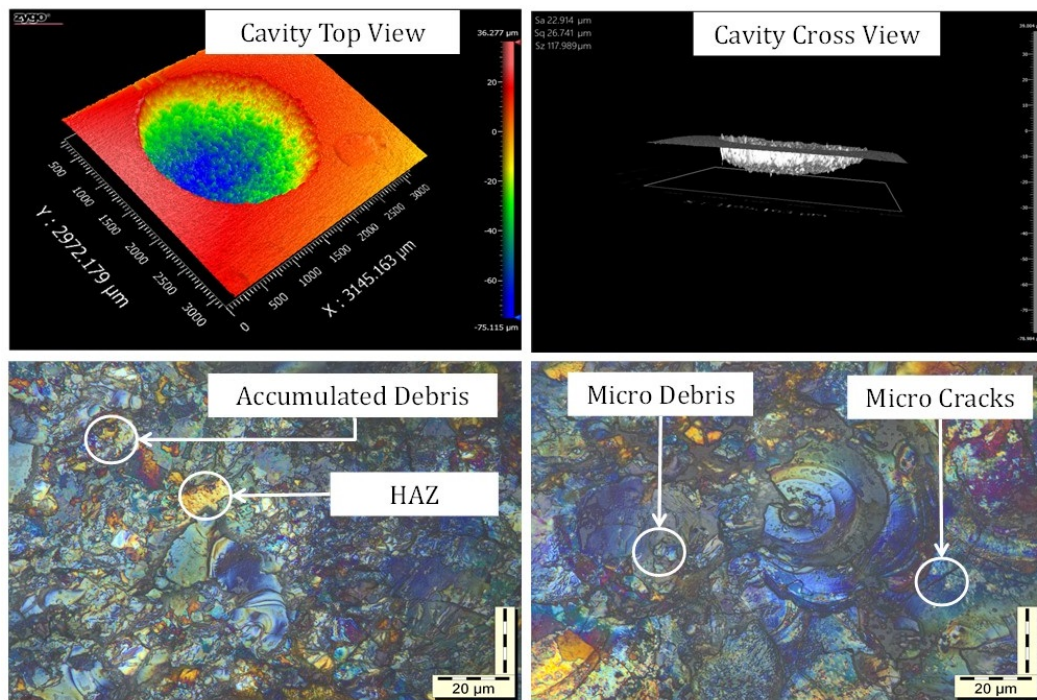


Figure 4.6: Optical microscope and profilometer images of surface morphology

During the EDM process, the temperature of the HAZ does not reach the melting point or vaporization stage. Hence, the heated material does not detach from the location, however, the properties of the micro-structure change.

Since the produced discharge energy is shared by each element of the process, namely, the workpiece, dielectric medium, and tool, a HAZ is formed in both electrodes[133]. More accurate results were obtained by re-tuning the machined surface using a profilometer, demonstrating the HAZ created during the construction of the appropriate 2 mm cavity. Furthermore, usage of natural flushing technique, in the current experiments, accumulated unwanted debris on the work-piece surface. The debris can be washed out or minimized by using forced pressure flushing and a fresh dielectric medium. During the Maglev EDM, some micro cracks are often seen in the work-piece surface of the thermal shocks and quenching of the newly machined surface. Since the specific energy density is predominantly influenced by the current-voltage characteristics and the gap state of the electrodes, the characterization of the surface morphology is more unstable.

In the present Maglev EDM, the waveforms and gap conditions were maintained to ensure a high surface finish with minimum loss of pulse discharge energy. In Maglev EDM, the primary value of the surface roughness varies from 3.08 to 5.17  $\mu\text{m}$ , and the average surface roughness is obtained at 4.085 $\mu\text{m}$ . In figure 4.7, the average surface roughness of the Maglev EDM is presented and compared with other micro EDM processes that have similar MRR ranges.

It has been observed that the range of the average surface roughness is lower in Maglev EDM compared with other conventional EDM. The average surface roughness in the current work was 4.3 $\mu\text{m}$ , which was slightly higher than the surface roughness obtained by Ahmed et al.[134], which was 3.67  $\mu\text{m}$ . They

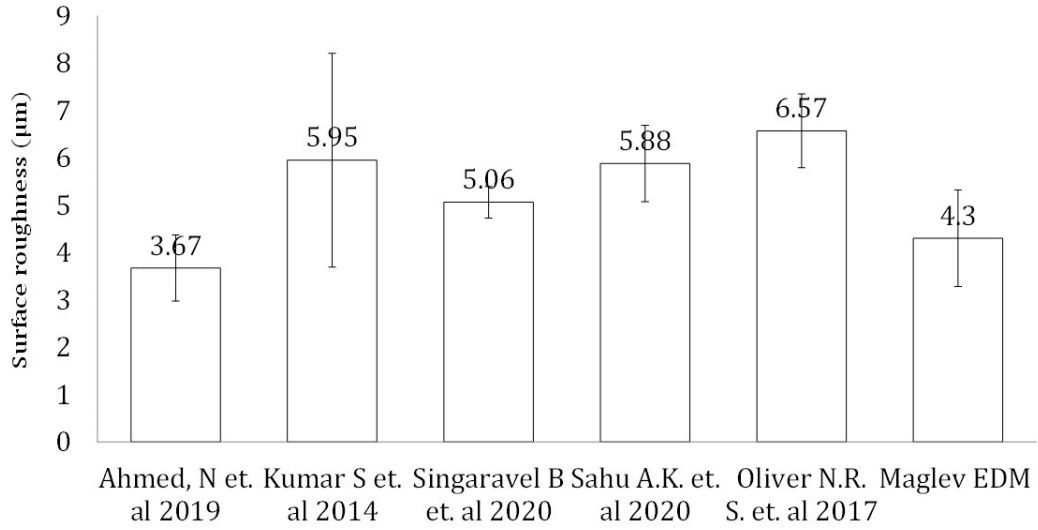


Figure 4.7: Comparison of the surface roughness

employed a forced flushing technique to carry out the debris and eroded metal particles, whereas natural flushing was applied in the current Maglev EDM case. However, other researchers have determined various surface roughness ranges, such as Kumar et al. [135] who obtained an average surface roughness in the range of  $5.95 \mu\text{m}$ . They used the hybrid Taguchi artificial neural network approach to predict the surface roughness under different conditions. The average surface roughness observed by Singaravel et al. [136] was  $5.06 \mu\text{m}$ . They tested and concluded that vegetable oil did not function as a dielectric medium in a few cases and enhanced the surface roughness compared to other dielectric media.

Sahu et al. [137] observed an average surface roughness in the range of  $5.88 \mu\text{m}$  during comparative experiments of various tools. The average surface roughness observed by Oliver et al. [138] was  $6.57 \mu\text{m}$ . The research that contributed to the field of EDM of hard-to-cut materials pointed out that the peak current

is the most significant parameter and leads to unwanted material removal during EDM. The pulse on time is the second factor that affects the surface roughness. Both parameters ultimately increase the specific energy density while machining and affect the mechanism of the material removal rate.

#### 4.4 Summary

The Maglev EDM is explored by experiments on the CPTI work-piece using the brass electrode. The results revealed that the proficiency of the Maglev EDM was higher than that of the conventional EDM. In addition, the material removal rate, specific energy, and surface morphology were studied as output responses and compared with the available literature. The following conclusions are drawn from the current work:

- MRR is higher in Maglev EDM than in conventional micro EDM due to the near-zero pulse of time. This relationship increases the desired discharge energy throughout a longer period.
- The IEG is precisely controlled and regulated by the maglev servo mechanism as per the requirement of the EDM. The spark gap is accurately maintained by the logical arrangement of the magnets using the Maglev lucidity and replacing them with a conventional servo mechanism.
- The short circuit is the prime concern in conventional micro EDM; short circuits deteriorate the surface quality and increase the Tool Wear Rate. At present, Maglev EDM has resolved such issues to a great extent.
- Maglev EDMs shows less specific energy than other conventional EDMs by replacing the conventional pulsed power supply and effectively utilizing maximum energy.

## CHAPTER 5

### FEASIBILITY ANALYSIS ON TITANIUM ALLOY WORK MATERIAL

Publication is under review<sup>1</sup>

#### 5.1 Introduction

The present chapter deals with the feasibility analysis of the proposed Maglev EDM (MEDM) through a series of experiments. The experiments were performed on the Ti-6Al-4V alloy with a tool made of soft brass (in comparison to Ti-6Al-4V) with a 2 mm diameter. Deionized water was used as a dielectric medium during the machining process. It is well known that titanium alloys, mainly Ti-6Al-4V, have wide application in the biomedical, aeronautical, and marine industries, as they have several excellent properties such as a high strength-to-weight ratio, high corrosive resistance, high wear resistance, and high strength at a higher temperature. Therefore, titanium is a suitable material to detect the feasibility of maglev EDM.

#### 5.2 Experimental method

A preliminary experiment was done, and the optimum initial electrode gap distance attained was  $\sim 1$  mm at 12 V open circuit voltage and 2 A peak current. The circular dimples were formed using three repetitions of 10 minutes and a 1 mm initial gap distance.

### 5.2.1 Discharge waveform

Various shapes of pulse have been revealed in studies, which are dependent upon the type of pulse generator applied during the EDM process. These pulses have exposed significant effect on MRR and surface roughness of the workpiece [139].

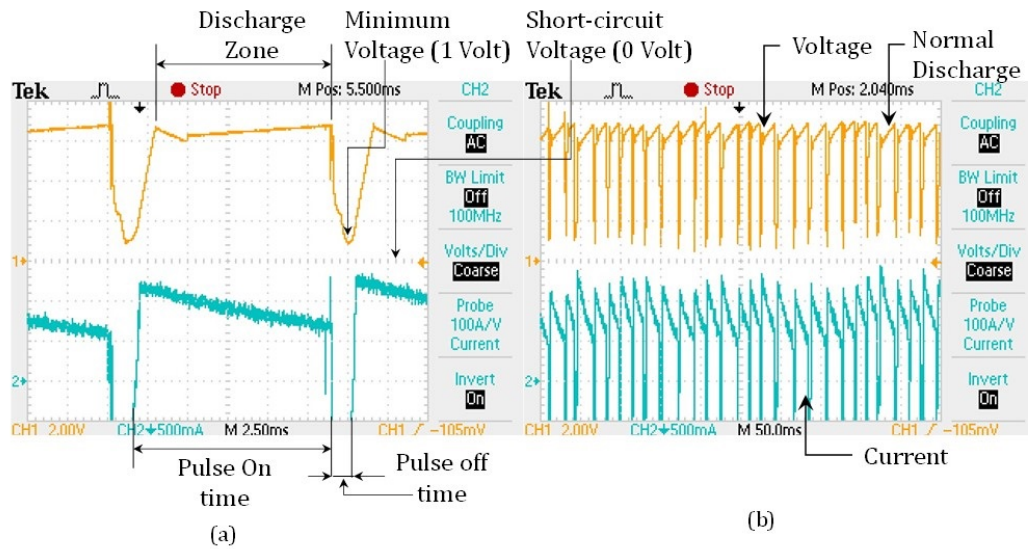


Figure 5.1: Discharge waveform of maglev EDM process (a) Single-pulse; (b) Multi-pulses

Therefore, pulse shape plays a crucial part in confirming that the newly developed maglev EDM works correctly in a continuous manner. The discharge waveform throughout maglev EDM process during single pulse and multiple pulses are shown in Fig 5.1 (a & b) respectively, which were taken on digital storage oscilloscope. Fig 5.1 (a & b) time vs. voltage and current graphs are shown. In this graph time is changing on X-axis, while voltage (yellow line) and current (blue line) are on Y-axis. From Fig 5.1a it is visible that the average discharge voltage and current are 6 volt and 1.2 Amp respectively. In maglev EDM short circuit is not obtained since the minimum voltage in the waveform is above

zero volt in fig 5.1 (a & b). Similarly, this figure is not showing open circuit voltage; it indicates no open circuit condition during the machining. Although it shows an instability for a fraction of a second in  $\sim 20$ -30 seconds, it may be due to the debris between the electrodes. Thus, stability during maglev EDM (without short circuit/open circuit) is higher than in the conventional EDM process (presence of short circuit). In figure 5.1 a, it is illustrated that the pulse width or pulse on time is very high as compared to pulse off time which results in ignition delay. Therefore, discharge energy from maglev EDM is very high compared to the conventional EDM method, since discharge energy is dependent upon pulse width. Resultantly, shorter ignition delay has produced higher discharge energy between the inter electrode gaps within the pulse duration. Therefore, larger volume of material is removed within a given amount of input power through maglev EDM. From discharge waveform in every chapter, it was observed that short circuit does not exist in maglev EDM mechanism, even with the usage of still dielectric. Therefore, higher duty cycle and continuous discharges were achieved. In Maglev EDM the duty cycle was achieved nearly 95%. Whereas it is quite difficult or nearly impossible to achieve the smooth waveform without short circuiting or arcing in conventional EDM process. Even the duty cycle usually observed in conventional EDM may be 50 to 70%.

In figure 5.1 b, the average discharge waveform is continuously observed without interruption. It is observed that during maglev EDM process, debris does not occur between inter electrode gaps, hence, stable discharge is achieved during



entire machining time. Further, the observed voltage-current plot of Maglev EDM with the time scale is presented in figure 5.1 a and b. It is observed that most of the voltage and current waves are stable and uniform. Only, the sudden downfall in the discharge voltage indicates the quick ionization without ignition delay which results in continuous EDM. In addition to the above the plot

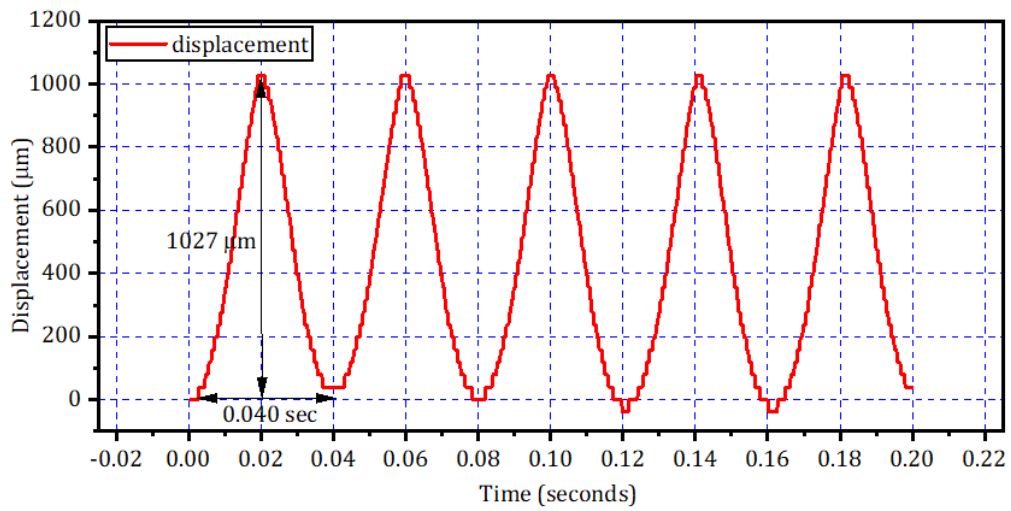


Figure 5.2: Positioning response of maglev EDM in terms of time displacement curve

[140]

of the time-electrode displacements were observed using a high-speed camera (FASTEC imaging, Model IL5LM4, USA, resolution SVGA 800 x 600, 12-bit CMOS sensor, shutter 3 μsec) during quick retraction and positioning. The time-electrode displacement curve for rapid positioning and retraction is presented in figure 5.2. The plot shows that for a unit mm positioning stroke, the machine accomplished a positioning resolution of nearly 10 μm. The initial interelectrode gap was set at 1 mm, and the maximum travel shown in figure 5.2 is 1000 μm. This additional 80 mm travel of the tool can be justified as the tool is returning to

its original set position; it crosses the initial set distance due to inertia. Further, the plot shows that the tool electrode is stable for microseconds on the topmost position for the stable gap condition before the forward stroke.

### **5.2.2 Predictive modeling**

In analytical approach researchers tried to develop a thermal model to predict MRR and surface roughness aimed at a single spark or pulse, then multiplied it with number of pulses to predict the final MRR and surface roughness. These approaches have taken various assumptions such as the size of plasma channel, crater size, temperature distribution and mode of heat transfer. Therefore, these models are validated through a specific, definite type of EDM process. In present modelling, dimensional analysis approach is taken through Buckingham's  $\pi$  theorem [141] and multi variable regression analysis[142] to find out values of power index and linear coefficient. Various researchers have done mathematical modelling of EDM process through dimensional analysis. These studies took discharge energy and workpiece material property during mathematical modelling. In actual practice, dielectric medium and tool material affects the MRR and average surface roughness (Ra) of EDM process, which has been observed in several studies [143] [144][145].

In present work, during dimensional analysis workpiece material properties such as melting point temperature, density and thermal conductivity were taken as non-variable by taking identical workpiece in modelling. These workpiece materials' values were included in the value of linear coefficient and power index

constant of Buckingham's  $\pi$  theorem. It is understood by the previous studies [144][145] that MRR and Ra are influenced by the energy density of plasma (dependent upon tool material characteristics which  $A$  and  $\sigma$  represent), the dielectric medium (represented by  $D_s$  and  $\alpha$ ); and the EDM machining condition parameters (represented by  $T_{on}, I_d, V_d, P$  and  $D_f$ ). These symbols have the usual meaning, which is given below in Table 5.1. From these parameters, a complete dimensionally independent (CDI) subset or repeating variables were selected to form a group of the dependent variable and other independent variables as non-dimensional  $\pi$ .

Table 5.1: Dimensions of parameters applied on dimensional analysis

Parameter Category	Parameter	Symbol	Dimension (MKSA)
CDI Subset	Discharge Time	$T_{on}$	T
	Surface Area of tool	$A$	L <sup>2</sup>
	Discharge voltage	$V_d$	ML <sup>2</sup> T <sup>-3</sup> I <sup>-1</sup>
	Flushing pressure	$P$	ML <sup>-1</sup> T <sup>-2</sup>
Independent term	Discharge current	$I_d$	I
	Duty factor	$D_f$	-
	Thermal diffusivity	$\alpha$	M <sup>-1</sup> L <sup>-3</sup> T <sup>3</sup> I <sup>2</sup>
	Dielectric strength	$D_s$	MLT <sup>-3</sup> I <sup>-1</sup>
	Tool electrical conductivity	$\sigma$	M <sup>-1</sup> L <sup>-3</sup> T <sup>3</sup> I <sup>-2</sup>
Dependent term	Material removal Rate	$M_r$	MT <sup>-1</sup>
	Surface roughness	$R_a$	L

The four parameters  $T_{on}, A, V_d,$  and  $P$  are selected as CDI subset and remaining 5 independent parameter are selected to form non dimensional  $\pi$  parameter indicated below in Table 5.1. The MRR and Ra can be expressed in a relationship as follows-

$$M_r = f(T_{on} \times I_d \times V_d \times P \times D_f \times A \times \sigma \times D_s \times \alpha) \quad (5.1)$$

$$R_a = f(T_{on} \times I_d \times V_d \times P \times D_f \times A \times \sigma \times D_s \times \alpha) \quad (5.2)$$

From equation 5.1 and equation 5.2, it is evident that both the dimensionless

homogeneous equations have ten variables with four fundamental dimensionless coefficients, therefore according to Buckingham's theorem [146] the solution can be given in the form of a product of six independent dimensionless  $\pi$  equations.

By applying Buckingham's theorem each dimensional term can be stated as shown in equation 5.3, 5.4, 5.4, 5.5, 5.6, 5.7, and,5.8.

$$\pi = f(T_{on}^{a1} A^{b1} V_d^{c1} P^{d1} M_r) \quad (5.3)$$

$$\pi = f(T_{on}^{a2} A^{b2} V_d^{c2} P^{d2} R_a) \quad (5.4)$$

$$\pi = f(T_{on}^{a3} A^{b3} V_d^{c3} P^{d3} I_d) \quad (5.5)$$

$$\pi = f(T_{on}^{a4} A^{b4} V_d^{c4} P^{d4} D_f) \quad (5.6)$$

$$\pi = f(T_{on}^{a5} A^{b5} V_d^{c5} P^{d5} \alpha) \quad (5.7)$$

$$\pi = f(T_{on}^{a6} A^{b6} V_d^{c6} P^{d6} D_s) \quad (5.8)$$

By solving the above equations as per Buckingham's  $\pi$  theorem [141] and replacing dimensionless parameters  $\pi$ s, equations can be rewritten as follows equation 5.9 and 5.10.

$$f\left(\frac{M_r}{T_{on} A^{0.5} P}, \frac{I_d T_{on} V_d}{A^{1.5} P}, D_f, \frac{D_s A^{0.5}}{V}, \frac{\sigma T_{on} V^2}{P}\right) = 0 \quad (5.9)$$

$$f\left(\frac{R_a}{T_{on} A^{0.5} P}, \frac{I_d T_{on} V_d}{A^{1.5} P}, D_f, \frac{D_s A^{0.5}}{V}, \frac{\sigma T_{on} V^2}{P}\right) = 0 \quad (5.10)$$

Applying power law to evaluate the eq. (5.9) and (5.10) give

$$\frac{M_r}{T_{on} A^{0.5} P} = K_1 \left(\frac{I_d T_{on} V_d}{A^{1.5} P}\right)^{v^{(1)}} D_F^{w^{(1)}} \left(\frac{\alpha T_{on} n}{A}\right)^{x^{(1)}} \left(\frac{D_s A^{(0.5)}}{V}\right)^{y^{(1)}} \left(\frac{\sigma T_{on} n}{P}\right)^{z^{(1)}} \quad (5.11)$$

$$\frac{R_a}{A^{0.5}} = K_2 \left( \frac{I_d T_{on} V_d}{A^{1.5} P} \right)^{v_2} D_F^{w_2} \left( \frac{\alpha T_{on}}{A} \right)^{x^{(2)}} \left( \frac{D_s A^{(0.5)}}{V} \right)^{y_2} \left( \frac{\sigma T_{on}}{P} \right)^{z_2} \quad (5.12)$$

In the above expression, equations 5.11 and 5.12 are the final equations from which prediction of MRR and Ra is achievable after finding the values of linear coefficients and power indexes of both equations.

To find the values of constants ( $K_1, K_2, v_1, v_2, w_1, w_2, x_1, x_2, y_1, y_2, z_1$ , and,  $z_2$ ) multi-variable regression analysis [142] is applied with the help of experimental values of previous published results. It is observed from various predictive models that; they were simply applying experimental values of their own EDM setup [147–149]. The predictive models were not feasible for other EDM setup since the servo mechanism or control mechanism changed during every setup. Therefore, in current predictive modelling, experimental results of different EDM setups were considered. The following table 5.2 shows the experimental values of previously published works [150–154] which were applied in multi variable regression analysis. Identical units were taken throughout the parameters to find the values of linear coefficients and power indexes. In general the noise is a part of the EDM process, but it does not affect the output parameters such as MRR, or surface roughness. Hence the present study did not consider noise for mathematical modeling. In mathematical modeling, the key factors which affect the output parameters were considered and some were neglected due to their relative insignificance.

Table 5.2: Parameters and their values applied to develop mathematical model

Parameter	[150]	[151]	[152]	[153]	[154]
Discharge Time (min)	3.33E-06	8.33E-07	0.000005	1.08E-06	2.50E-06
Surface Area of tool (mm <sup>2</sup> )	78.57	78.57	78.57	154	50.29
Discharge voltage (V)	200	20	25	115	75
Flushing pressure (Kgf/mm <sup>2</sup> )	0.005	0.00005	0.021414	0.005	0.0153
Discharge current (Amp)	20	20	10	20	6
Duty factor	0.3	0.5	0.85	0.6435	0.03
Thermal diffusivity (mm <sup>2</sup> /min)	5.34	8.58	4.428	4.428	4.428
Dielectric strength (V/mm)	18000000	80000000	4700000	4700000	4700000
Material removal Rate (Kg/min)	2.24E-05	2.98E-05	2.37E-05	3.04E-05	2.64E-06
Surface roughness(mm)	4.49E-03	2.65E-03	6.88E-03	5.38E-03	7.39E-03

### 5.3 Results and discussion

#### 5.3.1 Model validation and prediction

By multi variable regression analysis, values of linear coefficients and power indexes are found; hence equation 5.11 and 5.12 are established as follows.

$$M_r = 5.585E - 10(T_{on}A^{0.5}P) \left( \frac{I_d T_{on} V_d}{A^{1.5} P} \right)^{1.0614} \cdot D_F^{0.3123} \left( \frac{\alpha T_{on}}{A} \right)^{-1.6954} \left( \frac{D_s A^{(0.5)}}{V} \right)^{0.8303} \left( \frac{\sigma T_{on} V^2}{P} \right)^{-0.3235} \quad (5.13)$$

$$R_a = 14.289A^{0.5} \left( \frac{I_d T_{on} V_d}{A^{1.5} P} \right)^{0.1914} D_F^{0.0067} \left( \frac{\alpha T_{on}}{A} \right)^{0.1556} \cdot \left( \frac{D_s A^{(0.5)}}{V} \right)^{-0.2394} \left( \frac{\sigma T_{on} V^2}{P} \right)^{-0.2483} \quad (5.14)$$

The above equation 5.13 and 5.14 are the concluding equations of mathematical modeling, which were obtained with the help of the Buckingham theorem and multivariable regression analysis. This model is unique from earlier, since it includes experimental values of different experimental setup to facilitate the diversity of the EDM setup. This model includes properties that were not taken in the previous modeling and that affected the MRR and Ra with great extent.

The following formula calculates the experimental MRR of maglev.

This model includes properties that were not taken in the previous modeling, and they affect the MRR and Ra to a great extent. The following formula calculates the experimental MRR of Maglev EDM.

$$ExperimentalMRR = \frac{Finalweightofworkpiece - initialweightofworkpiece}{Machiningtime} \quad (5.15)$$

Prediction results of MRR and Ra excellently matched with the experimental

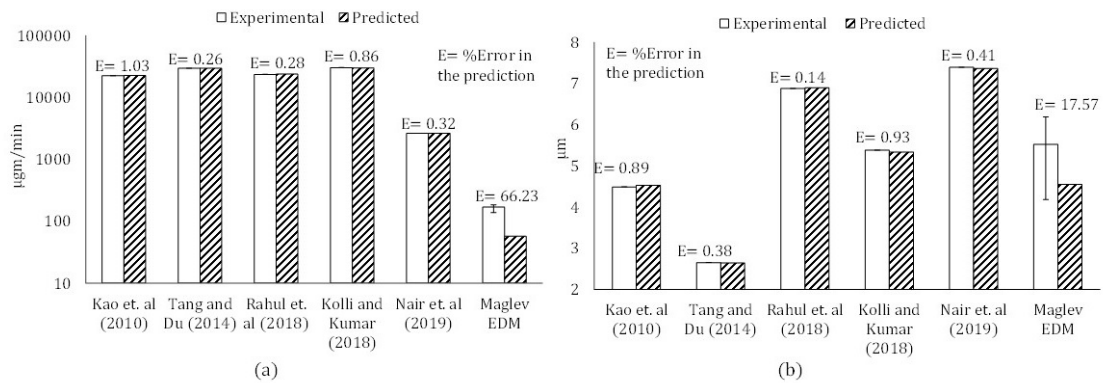


Figure 5.3: Experimental vs. Predicted result during different EDM process (a) MRR; (b) Average surface roughness

results of EDM setup which were taken into consideration during calculation of constant of model. Although, prediction results were not matched with maglev EDM setup results, a difference in prediction and experimental results of maglev EDM setup was observed. The reason for not including the maglev EDM experimental result is to compare it to the conventional EDM method and see how it differs.

Thus, evaluation of maglev EDM setup from other conventional EDM setup

can be achieved. Fig 5.3 a & b shows the experimental vs. predicted value of MRR and Ra, respectively. It is observed from fig 5.3 a that the experimental and predicted value of MRR is maximum during Kolli and Kumar[153] experimental setup while minimum in maglev EDM. Here the critical factor is discharge voltage and current, which is minimum during maglev EDM process. Additionally, several other parameters also affect the MRR and Ra. Since maximum discharge voltage and current were given during Kao et al. experiment, nevertheless, maximum MRR and Ra was not observed during their experimental setup. These parameters are duty cycle, pulse on time, dielectric medium, plasma density and tool electrode material which were included in present mathematical modeling. During the maglev EDM process the MRR was increased by 66.23% which was higher than the predicted results. This shows that maglev technology is better than the expected result in MRR. Experimental Ra in machined surface of maglev EDM is obtained from profilometer Zygo new view 9000 and it is explained below in next section; characterization of surface morphology. From figure 5.3 b, it is observed that experimental value of maglev EDM were varying higher than predicted value. Minor variation in Ra within predicted and experimental results can be concluded as the effect of deviation in quenching rate, which was not included in mathematical modelling.

Moreover, during maglev EDM process MRR result (66.23%) was increased higher than Ra (38.1%) result. Average % error observed in prediction of MRR and Ra was a mere, less than 1% in EDM setup, which was included during math-



emathical modelling. Hence, excellent prediction results were achieved through mathematical modelling. It is a general trend that increment in MRR will increase Ra. Although, by observing figure 5.3 a & b, it can be concluded that the general trend is wrong and MRR is not directly proportional to Ra of the material. There are certainly other factors on which Ra and MRR of material depends such as tool material, dielectric medium, quenching rate and energy density of plasma. In the maglev EDM process, small tool diameter was used and energy density of plasma is too high as mentioned in figure 5.3 b. As a result, Plasma energy density and specific energy during maglev EDM is maximum, accordingly, highest % error in prediction is obtained during Ra. Therefore, it can be concluded from mathematical modelling that MRR in maglev EDM is achieved more than the expected or predicted result, without ample increment in Ra of workpiece material.

### **5.3.2 Characterization of surface morphology**

The 3D machined surface on maglev EDM is characterized and analyzed using optical profilometer Zygo new view 9000. Fig 5.4 a & b depicts the three-dimensional surface topography taken on it. In this figure, height of the lump and depression on machined surface can be seen. In figure 5.4 a, it can be observed that the diameter of material removed from the machined surface was approximately 2 mm. From figure 5.4 a, it can be concluded that the value of over cut is relatively low during maglev EDM process. In maglev EDM process, continuous sparking phenomenon removes material to form craters and these craters play a crucial role in elaborating on surface topography.

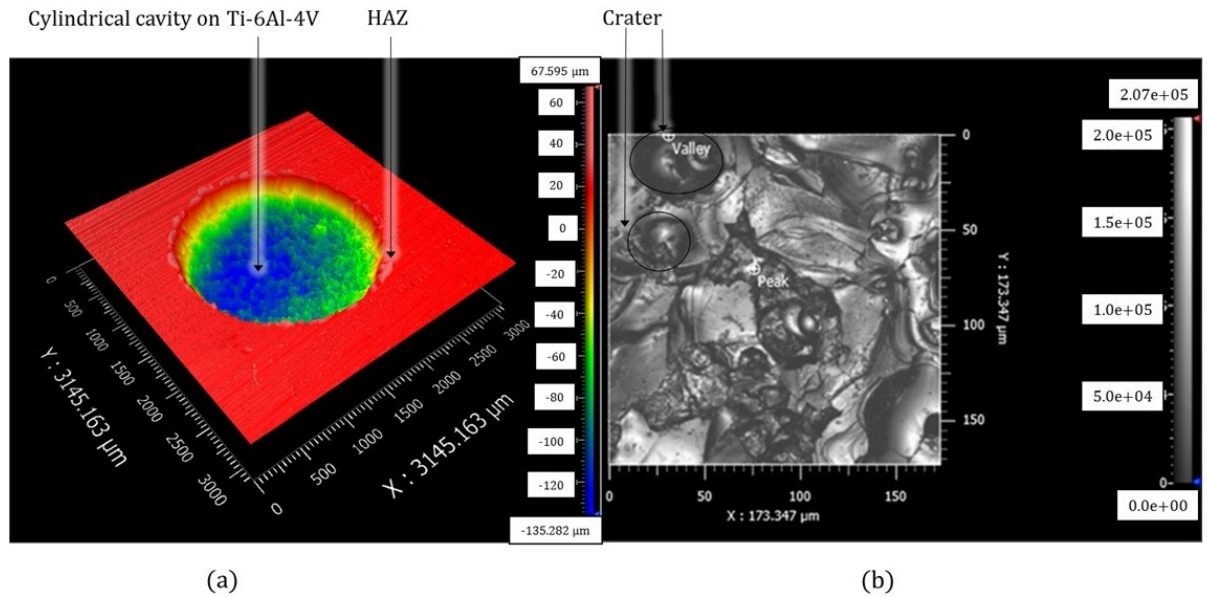


Figure 5.4: Surface morphology during maglev EDM (a) 3D profile map of whole texture; (b) 3D profile map of machined surface

It is clear from figure 5.4 a & b maximum height of the machined surface can be observed at approximately 250  $\mu\text{m}$ . In figure 5.4 b the highest valley and peak is  $173.347 \times 173.347 \mu\text{m}^2$  area and approximately micron size semi-spherical shapes craters are achieved through the maglev EDM process. Fig 5.5 shows the machined surface 2D profiles with different scale taken from the optical microscope Olympus BX-52 and Zeiss field emission scanning electron microscope (FESEM). Fig 5.5 b shows the image captured by the optical microscope and Fig 8(c) shows the FESEM image of the inside area within the machined surface. During maglev EDM process, de-ionized water was filled inside the workpiece holder. Combination of still water with concentrated discharge energy produced oxides layer on the upper surface of the workpiece. Fig 5.5 b & c show long micro cracks, micro pores, material accumulation and metal globules. The difference of contraction stress within surface surpasses the material's ultimate tensile stress.

Therefore, long micro cracks are formed.

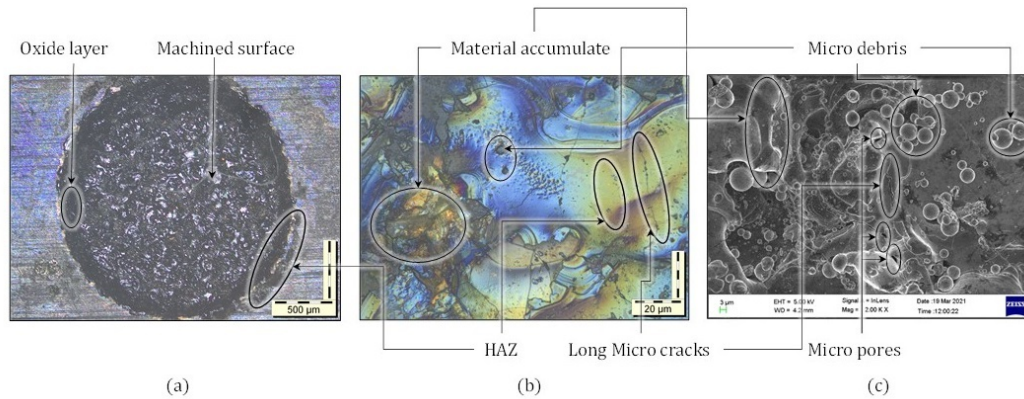


Figure 5.5: Surface morphology during maglev EDM (a) 2D profile of whole dimple (b) 2D profile with 20  $\mu\text{m}$  scale of maglev EDM taken from microscope (c) 2D profile with 3  $\mu\text{m}$  scale of maglev EDM taken from FESEM

It can be observed from surface morphology revealed in figure 5.5 b & c that the surface irregularities and color change with an increase in discharge power. Heat affected zone (HAZ) can be seen in figure 5.5 a & b, since Ti-6Al-4V has low thermal conductivity and the surface layer is heated up during these EDM process, however, the material is not removed. Therefore, from figure 5.5 c, it can be inferred that too much micro-debris are collected on machined surface in spherical nodules. Since, the quantity of micro size debris was excessive in maglev EDM, still deionized water was used. Therefore, debris of micron size were not removed from machined surface, while debris of macro size were removed by the oscillatory motion of the tool electrode.

figure 5.6 is plotted with the help of the optical profilometer Zygo new view 9000 and as per the ISO 4288-1997 standards, to measure the Ra between 2 -10  $\mu\text{m}$ , the sampling length should be between 2.5-12.5 mm. Although, machining

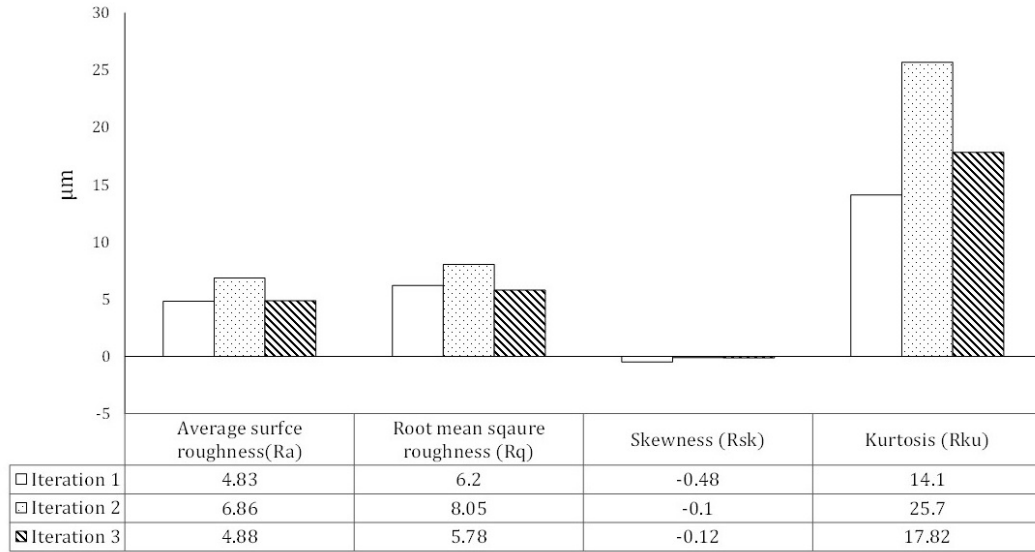


Figure 5.6: Roughness values observed on machined surface during maglev EDM by Optical profilometer

is achieved by 2 mm diameter tool, four slices of 2 mm length were made in machined area to measure the average value in iteration one, two and three. Filter was applied from 0 to 1 mm to measure the surface profile without form.

In figure 5.6 root mean square roughness (Rq), skewness (Rsk), Ra and Kurtosis (Rku) of the machined area is shown. Ra signifies the average deviation of asperities roughness from mean line throughout sampling length. Maximum Ra is observed in iteration two since the MRR is higher in it than the other two. Moreover, an additional reason of high Ra in iteration two in comparison to iteration one and three is high pulse on time. It has been reported that the higher pulse on time crater size is unavoidably larger [155], it results in higher Ra of workpiece. Rq shows the standard deviation of distribution of surface heights and maximum Rq is observed in iteration three than in iteration two. It displays that surface heights of machined surface during iteration three is more

randomly distributed. The skewness of a profile shows the profile's balance about the mean line, which means if several peaks and valley are equal, then it will show zero skewness. So a positive skewness value shows high peaks and negative skewness shows deep scratches or more valleys. During maglev EDM in all three iterations, negative skewness is detected. Therefore, it can be concluded that maglev EDM is constructing the craters and removing asperities, which existed before the machining workpiece surface. The present maglev EDM mechanism phenomena displays a perfect characteristic of EDM process. Moreover, minimum skewness value is observed in iteration two and maximum in iteration one, this value validates that the surface roughness is minimum in iteration one and MRR is maximum in iteration two. Kurtosis value is the sharpness of the probability density of a profile. According to it, a value lower than three, signifies less number of high peaks and low valleys present in profile, while value more than three indicates higher number of high peaks and low valleys. During maglev EDM process, kurtosis value shows minimum number of high peak and low valley in iteration two, which approves a high MRR value during iteration two [156].

### **5.3.3 Evaluation of the specific Energy**

In present work, specific energy is termed as the minimum amount of energy (in Joule) required to remove a unit mass (in  $\mu\text{gm}$ ) of workpiece material (Ti-6Al-4V). Minimum specific energy value means higher MRR with less discharge power supply. Therefore, performance of different experimental setup is evaluated based on it. According to it, an experimental setup with minimum value of specific energy is best and vice versa. In this calculation, duty cycle is

included to exclude the amount of discharge power that is wasted during pulse off time. Five published research articles were referred along with the results of the

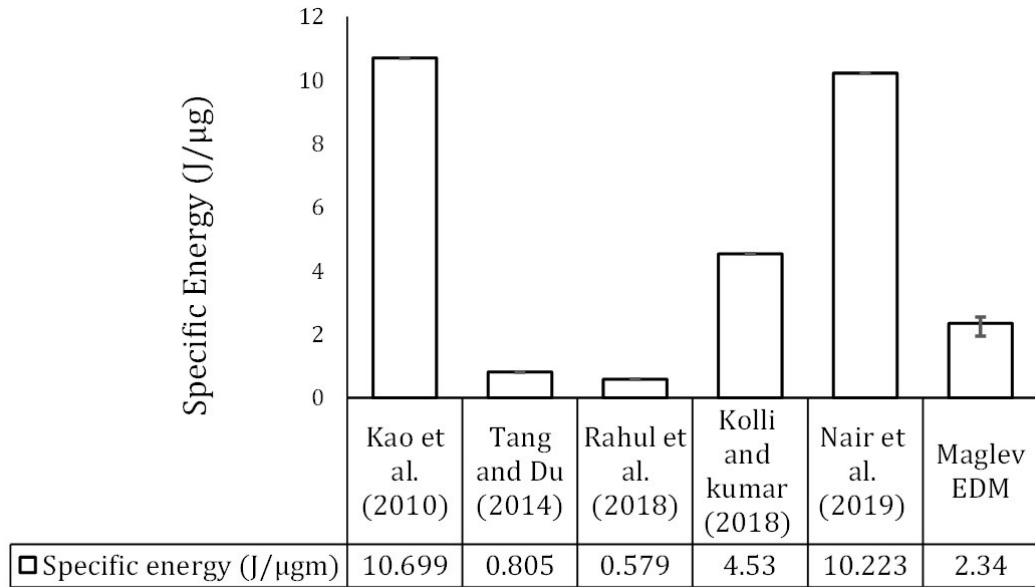


Figure 5.7: Specific energy comparison of different experimental setup [157]

maglev EDM to accomplish evaluation based on specific energy to remove material. The specific energy to remove the material from Ti-6Al-4V is calculated, and its assessment can be seen in figure 5.7. It shows Kao et al. EDM process, wherein the specific energy required to remove the material was approximately five times more than maglev EDM process. It can be observed that they have applied copper tool of 10 mm diameter with high amounts of input power. However, duty cycle, excessive voltage and dielectric medium (kerosene) increases the specific energy required to remove material. Moreover, excessive voltage develops arcing more than beneficial discharge pulses, which leads to the wastage of input power. Kerosene with higher amount of input power enhances the formation of carbide layer on upper surface, which results into an increment in the

wastage of discharge energy to remove it. In the assessment it was seen that Tang and Du EDM setup took less amount of specific energy than maglev EDM. They achieved it by optimized application of discharge voltage, current, dielectric medium (water) and duty cycle. However, the leading cause of difference between specific energy of reported work and maglev EDM is the excessive influence of tool material (copper vs. brass) and its diameter (10 vs. 2 mm) on the amount of plasma energy density. In assessment, it was observed that Rahul et al. applied cryogenically treated copper tool of 10 mm diameter with high flushing pressure. High flushing pressure reduced the occurrence of several short circuit and debris formation on the upper surface. Additionally, by cryogenic treatment of copper tool they improved electrical and thermal conductivity [152]. Subsequently, they achieved approximately five times less specific energy to remove material than maglev EDM. Kolli and Kumar have achieved highest MRR, however their specific energy was poor than maglev EDM. This condition arose because they applied excessive voltage and 14 mm diameter copper tool with EDM oil, producing excessive carbide layer and high plasma energy density. Additionally, pulse on time was very low, therefore excess arcs were produced than discharge pulses, which increased the wastage of input power. The duty cycle during Nair et al. experiment was the lowest (3%) which enhanced the wastage of input power. Moreover, instead of copper tool they applied a brass tool, with lower electrical conductivity, similar to the maglev EDM experiment.

In figure 5.7 it can be observed that Sisodiya et al. consumed more specific en-

ergy compared to other works. According to  $\lambda$ (thermal conductivity).  $\theta$ (melting point temperature) theory[158][159]machining through EDM process is low for the material which have high value of multiplication of  $\lambda$  &  $\theta$ .It was observed since CpTi is applied as workpiece material during Maglev EDM process and according to  $\lambda$ .  $\theta$  theory, CpTi has less machining capability during EDM process than Ti-6Al-4V alloy. Therefore, specific energy consumed in machining CpTi is higher than Ti-6Al-4V alloy. Additionally, CpTi has approximate double thermal conductivity than Ti-6Al-4V alloy, which allows heat to transfer through it more easily than Ti-6Al-4V alloy. Hence, material removal through melting and evaporation becomes difficult during machining of CPTI.The preceding comparison of specific energy consumption revealed significant differences from the reported work. So in one reported work, the author computed the actual energy and found that it is constant for multiple sets of parameters[160]. From above discussion it can be determined that the maglev EDM setup during machining Ti-6Al-4V alloy has shown comparably better specific energy as opposed to other EDM setups. Additionally, CpTi machining during Sisodiya et al[157] had higher specific energy due to the  $\lambda$ .  $\theta$  theory of EDM process. In the research stated in published articles, CNC EDM machines were used during experiments, whereas newly developed maglev EDM has no CNC control. When experimental parameters of experiments were compared, the reason for low specific energy was detected to be plasma energy density (tool electrode diameter), continuous flow of dielectric medium with pressure and copper electrode. It can thus be concluded that the cheaper maglev EDM setup can achieve better results than many other expensive



conventional EDM setup, if similar parameter of process are used, as it can work at higher duty cycle without short circuit throughout an extended period.

#### 5.3.4 Summary

The maglev EDM mechanism is developed to assist and drive the tool electrode to maintain the optimum electrode gap. Furthermore, the Maglev EDM control mechanism could reduce the possibility of irregular electric discharge, leading to enhanced machining efficiency. In this investigation, the stability of the maglev EDM was observed by the analysis of discharge waveforms, and the machining characteristics such as MRR and surface roughness parameters. The mathematical modelling was achieved with different experimental setup results to diminish the effect of similar servo mechanism. This study can be concluded as follows-

- The experimental results of discharge waveform, surface morphology and MRR validate that the maglev EDM mechanism can do a stable EDM process. The controlled spark between electrodes produces optimum amount of discharge energy to remove the material.
- From discharge waveform results it was observed that short circuit does not exist in maglev EDM mechanism, even with the usage of still dielectric. Therefore, higher duty cycle and continuous discharges were achieved as compared to conventional EDM process.
- Prediction error of MRR is higher than the prediction error in Ra since high plasma energy density is achieved during maglev EDM. A higher experimental result than prediction result of MRR shows that maglev EDM produces better results than expected without ample increment in Ra of Ti-6Al-4V alloy.
- It was observed from machined surface that during maglev EDM process, increase in pulse-on time causes enhancement in several craters and their

size, as a result MRR and Ra are increased.

- It is established from mathematical modeling prediction results that MRR and Ra have no direct relation with each other. Other factors include the amount of plasma energy density, tool material and dielectric medium, which have equivalent impact as discharge energy and workpiece material have on MRR and Ra.
- It was detected that static dielectric medium placed micro-debris on machined surface and macro-debris were removed by controlled oscillation of tool electrode.
- From the surface roughness parameters Ra, Rq, RSk and Rku, it is concluded that that maglev EDM control mechanism forms craters and remove asperities that existed on surface before the machining.
- Specific energy of material removal results have concluded that the maglev EDM generates excellent results as compared to various conventional EDM mechanisms. Therefore, the maglev EDM control mechanism can work as low cost sustainable manufacturing substitute for high cost conventional EDM machine.

## CHAPTER 6

### FEASIBILITY ANALYSIS ON INCONEL 625 WORK MATERIAL

(List of publications2)

#### 6.1 Introduction

This chapter deals with the feasibility analysis of the proposed Maglev EDM (MEDM) through a series of experiments. The workpiece and tool material for the experiment were Inconel 625 with a specimen size of 30 mm x 20 mm x 2 mm, and a cylindrical copper rod with a diameter of 3 mm and a length of 10 mm was used. The workpiece material was chosen because it falls into the difficult-to-cut category and presents research problems regarding machinability using traditional methods. Furthermore, the material has unique features such as good corrosion and wear resistance at high temperatures and pressures, making it popular in industrial applications [161].

The machining feasibility of maglev EDM was examined, and the findings were compared with those reported in the literature. The experimental results demonstrate that specific energy consumption (SEC), material removal rate (MRR), tool wear rate (TWR), and average surface roughness (Ra) were all within the ranges of reported work. The surface morphology, material migration, and diffusion phenomena were further examined using field emission scan-

ning electron microscopy (FESEM) and electron diffraction X-ray spectroscopy (EDX), respectively. The proposed technology might serve as an alternative to EDM's servo gap control.

## 6.2 Materials and Methods

### 6.2.1 Workpiece and tool material

The thermophysical characteristics of workpiece and tool materials, as well as their elemental composition and mechanical characteristics, have been highlighted in Tables 6.1 and 6.2. The dielectric medium utilized in the experiment was commercial grade EDM oil (specific gravity 0.753, kinematic viscosity (at 40 °C) 2–3 cSt, dielectric strength 45 KVA.

Table 6.1: Chemical constituents (% weight) and mechanical properties of Inconel 625 workpiece

Elemental composition	Ni	Cr	Mo	Ti	Fe	Mn	Nb+Ta	Si	C	Al	S
% Weight	58-71	19-23	08-10.	0.4	0.5	0.5	3.2-3.8	1	0.1	0.4	0.015
Mechanical properties											
Mass density	8.44 g/cm <sup>3</sup>										
Melting Point	1290-1350°C										
Elastic modulus	205.8 GPa										
Tensile strength	940 MPa										
Yield strength	430 MPa										
Hardness	88 (HC)										

Table 6.2: Thermo mechanical property of tool electrode (Copper) material

Thermo-physical Properties	Value
Composition	99.9% Cu
Density	8.904 g/cm <sup>3</sup>
Melting point	1083°C
Hardness	100 HB
Electrical resistivity	9 μΩ-cm

### 6.2.2 Experimental Procedure

Prior to machining, the tool and workpiece's cross-sections were polished on a disc polishing machine with emery polishing paper of grades 1500 and 1800. (Chennai Metco). After that, a velvet cloth with diamond paste is used to create a mirror-like finish. It is necessary for a clear view of the crater that has formed

on the machined surface. Pilot tests were used to identify the extremely low and high values of process parameters in terms of gap voltage, gap current, and duty factor. The machining is stable at a gap voltage of 6–8 V (no-load voltage 12 V) and a gap current of 400–500 mA, according to the results of pilot tests (peak current 1 A). The level of experimental condition for maglev EDM was determined based on the pilot experiment and is listed in Table 6.3 along with obtained output responses.

Table 6.3: The measured gap voltage, gap current and duty factor in four iterations during processing of Inconel 625

Open circuit voltage (V)	Discharge voltage (V)	Discharge current (A)	Duty factor	Machining time
12	7.12	0.47	0.9564	10 minutes
	6.8	0.45	0.9564	
	7.1	0.46	0.9564	
	7.15	0.48	0.9564	

In the current experimental work, the workpiece was connected to the positive terminal while the tool was connected to the negative terminal of the DC power supply. The workpiece is dipped in EDM oil and an open-circuit voltage of 12 V is applied by fixing the maximum peak current of 1 A across the load. The tool starts oscillating along the thrust direction to maintain the constant inter-electrode gap. The machining starts at a discharge voltage of 6.5–7.5 V and discharge current of 400–500 mA. During discharge, the electrical information in terms of the current-voltage waveform is captured in a digital storage oscilloscope (DSO) via a differential type current and voltage probe. This information was further used to calculate the discharge power and specific energy consumption rate of workpiece material. The material removal rate (MRR) and tool wear rate (TWR) was calculated using the weight reduction method i.e., by measuring the

difference between initial and final weight before and after the machining using a highly precise weighing machine (Mettler Toledo, accuracy one  $\mu\text{g}$ ). There were four trial experiments were carried out to observe the various readings. However, it was observed that to maintain the constant, the inter-electrode gap tool must be advanced, which is maintained with the help of driving voltage for the required adjustment in magnetic force. Sometimes, due to the mass inertia of the tool, the restoring force becomes larger than the repulsive force; hence, in order to maintain the constant inter-electrode gap, the tool realises some upward force in the Z direction. The upward force seems to be a thrust force.

### **6.3 Results and Discussions**

#### **6.3.1 Morphological characterization of the machined surface through FESEM**

The high-resolution field emission scanning electron microscopy (FESEM, SUPRA-55, ZEISS) was used to study and quantify the surface properties of the machined surface. Fig 6.1 shows the surface topography of the machined surface as a function of maglev EDM input parameters. Micro-holes, micro debris particles, micro globules, micro-pores, pinholes, lumps of debris particles, and other structures were observed on the machined surface, according to microscopic images. Micro-holes and pinholes may emerge as a result of trapped gas air bubbles in the melted material during solidification [162]. The reattachment of more than three irregular debris particles cause lumps of debris formation during solidification. Due to insufficient flushing or the mass density inertia property, certain debris particles were found perfectly spherical and stuck to the machined surface. Micro globules were named for the minuscule reattached spherical debris

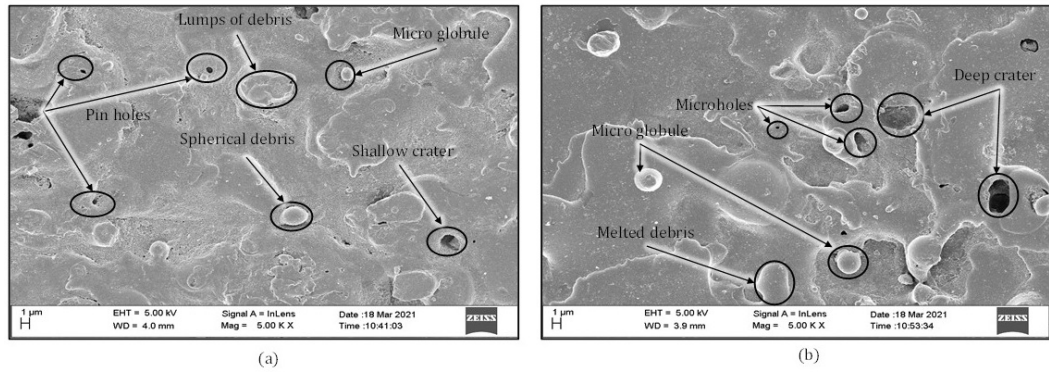


Figure 6.1: Surface topography/morphology analysis of machined workpiece parts through FESEM

particles. With an increase in discharge current value, the enrichment of micro holes, debris particles, micro globules, lumps of debris, micro-cracks, and so on increases. More craters and large debris will occur as thermal energy is derived from the discharge, potentially lowering the quality of the surface. In two iterations, the existence of the recast layer (white layer) at the edge surface is shown in figure 6.2 (a & b).

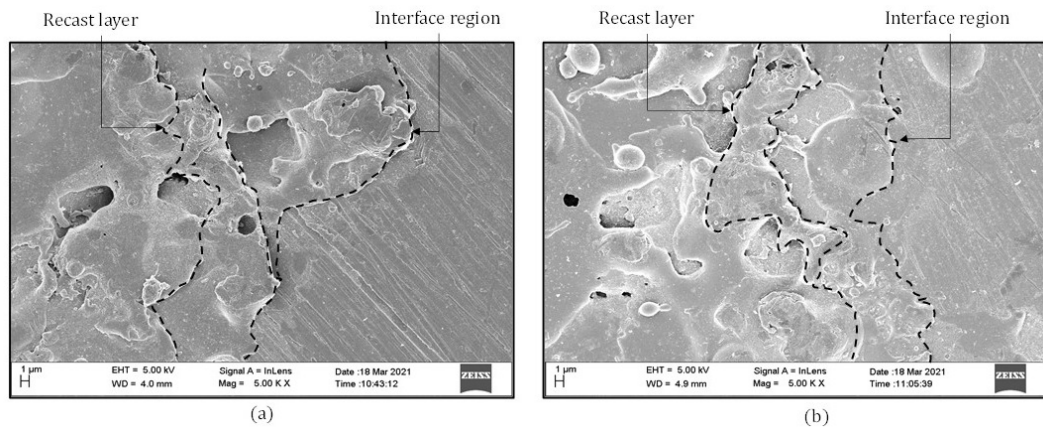


Figure 6.2: The re-solidified layer (recast layer) near the interface region of the machined surface

### 6.3.2 Material migration and diffusion analysis through EDX

Energy-dispersive X-ray spectroscopy was used to determine the elemental and chemical composition of the machined surface. It provides information about the availability of elemental peaks inside the material in terms of weight percentage or atomic percentage, at different positions of the machined product. The elemental peaks of the machined surface are shown in figure 6.3 as EDX spectra, while material migration and diffusion were depicted in figure 6.3b. Significant levels of nickel, ferrous, manganese, chromium, and copper suggest that most elements come from their compositional component. The fact that copper is available in a somewhat larger quantity implies that bidirectional material transfer and diffusion occur within the machined surface. The presence of carbon in a little bit higher quantity indicates that the carbon comes from the carbon stub (sample attached with it) and from the decomposition of hydrocarbon oil under high-temperature plasma. The presence of oxygen indicates that the surface gets oxidized, which may be due to the contact of atmospheric air. FESEM images were used to study the topography of the localized tool eroded part, and EDX was used to characterize the chemical composition. The EDX examination shows that nickel (0.66%) and hafnium (3.70%) are in significant concentrations on the tool's eroded surface. It means that there is bidirectional material movement and diffusion under the high-temperature plasma. A large amount of copper (68.31%) in the spectrum suggests that most of the portion comprises copper. The surface shape of the worn tool electrode surface is depicted in figure 6.4a, while the chemical characteristic and material movement are depicted in figure



6.4b. The tool has been worn at a specific spot, indicating localized tool erosion.

### 6.3.3 Material migration and diffusion analysis through EDX

Energy-dispersive X-ray spectroscopy was used to determine the elemental and chemical composition of the machined surface. The elemental peaks of the machined surface are shown in figure 6.3 a as EDX spectra while material migration and diffusion were depicted in 6.3 b.

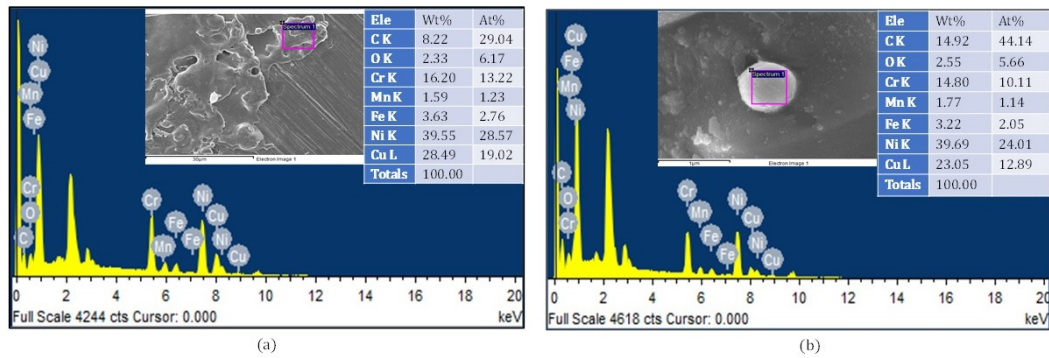


Figure 6.3: (a) Chemical characterization (b) material migration, and elemental diffusion analysis through EDX spectrum

The presence of significant levels of nickel (39.55–39.69, wt %), ferrous (3.22–3.63, wt%), manganese (1.59–1.77, wt%), chromium (14.80–16.20, wt%), and copper (23.05–28.49, wt%) suggest that the majority of the elements come from their compositional component. The copper is available in a somewhat larger quantity implies that bidirectional material transfer and diffusion occur within the machined surface [163]. The presence of carbon (8.22–14.92, wt%) in a little bit higher quantity indicates that the carbon comes from the carbon stub (sample attached with it) as well as from the decomposition of hydrocarbon oil under high-temperature plasma [164]. In order to characterize the chemical composition and investigate the topography of the localized tool degraded region,

FESEM pictures were used. The energy-dispersion X-ray spectroscopy (EDX) analysis reveals that the degraded surface of the tool contains substantial quantities of nickel (0.66, wt%) and hafnium (3.70, wt%). This implies that bidirectional material movement and diffusion take place within the high-temperature plasma. The spectrum shows a significant quantity of copper (68.31, wt%), indicating

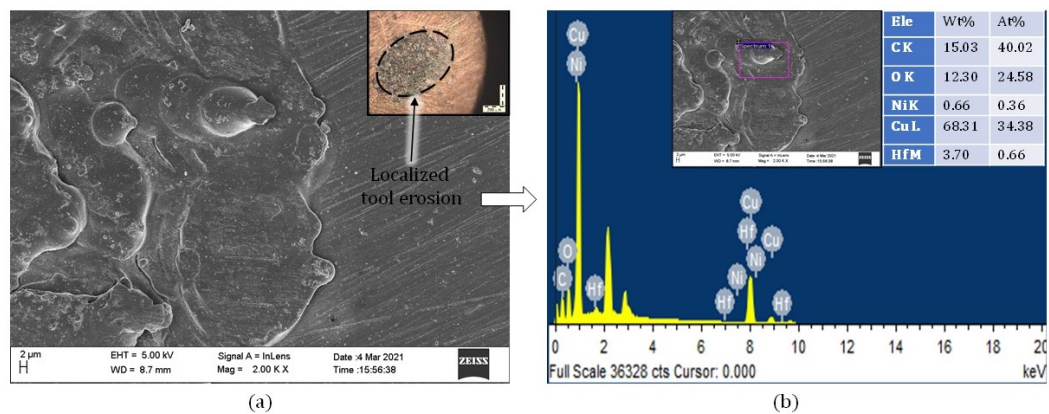


Figure 6.4: (a) Surface morphology of the eroded tool part (confined tool wear with their spark position) (b) material migration and diffusion within the tool eroded part

that copper makes up the majority of the component. Fig6.4a shows the surface profile of the worn tool electrode surface. Fig6.4 b illustrates the chemical characteristic and material flow. A specific area of the tool has been worn, indicating localized tool erosion.

### 6.3.4 Discharge characteristic curve analysis

The analysis of current and voltage pulses provides important insights into the gap condition and the type of discharge waveform. The duration of the ignition delay, during which the dielectric completes its ionisation process, is one of the most crucial factors determining the stability of the discharge phenomenon in the EDM process. Sometimes a discharge occurs without any ignition delay,

resulting in a transient arc. These transient arcs should be avoided during machining because they can impair surface integrity[165]. Another occurrence that

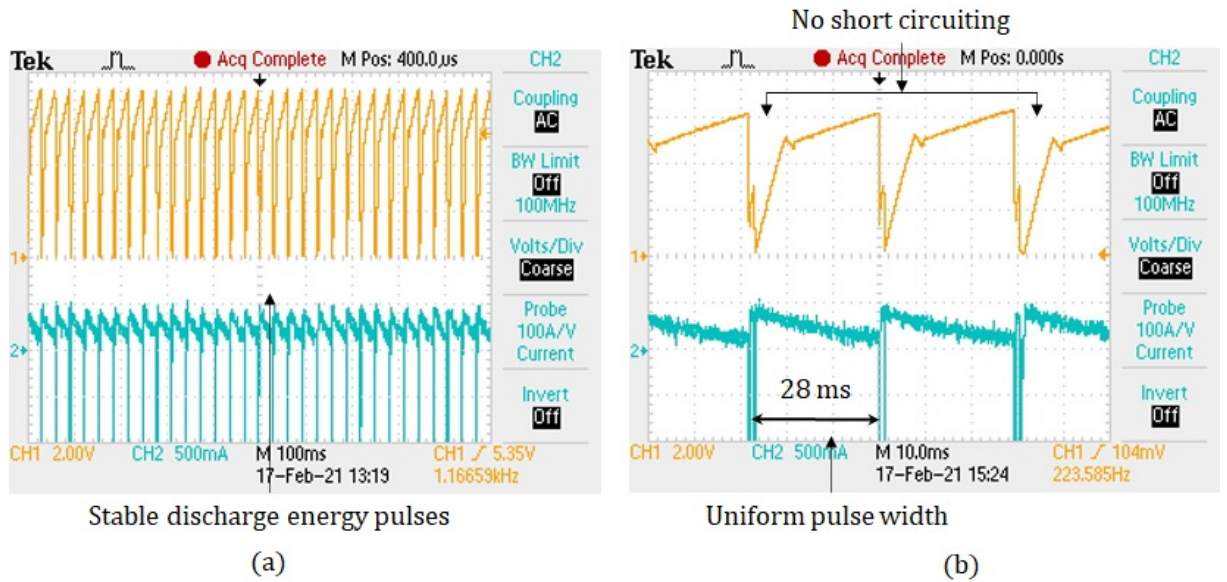


Figure 6.5: Real time voltage and current waveform at the time scale of (a) 100ms and (b) 10ms

is common in conventional EDM is short-circuiting. This is brought on by the servo head's poor response and ineffective flushing (unstable gap) of the debris particles from the discharge zone. The enormous current can flow with no discharge due to direct contact. This should also be avoided because it degrades the workpiece's machined surface. Fig6.5 shows the time transient discharge characteristic curve of Maglev EDM in terms of voltage and current (V-I) waveform. The machining occurs at the moment when the open-circuit voltage is dropped to discharge voltage and currents start raising during effective pulse on time. In the current system, the supplied power was pure DC type hence, no ignition delay and pulse off time is there. The channel is ionized very fast (short ionization) for creating continuous electrical discharge. Meanwhile, it was noticed that the

recorded duty factor was approximately 0.9564 in the digital storage oscilloscope (DSO). This indicates that most of the discharge energy part is utilized in removing the material during effective pulse on time. Moreover, it indicates the continuous EDM without any pulse interval time.

The fig 6.5 a indicates that most of the discharge energy pulses are stable and uniform. No ignition delay is found in the curve this means the ionization and discharge are happening simultaneously. The three discharge energy pulses are shown in Fig 6.5 b at a time scale of 10 ms. The majority of discharge energy pulses exhibit uniform pulse widths (28 ms) free of any undesirable signals like arcing and short-circuiting. The voltage-current waveform's overall analysis reveals that the process is extremely steady and efficient. Additionally, it shows that the suggested servo mechanism effectively controls the gap condition.

### **6.3.5 Surface integrity (SI) analysis**

In the EDM process, surface roughness is an important machining performance indicator. It is influenced by the presence of micro-pores, micro-holes, micro-cracks, and micro debris particles [166]. A non-contact type profilometer (Zygo, NewView-9000) was used to measure the arithmetic mean height ( $S_a$ ), root mean square roughness ( $S_q$ ), and maximum height ( $S_z$ ) roughness metrics. Fig 6.6 (a) indicates the 3D plot of area surface roughness for the scanned area of  $1562.870 \times 1562.870 \mu\text{m}^2$ . The  $S_a$ ,  $S_q$ , and  $S_z$  were found  $0.707 \mu\text{m}$ ,  $1.461 \mu\text{m}$ , and  $30.981 \mu\text{m}$  respectively. The 2D surface plot with three different slices over the machined part is presented in figure 6.6b. Later on, the actual variation

of linear surface integrity (local) parameters (Ra, Rq, and PV) over the three different slices were presented in figure 6.6c.

It was noted that the Ra, Rq, Rz, were changing between 0.899 and 1.057  $\mu\text{m}$ , 1.198–1.366  $\mu\text{m}$ , and 6.862–7.197  $\mu\text{m}$  respectively. In case of maglev EDM, the overall evaluation of the surface roughness and surface texture characteristics suggests that the surface integrity parameters have a low value. This is owing to the machining gap's availability of low discharge energy. The action of tool electrode oscillation quickly improves the flushing condition, resulting in a low roughness value. In the current study, the area surface roughness is quantified in terms of arithmetic mean height (Sa), root mean square roughness (Sq), and maximum height (Sz). A non-contact white light interferometer (Zygo, NewView-9000) was used to measure these roughness metrics. Fig 6.6 (a) indicates the 3D plot of area surface roughness for the scanned area of 1562.870 x 1562.870  $\mu\text{m}^2$ .

The Sa, Sq, and Sz were found at 0.707  $\mu\text{m}$ , 1.461  $\mu\text{m}$ , and 30.981  $\mu\text{m}$ , respectively. The 2D surface plot with three different slices over the machined part is offered in Later, the actual variation of linear surface integrity parameters (Ra, Rq, and PV) over the three different slices were presented in 6.6 (C). It was noted that the Ra, Rq, and Rz were changing between 0.899-1.057  $\mu\text{m}$ , 1.198-1.366  $\mu\text{m}$ , and 6.862-7.197  $\mu\text{m}$ , respectively. In the Maglev EDM, the overall evaluation of the surface roughness and surface texture characteristics suggests that the surface integrity parameters have a low value. It is owing to the machining gap's availability of low discharge energy. Moreover, the action of

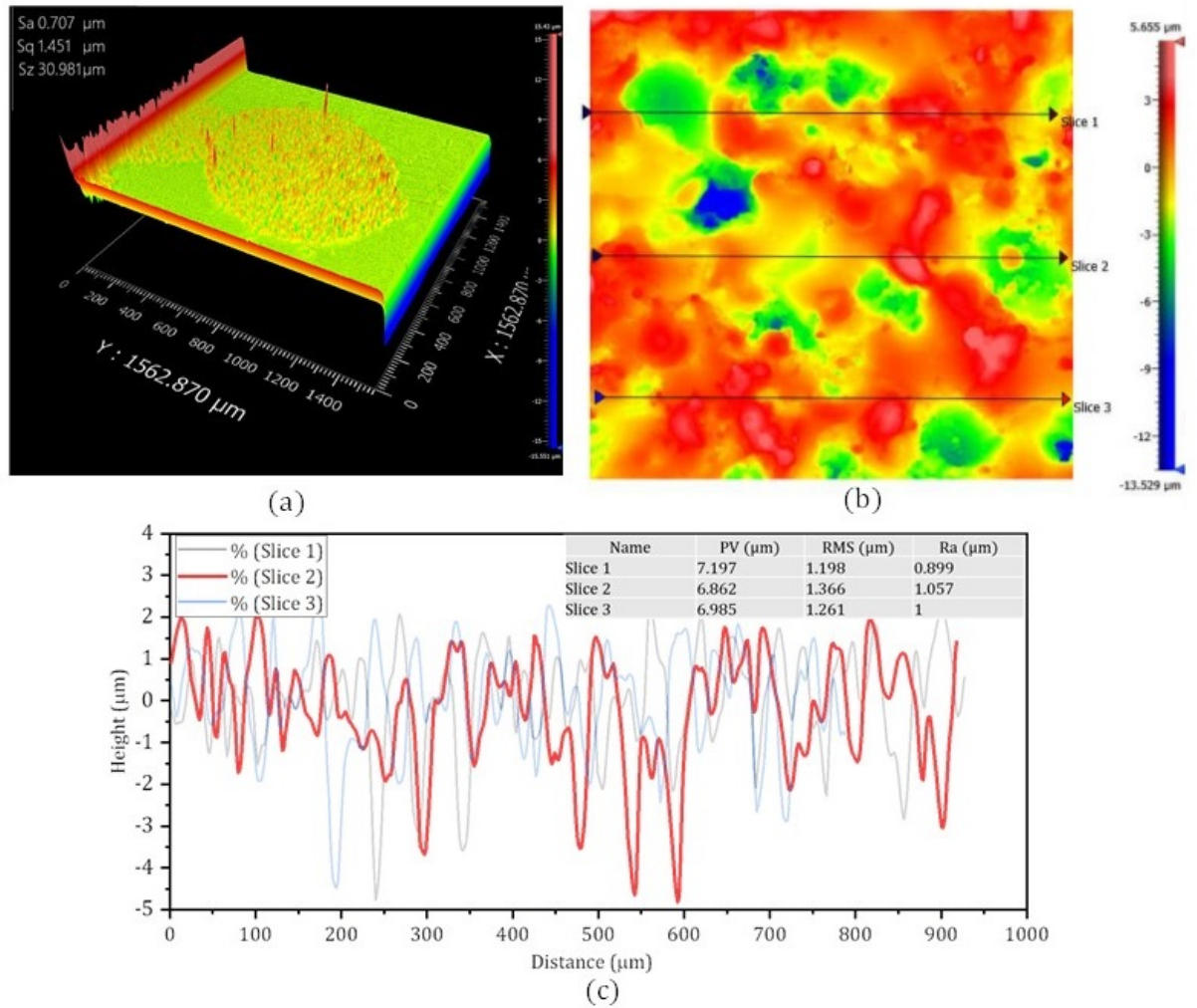


Figure 6.6: (a) 3D plot for area surface roughness for the scanned area (b) 2D surface roughness plot (c) variation of linear surface integrity parameters (Ra, Rq, and Rz) over three different slices

tool electrode oscillation quickly improves the flushing condition, resulting in a low roughness value.

### 6.3.6 Specific energy consumption (common performance index) analysis

The specific energy consumption (SEC) is defined as the amount of discharge energy required to remove a single unit of volume or mass. Initially, discharge power has been calculated based on the information obtained in the form of dis-

charge voltage, discharge current, and effective pulse on time. The specific energy consumption was obtained by dividing this discharge power by the material removal rate (MRR). The maximum specific energy consumption was (1.6284 J/ $\mu$ g) for the discharge power of 1.17 J/s (watt) while the minimum (1.2245 J/ $\mu$ g) for the discharge power was 1.06 J/s (watt). To assess its effectiveness, the specific energy consumption (SEC) of the current maglev EDM system was compared with the data from the published literature, as shown in figure 6.7. According to Ali et al. [167] the specific energy ranges from 0.1278 to 2.5265 J/ $\mu$ g for discharge powers between 66 and 408 J/s. The chosen dielectric medium was EDM oil in their case, and the working material was Inconel 718. Mishra et al. [168] reported that the EDM system's specific energy varies between 0.054 and 0.4789 J/ $\mu$ g for discharge powers between 300 and 700 J/s. Inconel 625 served as the material for the workpiece, electrolytic pure copper served as the tool, and the tool was a cylindrical graphite rod ( $\phi$ 12 mm). The examination of the data from this article showed that the system's specific energy ranges from 0.1820 to 1.7919 J/ $\mu$ g for discharge powers between 210 and 792 J/s. Similar to this, Datta et al.[169] revealed in another study that the EDM system's specific energy ranges from 0.03805 to 1.2085 J/ $\mu$ g for discharge powers between 97.7 and 743 J/s. Inconel 718 plate served as the workpiece material and copper ( $\phi$  20 mm) and EDM oil served as the tool and dielectric fluids respectively. Upadhyay et al.[170] evaluated performance indicators such as material removal rate (MRR), tool wear rate (TWR), surface roughness (Ra), and surface crack density (SCD) to examine the EDM system's ability to machine Inconel 601 material. The examination

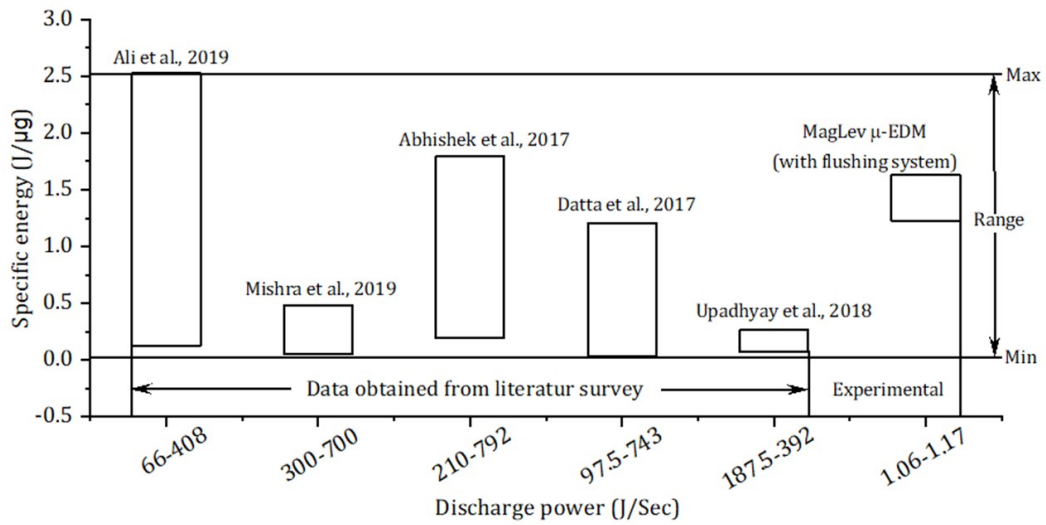


Figure 6.7: Comparative analysis of specific energy consumption (SEC) with the existing literature

of the data included in this work showed that over the discharge power range of 187.5–392 J/s, the specific energy varied between 0.07561 and 0.2632 J/μg. The maglev EDM system’s specific energy (1.2245–1.6284 J/μg) is within the same range as that previously reported in the literature (0.03805–2.5265 J/μg), according to the overall analysis of the specific energies of five distinct EDM studies. This means that the system requires very little servicing and maintenance costs and is just as effective as other commercial EDM systems.

### 6.3.7 Material removal rate (MRR) and tool wear rate (TWR) analysis

The material removal rate (MRR) is one of the important performance measures which significantly depends on the level of discharge energy in the machining gap. The maximum estimated material removal rate was found 57 μg/min for the discharge voltage of 7.12 V and discharge current of 470 mA. The mini-



mum material removal rate (MRR) was noted 39  $\mu\text{g}/\text{min}$  at a discharge voltage of 6.8 V and discharge current of 450 mA. The average material removal rate (MRR) in four iterations was 47  $\mu\text{g}/\text{min}$ . Fig 6.8a indicates the variation of material erosion rate from average value in four iterations with respect to discharge power. It was reported in the literature that as the discharge power increases the material erosion rate also increases but after achieving the maximum material removal rate (MRR) it starts decreasing despite increasing current and voltage [171]. The decreasing nature of MRR shows the condition of insufficient flushing. Moreover, it is well-known fact that insufficient flushing further leads to transient arc and short-circuiting formation which reduces the material removal rate by an appreciable amount.

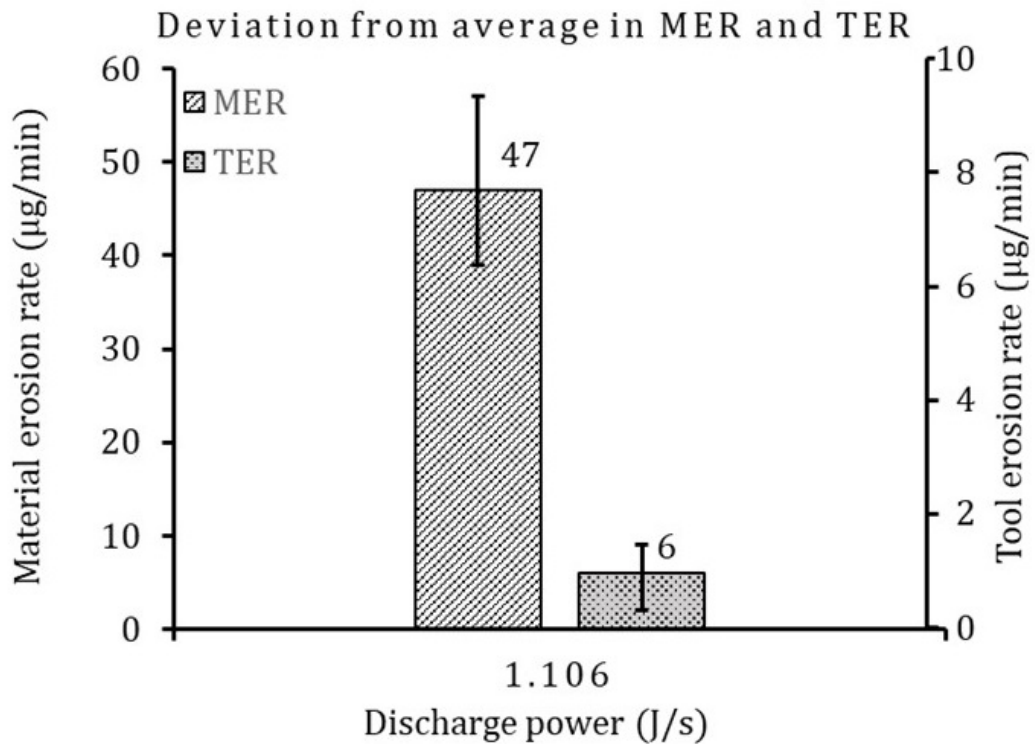


Figure 6.8: Average material removal rate (MRR) and tool wear rate (TWR)

It has been observed that high voltage potential and larger pulse width, the machining gap becomes wider which reduces the intensity of the flow of discharge current within the confined gap. The reduction in discharge current significantly reduces the material removal rate to a great extent. Tool wear is an unavoidable phenomenon in the  $\mu$ -EDM process and has a direct impact on machining accuracy and economics of the machining process. It is noted in the literature that the tool wear rate decreases with increasing conductivity. It is reliant on the density of the electrode material and the availability of the discharge energy in the machining gap. The maximum tool wear rate was observed 9  $\mu\text{g}/\text{min}$  when the discharge voltage was 7.12 V. The minimum tool wear rate was noted 4  $\mu\text{g}/\text{min}$  when the discharge voltage was 7.10 V. The average tool wear rate (TWR) was found 6  $\mu\text{g}/\text{min}$  in four iterations. Fig6.8b indicates the average variation of tool wear rate in four iterations with respect to discharge power.

#### **6.4 Summary**

The following conclusions can be derived based on the current study and experimental examination.

- In present chapter the feasibility of the Maglev EDM was observed using Inconel 625 material as a workpiece.
- In four iterations, the feasibility study found that performance metrics such as material removal rate (MRR), tool wear rate (TWR), and surface roughness (SR) fluctuate in the range of 39–57  $\mu\text{g}/\text{min}$ , 4–9  $\mu\text{g}/\text{min}$ , and 0.899–1.057  $\mu\text{m}$  (Ra) respectively.
- The time transient voltage-current (V-I) waveform shows that the majority of the discharge energy pulses are steady and uniform (28 ms), and there

is no ignition delay (short ionization). The absence of arcing and short-circuiting signals indicates that the process is highly efficient.

- The recast layer thickness is frequently greater towards the interface because flushing pressure is lower. The fractured dielectric has left behind fine granules that are alloyed with carbon in this hard, resolidified layer. The parent material's carbon content, the type of dielectric fluid utilised (1.06-1.17 J/s), and the discharge power were found to have a significant influence on the white layer thickness.
- The chemical characterization of the substance using EDX analysis shows that it migrates and diffuses in both directions. Due to the surface alloying process within the machined surface, this could result in the formation of an intermetallic compound under high plasma region.
- The maglev EDM system had specific energy of 1.2245–1.6284 J/ $\mu\text{g}$ , which was consistent with the earlier research range (0.03805–2.5265 J/ $\mu\text{g}$ ).

## CHAPTER 7

### FEASIBILITY ANALYSIS ON NIMONIC ALLOY WORK MATERIAL

(List of publications<sup>3</sup>)

#### 7.1 Introduction

The present chapter deals with the feasibility of a gap-controlled strategy for EDM processes using magnetic levitation. The tool is levitated and positioned accurately using a unique actuator arm. The actuator arm attained the required positioning accuracy in the thrust ( $Z$ ) direction to ensure a uniform and smooth discharge free of arcing and short circuits. Experiments were carried out using a copper tool and EDM oil on Nimonic superalloy (Grade C-263).

In present chapter comparison of voltage- current (V-I) curve, FESEM observations for microholes, micropores, the recast layer, and other surface topographical features are presented. Further, the bidirectional material movement and elemental diffusion are shown by elemental characterization using EDX analysis.

#### 7.2 Materials and Methods

##### 7.2.1 Workpiece and tool material

A Nimonic alloy of Grade C-263 with a specimen size of 30 mm x 30 mm x 2 mm was the work material while 3 mm copper rod was the tool material. Table 7.1 illustrates the compositional and thermophysical properties of the work

material. The material was chosen due to its inherent superior mechanical and physical properties, such as high oxidation strength and corrosion resistance at elevated temperature and pressure [172]. Furthermore, the material belongs to the category of exotic material and poses research challenges in machinability by the conventional methods. Also, it is a widely utilized material for avionic, bio implant, automotive, gas turbine, and heat exchanges industries [173].

Table 7.1: Chemical constituents (%weight) of Nimonic C-263 workpiece(under Mass Density=  $8.36 \text{ g/cm}^3$  and Melting Point  $1300 - 1355^\circ\text{C}$  )

Elemental composition	% weight
Al	0.6
B	0.005
C	0.040-0.080
Co	19.0-21.0
Cr	19.0-21.0
Cu	0.2
Fe	0.7
Mn	0.6
Mo	5.60-6.10
Ni	49
S	0.007
Si	0.4
Ti	1.90-2.40

A pure copper rod of diameter 3mm having a length of 10mm was used as tool electrode material (cathode) for the experimentation. The material is very soft and widely adopted as a tool material for EDM operation. The thermo-physical characteristics of the tool material are registered in Table 7.2.

Table 7.2: Thermo-physical property of tool electrode (Copper) material

Thermo-physical properties	value
Composition	99.9% Cu
density	$8.904 \text{ g/cm}^3$
Melting point	10830C
Hardness	100 HB
Electrical resistivity	$9\mu\Omega$ -cm

## 7.2.2 Experimental Procedure

It is a well-known fact in EDM that the negative imprint of the tool is shaped over the workpiece surface, therefore the cross-sectional part of the tool and workpiece were refined before machining. The initial finishing is done using a disk polishing machine (Chennai Metco) with emery paper grades 1500 and 2000. To produce the mirror quality, a velvet cloth with diamond paste was used later. The measured experimental condition for cutting the workpiece on maglev EDM on open circuit voltage 12V is shown in table 7.3 whereas the table 7.4 depicts the experimental conditions on traditional EDM on open circuit voltage 180-220V in the same way.

Table 7.3: Measured voltage and current signal in four iterations (IT1–IT4) via digital storage oscilloscope during machining on maglev EDM

Discharge voltage (V)	Discharge current (A)	Pulse on time ( $\mu$ s)	Duty factor	Machining time
7.2	0.69	29	0.9564	
7	0.67	29	0.9564	10 minutes
7.1	0.71	29	0.9564	
7.3	0.72	29	0.9564	

Table 7.4: Parameter setting for machining of Nimonic alloy (C-263) on conventional EDM

Gap voltage (V)	Gap current (A)	Discharge Voltage	Pulse on time ( $\mu$ s)	Duty factor	Machining time
12	3	10.5-13.5	20	0.5633	
16	4	15-17	70	0.7446	10 minutes
20	5	18-22	170	0.8333	
24	6	20-28	270	0.8544	

The workpiece was now connected to the positive terminal of the DC power supply, while the tool was attached to the negative terminal. The workpiece is immersed in high-performance EDM oil (specific gravity 0.753, dielectric strength 45 kVA), and a 12 V open-circuit voltage is applied by fixing the maximum peak current of 1 A. To maintain a steady inter electrode gap, the tool begins to

oscillate. With variable discharge current (650–750 mA), discharge happens at different voltage potentials (6.5–7.5 V) for the same open-circuit voltage (12 V). The electrical information is collected in a digital storage oscilloscope (excel file) for the calculation of discharge power and specific energy. The weight reduction method is used for the calculation of MRR, and TWR using a weight balance machine (MettlerToledo, accuracy 10  $\mu\text{g}$ ).

### 7.3 Results and Discussions

#### 7.3.1 Discharge stability monitoring through V-I curve

The measured voltage-current waveform on Maglev EDM during multiple discharges is depicted in Fig7.1a. The majority of the voltage and current signals were determined to be stable and uniform. The rapid drop in discharge

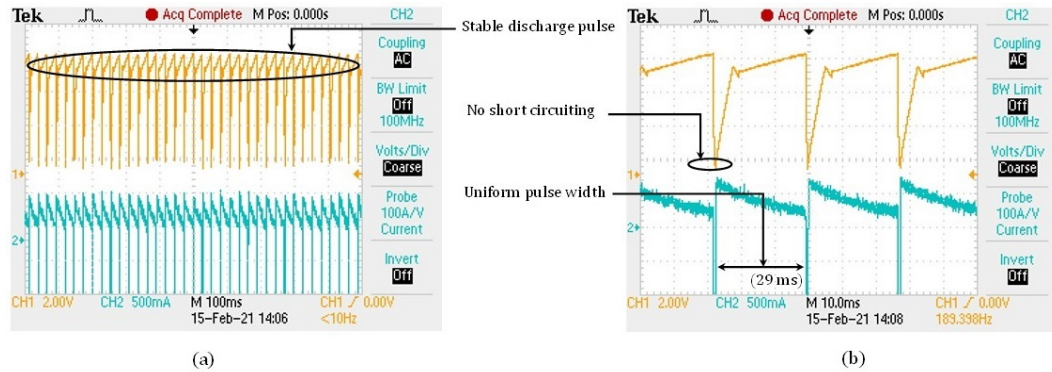


Figure 7.1: Real-time voltage-current waveforms (as measured) of maglev EDM at (a) 100ms and (b) 10ms time scale

voltage implies that ionization is occurring rapidly and without any ignition delay. This indicates that EDM is of continuous type. There is no provision of OFF time as DC power has no switching mechanism (ON/OFF). Here, ionization and discharge happen simultaneously. When the circuit tries to attain the open circuit condition there is cut-off in the flowing current for short duration of

time which seems as OFF time in the current mechanism. In this situation the electromagnetic force become higher than restoring force which pushes the tool toward workpiece for generating discharge. Fig 7.1b indicates the three discharge energy pulses at the time scale of 10 ms. The uniform pulse width was 29 ms. There were no arcing or short-circuiting signals, indicating that the process is very efficient and stable.

Fig7.2 indicates voltage-current curve of conventional EDM at a gap voltage of 12V and duty factor of 0.56. It was found that most of the voltage pulses are arises without any ignition delay. This indicates that the machining is happening with short ionization time. In further stages, these no ignition delays form transient arc. The transient arc indicates that the deionization is not fully complete after the previous pulse and there is a remnant of residual conductivity in the plasma channel [174]. In the same curve, the discharge current varies in both directions which indicates the current is of bipolar type. The bipolar nature of current may arise due to the polarity change (instantaneous rush of ions and electrons causes short-term swap or residual magnetization within the gap[175]. Fig 7.2b indicates the normal discharge of conventional EDM at gap voltage of 16 V and duty factor of 0.74. The presence of a significant amount of ignition delay indicates that the gap is getting enough time to get it completely ionized. Fig7.2c indicates the current-voltage curve at gap voltage of 20 V and duty factor of 0.83. The curve contains all types of discharge energy pulses such as normal discharge, transient arc, short-circuiting, etc. As the duty factor increases the



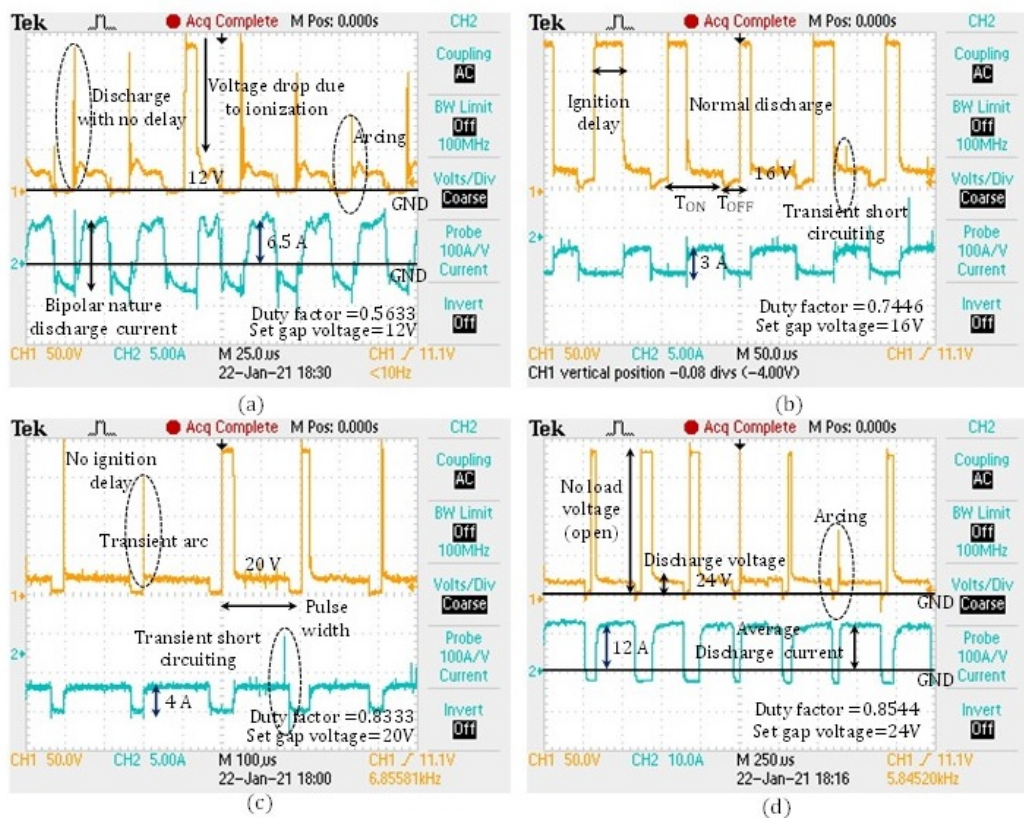


Figure 7.2: Real time pulse characteristics (as measured in DSO) and machining stability testing in conventional EDM through voltage current waveforms

amount of effective pulse on time also increases. The increase in effective pulse on time denotes that most of the discharge energy pulses are involved in removing the material. Fig7.2d indicates the current-voltage pulse at gap voltage of 24 V and duty factor of 0.85. The curve denotes that most of the discharge energy pulses are normal however some energy pulses are posing very little ignition delay time which may form the condition for arcing.

### **7.3.2 MRR and Specific energy consumption (SE) analysis**

Material removal rate (MRR) is one of the critical performance parameters which significantly depend on discharge energy level. This discharge energy level is further reliant on discharge voltage, discharge current, and duty factor. The duty factor is important because it decides the time of effective machining for a particular pulse. In present experimental work on maglev EDM, the duty factor (0.9564) is stable. The maximum estimated MRR was found  $102\mu\text{g}/\text{min}$  while the minimum MRR was found  $60\mu\text{g}/\text{min}$ . Average MRR was  $79.260\mu\text{g}/\text{min}$ . Fig 7.3a shows the impact of discharge power on MRR in Mgalev EDM, and Fig 7.3b conventional EDM. It was noted that the discharge power has an eminence impact on MRR as compared to voltage only.

With the increase in discharge power, the material removal also increases. The MRR is much higher in conventional EDM due to the high energy flow. However, it was also found that the MRR decreases after some time instead of increasing voltage. The reason may be the insufficient exclusion of debris particles from the machining zone or due to low plasma strength. Instead of better flushing

in conventional EDM, transient arcing and short-circuiting arise. The reason may be the slow response frequency of conventional servo EDM head and gathering of debris particles. Additionally, the previous study says that MRR is decrease with the of plasma density. It is mean that for long pulse duration the MRR decrease due to the arcing [176].

The specific energy (SE) is the another significant performance response which indicates the amount of discharge energy that is utilized for removing a single unit of volume. From fig 7.4 it was observed that the specific energy was maximum ( $2.2142 \text{ J}/\mu\text{g}$ ) for the discharge power of  $2.26 \text{ J/s}$  while the minimum ( $1.2558 \text{ J}/\mu\text{g}$ ) for the discharge power of  $2.08 \text{ J/s}$  in maglev EDM. This means, with increasing discharge power, the specific energy is increasing. The specific energy in the maglev EDM system is higher due to low discharge power which causes lower erosion rate.

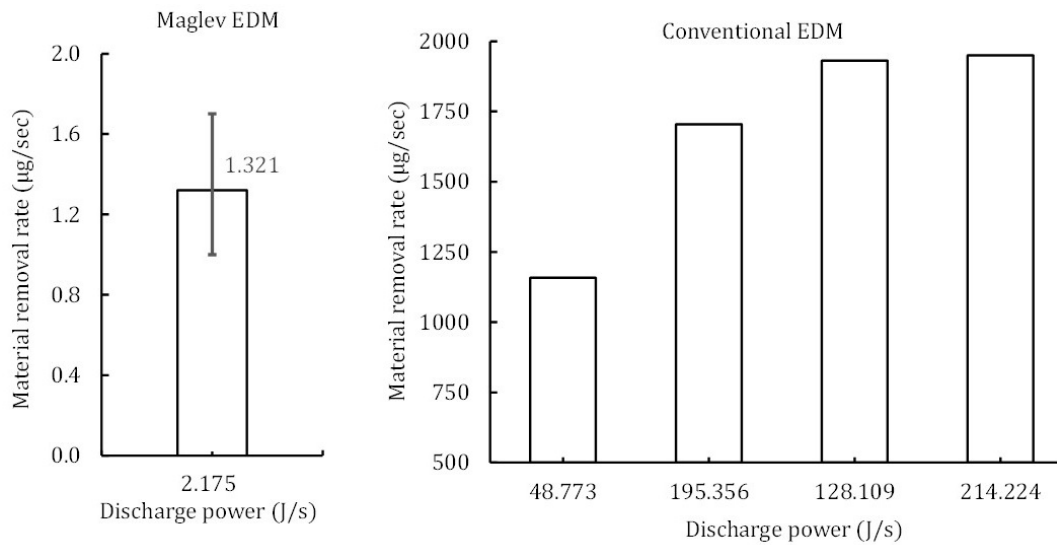


Figure 7.3: Variation in MRR with respect to discharge power in (a) Maglev EDM (deviation from average MRR) (b) conventional EDM

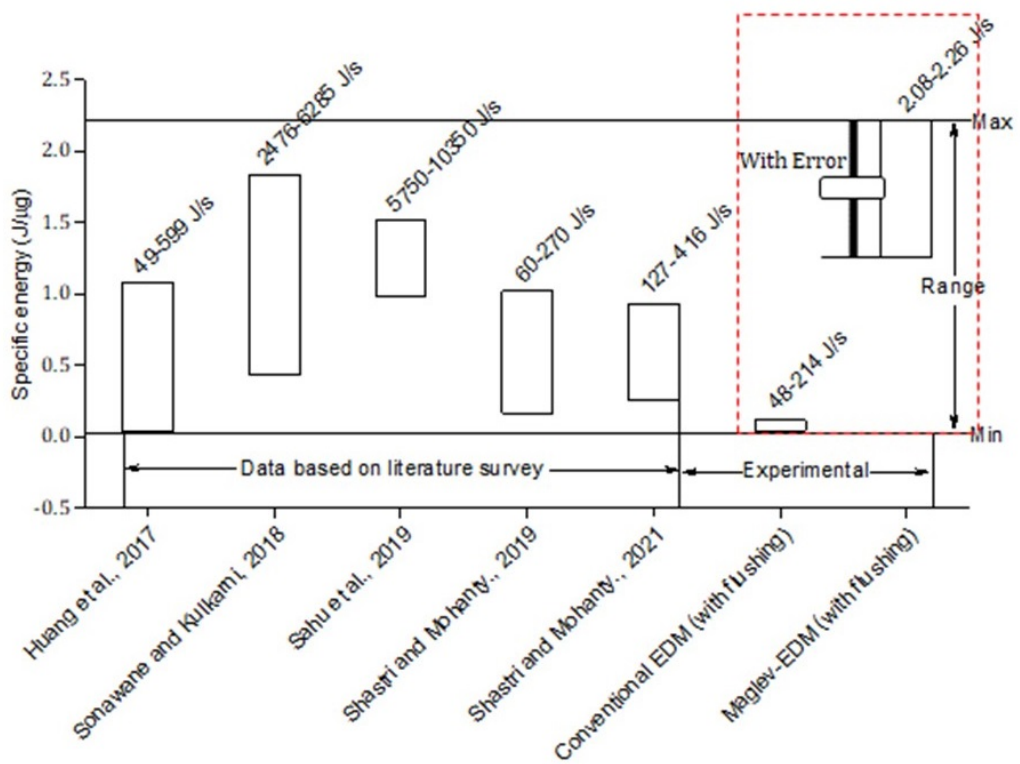


Figure 7.4: Comparative analysis of specific energy consumption (SEC) rate at varying range of discharge power (a) Maglev EDM (b) conventional EDM and in the reported literature

A similar type of pattern was also observed in conventional EDM. The maximum specific energy of  $0.1144 \text{ J}/\mu\text{g}$  was found at discharge power of  $195 \text{ J/s}$ . Later on, the specific energy of the maglev EDM system is compared with the data available in the open literature. Huang et al. [177] estimated the specific energy in the range of  $0.03433\text{--}1.07978 \text{ J}/\mu\text{g}$  for the discharge power range  $49\text{--}599 \text{ J/s}$ . Sonawane and Kulkarni [178] illustrated that the specific energy varies in the range of  $0.4297\text{--}1.8367 \text{ J}/\mu\text{g}$ . Sahu et al. [179] designates that the specific energy is lying between  $0.9854 \text{ J}/\mu\text{g}$  to  $1.5133 \text{ J}/\mu\text{g}$ . Shastri and Mohanty [180] indicated that the specific energy varies in the range of  $0.1670\text{--}1.0200 \text{ J}/\mu\text{g}$  for the discharge power range of  $60\text{--}270 \text{ J/s}$ . Shastri and Mohanty [181] showed that the specific energy varies in the range of  $0.2575\text{--}0.93026 \text{ J}/\mu\text{g}$  for the discharge power range of  $127\text{--}416 \text{ J/s}$ .

### **7.3.3 Surface roughness (SR) and tool wear analysis**

Surface roughness is another indicator of a machining performance measure, which deals with the surface integrity of the machined parts. In the current work, the surface integrity of the machined surface was analyzed by Zygo profilometer (New View 9000). The 3D plot for crater geometry is illustrated in figure 7.5a. The surface texture parameters ( $S_a$ ,  $S_q$ ,  $S_z$ ) for the scanned area of  $1562.870 \times 1562.870 \mu\text{m}^2$  are represented in figure 7.5b. The observed value of  $S_a$ ,  $S_q$ , and  $S_z$  was  $0.719$ ,  $1.192$ , and  $17.802 \mu\text{m}$ , respectively. To examine the linear surface integrity parameters ( $R_a$ ,  $R_q$ ,  $R_{sk}$ ,  $R_{ku}$ , and  $PV$ ), three different slices (line) were taken. The actual variation of surface roughness is denoted in figure 7.5c. It was observed that  $R_a$ ,  $R_q$ ,  $R_z$ ,  $R_{sk}$ , and  $R_{ku}$  were varying between  $0.931$  and

1.442, 1.171 and 1.861, 6.227–9.331, 0.66–1.04, and 2.82–3.57 $\mu\text{m}$  respectively. In maglev EDM, the overall evaluation of the surface roughness and surface texture parameters shows that the surface integrity parameters have a low value due to flow of low discharge energy. In EDM, tool wear is an unavoidable phenomenon. It depends on the density of the electrode material and the amount of discharge power available [182].

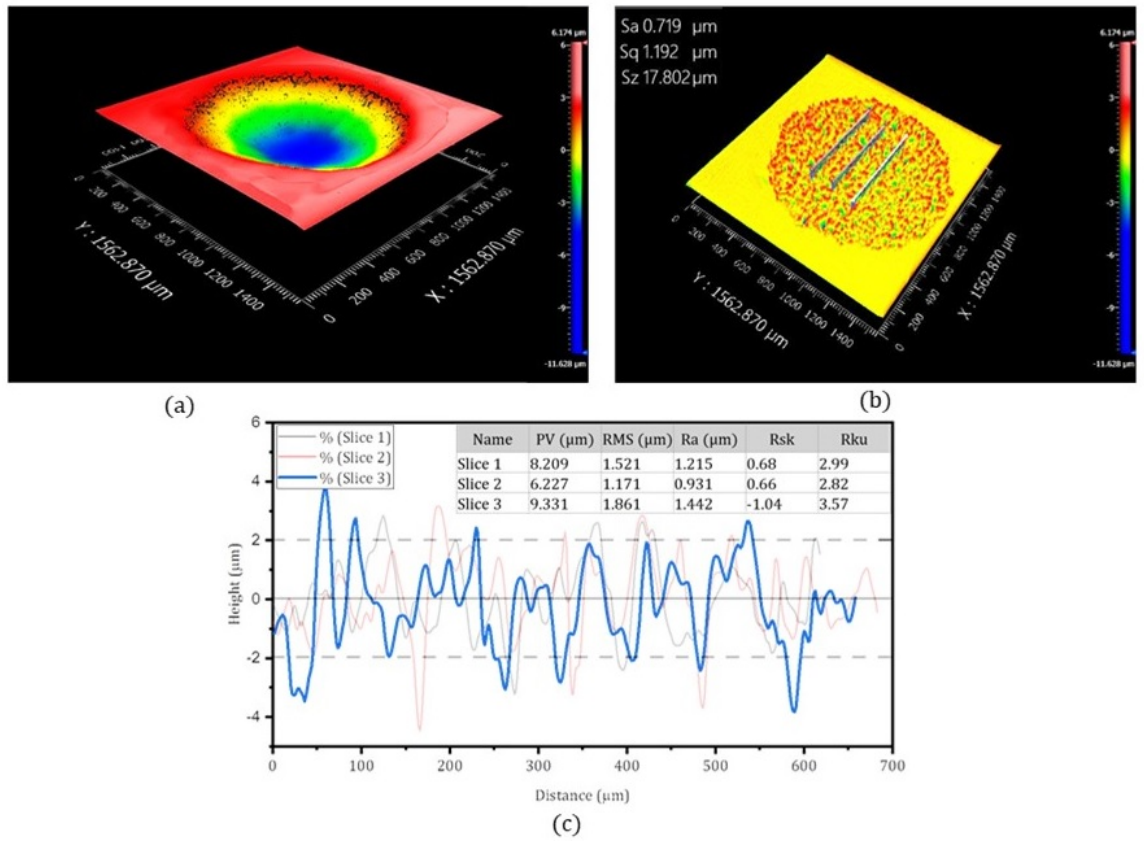


Figure 7.5: (a) 3D plot for surface roughness variation and crater geometry (b) area surface roughness and their variation (c) variation of linear surface integrity parameters (Ra, Rq, and Rz)

The tool wear rate first increases as the gap voltage increases, but after a while, despite increasing the gap voltage, the tool wear rate progressively starts to decrease. The cause could be work material deposition on the tool surface

as a result of diffusion and material migration. The maximum and minimum tool wear rates in maglev EDM were observed to be 28 and 14 $\mu\text{g}/\text{min}$  in the present four cycles of work. The average rate of tool wear was 19.75  $\mu\text{g}/\text{min}$ . This suggests TWR is 25% of MRR and needs to be improved. The following relation was used to evaluate the tool wear rate.

$$TWR = \frac{T_{(wi)} - T_{(vf)}}{\text{MassDensity} \times T_m} \quad (7.1)$$

Where  $T_{(wi)}$  indicates the initial tool weight,  $T_{(vf)}$  indicates the final tool weight after machining, and  $T_m$  indicates the total machining time in minutes.

#### **7.3.4 Surface topography analysis by FESEM**

The impact of input variables on the machined surface was examined in terms of surface morphology and topography through field emission scanning electron microscopy (FESEM) (Zeiss, Supra-55). surface characteristics are illustrated in figure 7.6. The presence of micropores, microholes, micro-pockets, micro-globules, and reattachment of melted debris particles, etc., were noted. These are due to thermal impact of electrical discharge and improper splashing of molted material [183].

The formation of the recast layer was found near the edge of the machined part. Mostly, it is formed at the termination of pulse on time because at that time the molten material is neither ejected nor completely flushed away. This re-solidified layer was hard and contains fine grains alloyed with the carbon that comes from the cracked dielectric. The re-solidified layer is appearing white

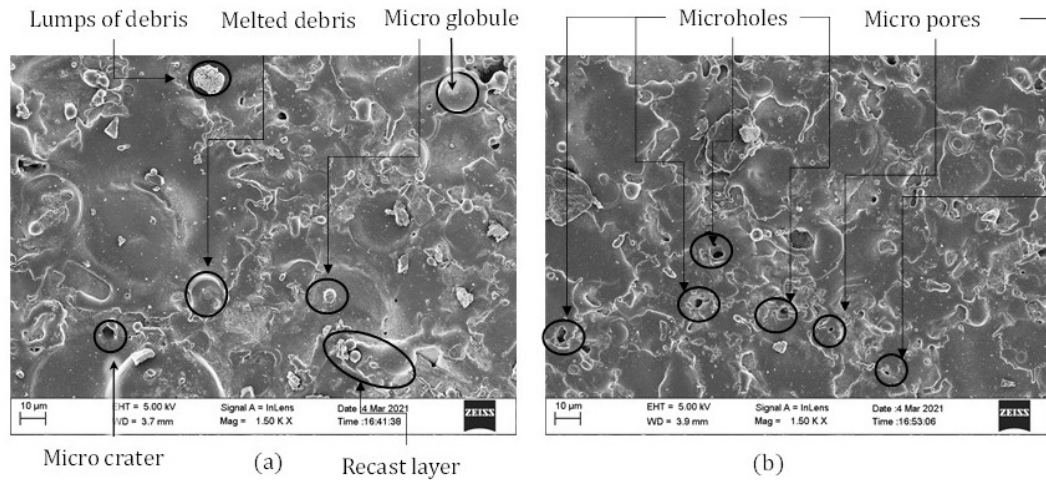


Figure 7.6: Surface morphology/topography analysis of machined workpiece parts through FESEM in two iterations at the same location

and unaffected by the etching process[184]. Micro-pores and pinholes were also observed on machined surfaces which is due to the trapping of gas bubbles in molten material during solidification[185].

### 7.3.5 Bidirectional material migration and diffusion analysis through EDX

Energy-dispersion X-ray spectroscopy analysis is carried out to determine the elemental and chemical composition of the machined surface. Moreover, it enables the analysis of near-surface elements and offers number of various element peaks at different locations, which appear as a sample mapping. Fig7.7a indicates the chemical characterization of the workpiece machined surface. The material migration and elemental diffusion analysis are shown Fig 7.7b. The presence of an appreciable amount of nickel, chromium, molybdenum, titanium, iron, and silicon indicates that most of the parts come from the parent material composition. The availability of copper signifies the bidirectional material transfer and diffusion from the tool electrode[186]. The surface alloying phenomenon



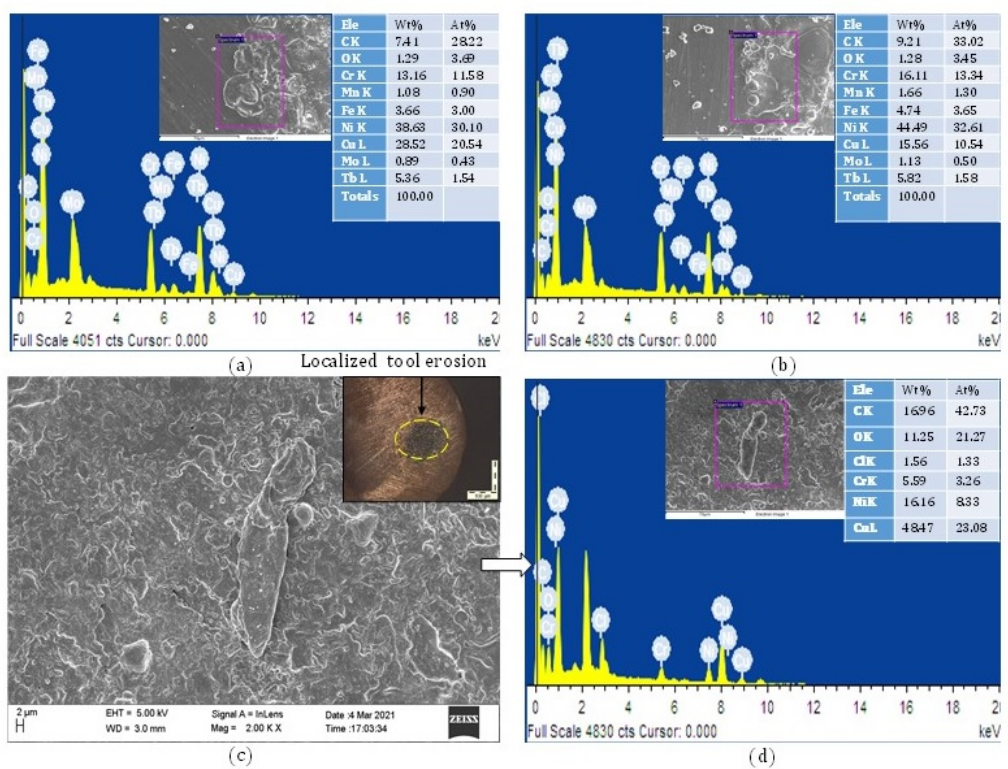


Figure 7.7: (a) Chemical characterization (b) material migration, and elemental diffusion analysis (c) machined copper tool electrode surface (inset: localized tool erosion with their spark location) (d) bidirectional material transfer in EDX spectra after machining on the tool surface

may happen under high temperatures and pressure in plasma region. At last, the presence of carbon indicates that carbon comes from the carbon stub or from decomposition of hydrocarbon oil (EDM oil) under high-temperature plasma. Fig 7.7c demonstrates the surface characteristics of the tool electrode (copper) after machining. The analysis of tool wear surface through EDX indicates that the material is migrated from both electrodes. The presence of nickel (16.16% weight) and chromium (5.59% weight) in an appreciable amount indicate the molecular diffusion and transfer of material in figure 7.7d.

#### 7.4 Summary

The following conclusions can be derived based on current experimental work.

- In the present chapter, a feasibility study was performed on the difficult-to-cut material nimonic alloy under the defined conditions.
- According to the feasibility study, the material removal rate varies between 60 and 102  $\mu\text{g}/\text{min}$ . The tool wear rate ranges from 14 to 28  $\mu\text{g}/\text{min}$ . In four iterations, the average tool wear rate was 19.75  $\mu\text{g}/\text{min}$ , or 25% of the MRR, and has to be improved.
- The average specific energy (1.735  $\text{J}/\mu\text{g}$ ) of the maglev EDM system is almost identical to that published in the open literature (0.0343–1.837  $\text{J}/\mu\text{g}$ ).
- The machined surface's average roughness (Ra) was 0.931–1.442  $\mu\text{m}$ , indicating a smooth surface when compared to the existing EDM.
- The EDX examination of the machined surface confirms the machined surface's bidirectional material transfer and elemental diffusion.

## CHAPTER 8

### CONCLUSION AND FUTURE SCOPE

#### 8.1 Conclusion

When it comes to cutting complicated shapes of hard-to-cut materials, electrical discharge machining (EDM) has many advantages over traditional machining methods. It is true that advancements in the field of EDM have refined cutting-edge technology over time. Although it is often true that there is scope for improvement due to significant reasons, It is considered less effective and reliable because of its statistical nature and unstable discharge energy. Despite multiple attempts to improve the settings, failures have been attributed to a stochastic process mechanism and the inclusion of a number of uncontrollable parameters. In order to ensure the long-term viability, efficiency, and robustness of the process, it is necessary to have a system that can adjust as a self-adaptive measure to address the occurrence of process failures and be consistent against power interruptions. In response, a technology called the Maglev Electrical Discharge Machine (MEDM) was developed, aiming to overcome the lacunae or limitations of conventional EDM. The current research objective is to test the feasibility of MEDM by comparing its response to the same range of process parameters as conventional EDM.

The feasibility of MEDM was tested on hard-to-cut metals like commercially pure titanium, titanium alloy, Inconel 625, and Nimonic alloy. The response based

on experimentation with the various materials is presented in the different chapters. The quantitative comparison in graphical form of material removal rate, surface finish, tool wear, and specific energy is presented in the respective chapters wherever applicable. It was observed that the undesirable process output of conventional EDM is due to the conventional servo mechanism. The delayed response, backlash, and gear hysteresis caused the harmful effect in the conventional servo system. Further, in the existing EDM technology, the traditional power source also affects the machining rate. Unfavorable process output, like inconsistency in discharge energy, affects the process economy and productivity. During the feasibility test it was observed that MEDM is a superior technology that addresses all major concerns and challenges of conventional EDM. Since the MEDM is based on the magnetic levitation concept, it eliminates the need for a conventional servo mechanism for tool feeding. Moreover, MEDM uses a pure DC power supply by replacing the conventional pulse power supply. The machining responses on the hard-to-cut materials proclaim that the MEDM is feasible, and its outputs are comparable with the same range of process parameters as conventional EDM technology.

Following are the salient conclusions drawn from this feasibility analysis:

- The MEDM is free of mass inertia and backlash, because of the replacement of older tool feeding servo mechanisms.
- The positioning response of maglev EDM is very fast compared to traditional EDM due to the self-adaptive system.
- MEDM runs on a pure DC power source, hence, the complex power source (transistor or capacitive) is eliminated.

- The maintenance cost of the servo mechanism and complex circuitry was eliminated.
- A comparison of the discharge characteristic curves of conventional EDM and MEDM shows that the voltage-current in MEDM is more stable. Unwanted signals like arcing and short-circuiting were not present, indicating that machining speed and stability have improved.
- The response output in terms of material removal rate, surface finish, and specific energy were comparable with conventional EDM.

However, the MEDM is in an early stage, but it might be used in industry with a few upgrades and could replace conventional EDM technology. The industrial applications of MEDM will be revolutionary for exceptional economy and higher productivity in the machining of hard-to-cut metals.

## **8.2 Future Scope**

The presently developed MEDM technology is in its early stages. Hard and challenging materials such as duplex steel with different tool materials and dielectric media (hydrocarbons and gases) are under examination. The feasibility analysis of maglev EDM (MEDM) on four hard-to-cut metals is shown in this document. As a future area of research, MEDM's current design can be improved to make more advanced technology, such as by making the flushing system better. At the present stage, only voltage variation is possible to a limited extent, and other process parameters cannot be changed. In the future, MEDM can be compared with conventional EDM for the same discharge energy at the laboratory for a true comparison and to validate the developed technology. These factors may improve further with future technologies. The rectified power supply may replace

the DC power supply. A high-power generator could improve material removal. At present, the feasibility investigation is done by running the machinery for up to 15 minutes. However, in the next phase, the durability test may extend the machine's runtime by several hours. Such improvements in the present MEDM can make the technology more capable for industrial applications.

## List of Publications by Scholar

### Published Journal papers

1. Sisodiya, M.S., Shukla, S. and Bajpai, V., 2022. "Feasibility analysis of novel Maglev EDM by comparing with conventional micro EDM" *Scientific Reports*, 12(1), pp.1-13
2. Kumar, D., Sisodiya, M.S., Mandal, D.K. and Bajpai, V., 2023. "Maglev micro-EDM: Feasibility and performance on Inconel 625" *CIRP Journal of Manufacturing Science and Technology*, 40, pp.155-166.
3. Kumar, D., Sisodiya, M.S. and Bajpai, V., 2022. "A novel servo-stabilized electromagnetic levitation for micro-EDM processing and its feasibility analysis" *Proceedings of the Institution of Mechanical Engineers, Part B: Journal of Engineering Manufacture*, p.09544054221124473.

### Under Review paper

1. Shukla, S., Sisodiya, M.S. and Bajpai, V. "Analytical modelling of material removal rate and surface finish in Maglev EDM on Ti-6Al-4V" in *Microsystem Technologies*,

## REFERENCES

- [1] Elman C Jameson. *Electrical discharge machining*. Society of Manufacturing Engineers, 2001.
- [2] Norliana Mohd Abbas, Darius G. Solomon, and Md. Fuad Bahari. A review on current research trends in electrical discharge machining (EDM). *International Journal of Machine Tools and Manufacture*, 47(7-8):1214–1228, June 2007.
- [3] C.J. Luis, I. Puertas, and G. Villa. Material removal rate and electrode wear study on the EDM of silicon carbide. *Journal of Materials Processing Technology*, 164-165:889–896, May 2005.
- [4] Deepak Kumar, Nirmal Kumar Singh, and Vivek Bajpai. Recent trends, opportunities and other aspects of micro-edm for advanced manufacturing: a comprehensive review. *Journal of the Brazilian Society of Mechanical Sciences and Engineering*, 42(5):1–26, 2020.
- [5] R.E. Williams and K.P. Rajurkar. Study of wire electrical discharge machined surface characteristics. *Journal of Materials Processing Technology*, 28(1-2):127–138, September 1991.
- [6] Ahmet Haşçalık and Ulaş Çaydaş. Electrical discharge machining of titanium alloy (ti-6al-4v). *Applied Surface Science*, 253(22):9007–9016,



September 2007.

- [7] Qi Jing, Jian Li, Yongbin Zhang, Lingbao Kong, and Min Xu. A study of influence of servo-control strategy on machining efficiency in micro-edm. *Nanomanufacturing and Metrology*, 3(1):83–90, 2020.
- [8] Yongshun Zhao, Xingquan Zhang, Xianbing Liu, and Kazuo Yamazaki. Geometric modeling of the linear motor driven electrical discharge machining (EDM) die-sinking process. *International Journal of Machine Tools and Manufacture*, 44(1):1–9, January 2004.
- [9] Yongfeng Guo, Zebin Ling, Xiaoyou Zhang, and Yerui Feng. A magnetic suspension spindle system for small and micro holes edm. *The International Journal of Advanced Manufacturing Technology*, 94(5):1911–1923, 2018.
- [10] B. Sen, N. Kiyawat, P.K. Singh, S. Mitra, J.H. Yew, and P. Purkaitl. A survey of servo-drive control schemes for electric discharge machining (edm). In *The Fifth International Conference on Power Electronics and Drive Systems, 2003. PEDS 2003.*, volume 2, pages 998–1003 Vol.2, 2003.
- [11] D De Wolf, L Cardon, and J Balic. Parameters affecting the quality of the electrical discharge machining process. *Adv Prod Eng Manag*, 5(4):245–252, 2010.
- [12] SI Drabkina. The theory of the development of the spark channel. *J. Exper. Theoret. Phys*, 21:473–483, 1951.

- [13] AS Zingermann. About the development of the discharge channel in electroerosive metal machining. *Journal Techn. Phys*, 26(5):1015–1020, 1956.
- [14] Bernd M Schumacher. After 60 years of EDM the discharge process remains still disputed. *Journal of Materials Processing Technology*, 149(1-3):376–381, June 2004.
- [15] John Milton Amiss, Franklin D Jones, and Christopher J McCauley. *Guide to the Use of Tables and Formulas in Machinery’s Handbook*. Industrial Press Inc., 2004.
- [16] T.B. Thoe, D.K. Aspinwall, M.L.H. Wise, and I.A. Oxley. Polycrystalline diamond edge quality and surface integrity following electrical discharge grinding. *Journal of Materials Processing Technology*, 56(1-4):773–785, January 1996.
- [17] CJ Luis and I Puertas. Methodology for developing technological tables used in edm processes of conductive ceramics. *Journal of materials processing technology*, 189(1-3):301–309, 2007.
- [18] Guo Zhe Yang, Feng Liu, and Hai Bo Lin. Research on an embedded servo control system of micro-edm. In *Applied Mechanics and Materials*, volume 120, pages 573–577. Trans Tech Publ, 2012.
- [19] M. Kunieda, B. Lauwers, K.P. Rajurkar, and B.M. Schumacher. Advancing EDM through fundamental insight into the process. *CIRP Annals*, 54(2):64–87, 2005.

- [20] A Yahya and CD Manning. Modelling, simulation and controller design for electro discharge machine system. *system*, 2(1):1, 2003.
- [21] B. Sen, N. Kiyawat, P.K. Singh, S. Mitra, J.H. Yew, and P. Purkait. A survey of servo -drive control schemes for electric discharge machining (EDM). In *The Fifth International Conference on Power Electronics and Drive Systems, 2003. PEDS 2003*. IEEE.
- [22] KP Rajurkar, G Levy, A Malshe, MM Sundaram, J McGeough, X Hu, R Resnick, and A DeSilva. Micro and nano machining by electro-physical and chemical processes. *CIRP annals*, 55(2):643–666, 2006.
- [23] Rosario Casanueva, Luis A Chiquito, Francisco J Azcondo, and Salvador Bracho. Electrical discharge machining experiences with a resonant power supply. In *IEEE 2002 28th Annual Conference of the Industrial Electronics Society. IECON 02*, volume 2, pages 1324–1329. IEEE, 2002.
- [24] G D’urso and Chiara Ravasio. Material-technology index to evaluate micro-edm drilling process. *Journal of Manufacturing Processes*, 26:13–21, 2017.
- [25] T Muthramalingam and B Mohan. A review on influence of electrical process parameters in edm. *Arch Civ Mech Eng*, 15(1):87–94, 2015.
- [26] MS Hewidy, TA El-Taweel, and MF El-Safty. Modelling the machining parameters of wire electrical discharge machining of inconel 601 using rsm. *Journal of Materials Processing Technology*, 169(2):328–336, 2005.

- [27] I Puertas, CJ Luis, and L Alvarez. Analysis of the influence of edm parameters on surface quality, mrr and ew of wc-co. *Journal of Materials Processing Technology*, 153:1026–1032, 2004.
- [28] Jun Qu, Albert J Shih, and Ronald O Scattergood. Development of the cylindrical wire electrical discharge machining process, part 2: surface integrity and roundness. *J. Manuf. Sci. Eng.*, 124(3):708–714, 2002.
- [29] Yongfeng Guo, Zebin Ling, Xiaoyou Zhang, and Yerui Feng. A magnetic suspension spindle system for small and micro holes EDM. *The International Journal of Advanced Manufacturing Technology*, 94(5-8):1911–1923, August 2017.
- [30] Muhammad P Jahan. Micro-electrical discharge machining. In *Nontraditional machining processes*, pages 111–151. Springer, 2013.
- [31] Chen-Chun Kao, Albert J. Shih, and Scott F. Miller. Fuzzy logic control of microhole electrical discharge machining. *Journal of Manufacturing Science and Engineering*, 130(6), October 2008.
- [32] Nor Liyana Safura Hashim, Azli Yahya, Md Daud, Syahrullail Samion, Ameruddin Baharom, Nor Hisham Haji Khamis, Nazriah Mahmud, et al. A review on electrical discharge machining servomechanism system. *Scientia Iranica*, 22(5):1813–1832, 2015.
- [33] B Sen, N Kiyawat, PK Singh, S Mitra, JH Yew, and P Purkaitl. A survey of servo-drive control schemes for electric discharge machining (edm). In *The*

*Fifth International Conference on Power Electronics and Drive Systems, 2003. PEDS 2003.*, volume 2, pages 998–1003. IEEE, 2003.

- [34] Yoshihito Imai, Akira Satake, Atsushi Taneda, and Kazuhiko Kobayashi. Improvement of edm machining speed by using high frequency response actuator. *Int. J. Electr. Mach*, 1:21–26, 1996.
- [35] Fumio MATSUMURA, Yohji OKADA, Masayuki FUJITA, and Toru NAMERIKAWA. Magnetic bearings. state of the art of magnetic bearings. (overview of magnetic bearing research and applications). *JSME International Journal Series C*, 40(4):553–560, 1997.
- [36] Xiaoyou Zhang, Tadahiko Shinshi, Go Kajiwara, Akira Shimokohbe, Yoshihito Imai, Hidetaka Miyake, and Takayuki Nakagawa. A 5-DOF controlled maglev local actuator and its application to electrical discharge machining. *Precision Engineering*, 32(4):289–300, October 2008.
- [37] Yong Li, Min Guo, Zhaoying Zhou, and Min Hu. Micro electro discharge machine with an inchworm type of micro feed mechanism. *Precision Engineering*, 26(1):7–14, January 2002.
- [38] Jian Li, Ramin Sedaghati, Javad Dargahi, and David Waechter. Design and development of a new piezoelectric linear inchworm actuator. *Mechatronics*, 15(6):651–681, July 2005.
- [39] Min Hu, Zhaoying Zhou, Yong Li, and Hejun Du. Development of a linear electrostrictive servo motor. *Precision engineering*, 25(4):316–320, 2001.

- [40] Yoshihito Imai, Takayuki Nakagawa, Hidetaka Miyake, Hirofumi Hidai, and Hitoshi Tokura. Local actuator module for highly accurate micro-edm. *Journal of Materials Processing Technology*, 149(1-3):328–333, 2004.
- [41] Xiaoyou Zhang, Tadahiko Shinshi, Hiroki Endo, Akira Shimokohbe, Yoshihito Imai, Hidetaka Miyake, and Takayuki Nakagawa. Development of a 5-dof controlled, wide-bandwidth, high-precision maglev actuator for micro electrical discharge machining. In *2007 International Conference on Mechatronics and Automation*, pages 2877–2882. IEEE, 2007.
- [42] Fuzhu Han, Yongxain Wang, and Ming Zhou. High-speed edm milling with moving electric arcs. *International journal of machine tools and manufacture*, 49(1):20–24, 2009.
- [43] Dongjue He, Hiroki Morita, Xiaoyou Zhang, Tadahiko Shinshi, Takayuki Nakagawa, Tatsusi Sato, and Hidetaka Miyake. Development of a novel 5-dof controlled maglev local actuator for high-speed electrical discharge machining. *Precision Engineering*, 34(3):453–460, 2010.
- [44] Haiyue Zhu, Tat Joo Teo, and Chee Khiang Pang. Magnetically levitated parallel actuated dual-stage (maglev-PAD) system for six-axis precision positioning. *IEEE/ASME Transactions on Mechatronics*, 24(4):1829–1838, August 2019.
- [45] KP Rajurkar, WM Wang, and RP Lindsay. A new model reference adaptive control of edm. *CIRP Annals*, 38(1):183–186, 1989.

- [46] JY Kao and YS Tarn. A neural-network approach for the on-line monitoring of the electrical discharge machining process. *Journal of Materials Processing Technology*, 69(1-3):112–119, 1997.
- [47] S Assarzadeh and M Ghoreishi. Neural-network-based modeling and optimization of the electro-discharge machining process. *The International Journal of Advanced Manufacturing Technology*, 39(5):488–500, 2008.
- [48] Ming Zhou and Fuzhu Han. Adaptive control for edm process with a self-tuning regulator. *International Journal of Machine Tools and Manufacture*, 49(6):462–469, 2009.
- [49] Raymond Snoeys, Dirk Dauw, and Jean-Pierre Kruth. Improved adaptive control system for edm processes. *CIRP Annals*, 29(1):97–101, 1980.
- [50] Marco Boccadoro and DF Dauw. About the application of fuzzy controllers in high-performance die-sinking edm machines. *CIRP annals*, 44(1):147–150, 1995.
- [51] RA Mahdavinejad. Edm process optimisation via predicting a controller model. *Archives of computational materials science and surface engineering*, 1(3):161–167, 2009.
- [52] JH Zhang, H Zhang, DS Su, Y Qin, MY Huo, QH Zhang, and L Wang. Adaptive fuzzy control system of a servomechanism for electro-discharge machining combined with ultrasonic vibration. *Journal of Materials Processing Technology*, 129(1-3):45–49, 2002.

- [53] Chen-Chun Kao and Albert J Shih. Design and tuning of a fuzzy logic controller for micro-hole electrical discharge machining. *Journal of Manufacturing Processes*, 10(2):61–73, 2008.
- [54] Chen-Chun Kao, Albert J Shih, and Scott F Miller. Fuzzy logic control of microhole electrical discharge machining. *Journal of Manufacturing Science and Engineering*, 130(6), 2008.
- [55] Yih-Fang Chang and Bor-Sen Chen. A robust performance variable structure PI/p control design for high precise positioning control systems. *International Journal of Machine Tools and Manufacture*, 35(12):1649–1667, December 1995.
- [56] Ho Seong Lee and Masayoshi Tomizuka. Robust motion controller design for high-accuracy positioning systems. *IEEE Transactions on Industrial Electronics*, 43(1):48–55, 1996.
- [57] Xiaoyou Zhang, Tadahiko Shinshi, Go Kajiwara, Akira Shimokohbe, Yoshihito Imai, Hidetaka Miyake, and Takayuki Nakagawa. A 5-dof controlled maglev local actuator and its application to electrical discharge machining. *Precision Engineering*, 32(4):289–300, 2008.
- [58] Yih-Fang Chang. Robust PI controller design for EDM. In *IECON 2007 - 33rd Annual Conference of the IEEE Industrial Electronics Society*. IEEE, November 2007.



- [59] Chen-Chun Kao. *Monitoring and control of micro-hole electrical discharge machining*. PhD thesis, University of Michigan., 2007.
- [60] Juan Pablo Segovia, Daniel Sbarbaro, and Eric Ceballos. An adaptive pattern based nonlinear PID controller. *ISA Transactions*, 43(2):271–281, April 2004.
- [61] Chingyei Chung, S Lu, and JS Deng. Modeling and control of die-sinking edm. In *WSEAS International Conference. Proceedings. Mathematics and Computers in Science and Engineering*, number 9. Citeseer, 2009.
- [62] W. M. Wang, K. P. Rajurkar, and K. Akamatsu. Digital gap monitor and adaptive integral control for auto-jumping in EDM. *Journal of Engineering for Industry*, 117(2):253–258, May 1995.
- [63] Wansheng ZHAO and Takahisa MASUZAWA. Adaptive control of EDM-JUMP with self-tuning approach. *Journal of The Japan Society of Electrical Machining Engineers*, 24(47):23–31, 1990.
- [64] K. P. Rajurkar and W. M. Wang. Improvement of EDM performance with advanced monitoring and control systems. *Journal of Manufacturing Science and Engineering*, 119(4B):770–775, November 1997.
- [65] K.P. Rajurkar, W.M. Wang, and R.P. Lindsay. A new model reference adaptive control of EDM. *CIRP Annals*, 38(1):183–186, 1989.

- [66] YS Liao and JC Woo. Design of a fuzzy controller for the adaptive control of wedm process. *International Journal of Machine Tools and Manufacture*, 40(15):2293–2307, 2000.
- [67] Mu-Tian Yan and Hsing-Tsung Chien. Monitoring and control of the micro wire-edm process. *International Journal of Machine Tools and Manufacture*, 47(1):148–157, 2007.
- [68] Mu-Tian Yan and Tun-Hua Cheng. High accuracy motion control of linear motor drive wire-edm machines. *The International Journal of Advanced Manufacturing Technology*, 40:918–928, 2009.
- [69] Trung Kien Hoang. Development of a wedm system with high machining efficiency. In *2017 international conference on system science and engineering (ICSSE)*, pages 397–399. IEEE, 2017.
- [70] PM Abhilash and Dupadu Chakradhar. Anfis modelling of mean gap voltage variation to predict wire breakages during wire edm of inconel 718. *CIRP Journal of Manufacturing Science and Technology*, 31:153–164, 2020.
- [71] Minhat Ade Erawan, Azli Yahya, Khamis Nor Hisham, Ahmad Saudi Samosir, Muhammad Arif Abdul Rahim, Andromeda Trias, and Juli Purwanto Nugroho Kartiko. Model of pulse power generator in electrical discharge machining (EDM) system. *Applied Mechanics and Materials*, 554:613–617, June 2014.

- [72] Marin Gostimirovic, Pavel Kovac, Milenko Sekulic, and Branko Skoric. Influence of discharge energy on machining characteristics in edm. *Journal of mechanical science and technology*, 26(1):173–179, 2012.
- [73] Azli Yahya, Andromeda Trias, Minhat Ade Erawan, Khamis Nor Hisham, Kamal Khalil, and Muhammad Arif Abdul Rahim. Comparison studies of electrical discharge machining (EDM) process model for low gap current. *Advanced Materials Research*, 433-440:650–654, January 2012.
- [74] R. Khokhlov. A method of analysis in the theory of sinusoidal self-oscillations. *IRE Transactions on Circuit Theory*, 7(4):398–413, December 1960.
- [75] Andreas Schubert, Henning Zeidler, Ralf Kühn, and Matthias Hackert-Oschätzchen. Microelectrical discharge machining: A suitable process for machining ceramics. *Journal of Ceramics*, 2015:1–9, August 2015.
- [76] Ved Prakash, P Kumar, PK Singh, M Hussain, AK Das, and S Chattopadhyaya. Micro-electrical discharge machining of difficult-to-machine materials: A review. *Proceedings of the Institution of Mechanical Engineers, Part B: Journal of Engineering Manufacture*, 233(2):339–370, July 2017.
- [77] Trias Andromeda, Azli Yahya, Nor Hisham Haji Khamis, Ameruddin Baharom, and Muhammad Arif Abdul Rahim. PID controller tuning by particle swarm optimization on electrical discharge machining servo control

- system. In *2012 4th International Conference on Intelligent and Advanced Systems (ICIAS2012)*. IEEE, June 2012.
- [78] Nazriah Mahmud, Azli Yahya, Mohammed Rafiq Abdul Kadir, and Nor Liyana Safura Hashim. Pulse power generator design for machining micro-pits on hip implant. *Jurnal Teknologi*, 61(2), 2013.
- [79] Muhammad Pervej Jahan, Yoke San Wong, and Mustafizur Rahman. A comparative study of transistor and rc pulse generators for micro-edm of tungsten carbide. *International Journal of Precision Engineering and Manufacturing*, 9(4):3–10, 2008.
- [80] Ade Erawan Minhat, Nor Hisham Hj Khamis, Azli Yahya, Trias Andromeda, and Kartiko Nugroho. Pulses model of electrical discharge machining (edm). *Proceeding of the Electrical Engineering Computer Science and Informatics*, 1:259–264.
- [81] Fuzhu Han, Shinya Wachi, and Masanori eda. Improvement of machining characteristics of micro-EDM using transistor type isopulse generator and servo feed control. *Precision Engineering*, 28(4):378–385, October 2004.
- [82] J Simao, H.G Lee, D.K Aspinwall, R.C Dewes, and E.M Aspinwall. Workpiece surface modification using electrical discharge machining. *International Journal of Machine Tools and Manufacture*, 43(2):121–128, January 2003.

- [83] K.P. Rajurkar, W.M. Wang, and J.A. McGeough. WEDM identification and adaptive control for variable-height components. *CIRP Annals*, 43(1):199–202, 1994.
- [84] M Ghoreishi and C Tabari. Investigation into the effect of voltage excitation of pre-ignition spark pulse on the electro-discharge machining (edm) process. *Materials and Manufacturing Processes*, 22(7-8):833–841, 2007.
- [85] Thangaraj Muthuramalingam and B Mohan. Enhancing the surface quality by iso pulse generator in edm process. In *Advanced Materials Research*, volume 622, pages 380–384. Trans Tech Publ, 2013.
- [86] Fuzhu Han, Shinya Wachi, and Masanori Kunieda. Improvement of machining characteristics of micro-edm using transistor type isopulse generator and servo feed control. *Precision Engineering*, 28(4):378–385, 2004.
- [87] Mu-Tian Yan and Tsung-Chien Lin. Development of a pulse generator for rough cutting of oil-based micro wire-edm. *Procedia Cirp*, 42:709–714, 2016.
- [88] YS Liao and YP Yu. Study of specific discharge energy in wedm and its application. *International Journal of Machine Tools and Manufacture*, 44(12-13):1373–1380, 2004.
- [89] FL Amorim and WL Weingaertner. The influence of generator actuation mode and process parameters on the performance of finish edm of a tool steel. *Journal of Materials Processing Technology*, 166(3):411–416, 2005.

- [90] KP Rajurkar, WM Wang, and RP Lindsay. On-line monitor and control for wire breakage in wedm. *CIRP annals*, 40(1):219–222, 1991.
- [91] Shun-Tong Chen and Chi-Hung Chen. A novel power source for high-precision, highly efficient micro w-edm. *Journal of Micromechanics and Microengineering*, 25(7):075027, 2015.
- [92] MP Jahan, YS Wong, and M Rahman. A study on the fine-finish die-sinking micro-edm of tungsten carbide using different electrode materials. *Journal of materials processing technology*, 209(8):3956–3967, 2009.
- [93] Fatemeh Karimi Pour, MAHROKH Bavandi, and AZLI Yahya. Simulation and analysis of rc type relaxation power generator for electrical discharge machines (edm) in laplace transform. In *Applied Mechanics and Materials*, volume 818, pages 112–116. Trans Tech Publ, 2016.
- [94] Do Kwan Chung, Hong Shik Shin, Min Soo Park, and Chong Nam Chu. Machining characteristics of micro edm in water using high frequency bipolar pulse. *International Journal of Precision Engineering and Manufacturing*, 12(2):195–201, 2011.
- [95] CJ Li, JJ Ding, SQ Yang, YS Fang, and QC Kong. Discharge current shape control method and experiment in wire edm. *The International Journal of Advanced Manufacturing Technology*, 87:3271–3278, 2016.
- [96] Deepak Kumar, Mangal Singh Sisodiya, and Vivek Bajpai. A novel servo-stabilized electromagnetic levitation formicro-EDM processing and its fea-

- sibility analysis. *Proceedings of the Institution of Mechanical Engineers, Part B: Journal of Engineering Manufacture*, page 095440542211244, October 2022.
- [97] SL Chen, BH Yan, and FY Huang. Influence of kerosene and distilled water as dielectrics on the electric discharge machining characteristics of ti-6al-4v. *Journal of Materials Processing Technology*, 87(1-3):107–111, 1999.
- [98] Yan Cherng Lin, Biing Hwa Yan, and Yong Song Chang. Machining characteristics of titanium alloy (ti-6al-4v) using a combination process of edm with usm. *Journal of Materials Processing Technology*, 104(3):171–177, 2000.
- [99] Masahiro Fujiki, Jun Ni, and Albert J Shih. Investigation of the effects of electrode orientation and fluid flow rate in near-dry edm milling. *International Journal of Machine Tools and Manufacture*, 49(10):749–758, 2009.
- [100] Yves Wouters, Alain Galerie, and Jean-Pierre Petit. Thermal oxidation of titanium by water vapour. *Solid State Ionics*, 104(1-2):89–96, 1997.
- [101] G Kibria, BR Sarkar, BB Pradhan, and B Bhattacharyya. Comparative study of different dielectrics for micro-edm performance during microhole machining of ti-6al-4v alloy. *The International Journal of Advanced Manufacturing Technology*, 48(5):557–570, 2010.

- [102] Yanzhen Zhang, Yonghong Liu, Renjie Ji, Baoping Cai, and Yang Shen. Sinking edm in water-in-oil emulsion. *The International Journal of Advanced Manufacturing Technology*, 65(5):705–716, 2013.
- [103] Sharanjit Singh, Arvind Bhardwaj, et al. Review to edm by using water and powder-mixed dielectric fluid. *Journal of Minerals and Materials Characterization and Engineering*, 10(02):199, 2011.
- [104] Gunawan Setia Prihandana, Muslim Mahardika, Mohd Hamdi, YS Wong, and Kimiyuki Mitsui. Accuracy improvement in nanographite powder-suspended dielectric fluid for micro-electrical discharge machining processes. *The International Journal of Advanced Manufacturing Technology*, 56(1):143–149, 2011.
- [105] Fumio Matsumura, Yohji Okada, Masayuki Fujita, and Toru Namerikawa. State of the art of magnetic bearings: Overview of magnetic bearing research and applications. *JSME International Journal Series C Mechanical Systems, Machine Elements and Manufacturing*, 40(4):553–560, 1997.
- [106] X Zhang, Y Ueyama, T Shinshi, Akira Shimokohbe, T Sato, H Miyake, and T Nakagawa. High-speed and high-accuracy edm of micro holes by using a 5-dof controlled maglev local actuator. In *Materials Science Forum*, volume 626, pages 255–260. Trans Tech Publ, 2009.
- [107] Ji-An Duan, Hai-Bo Zhou, and Ning-Ping Guo. Electromagnetic design of a novel linear maglev transportation platform with finite-element analysis.



- IEEE Transactions on Magnetics*, 47(1):260–263, January 2011.
- [108] Dong Jue He, Tadahiko Shinshi, and Takahiro Nakai. Development of a lens driving maglev actuator for laser beam off-axis cutting and deep piercing. *Key Engineering Materials*, 523-524:774–779, November 2012.
- [109] Xiao You Zhang, Kouki Uchiyama, and Tomohiro Ishizuka. High-speed, high-precision magnetic/piezoelectric hybrid drive actuator for micro electrical discharge machining. In *Advanced Materials Research*, volume 941, pages 2112–2115. Trans Tech Publ, 2014.
- [110] Changhao Chen, Yefa Hu, Huachun Wu, and Chunsheng Song. Parametric design and experiment of maglev actuators for microgravity vibration isolation system. *International Journal of Applied Electromagnetics and Mechanics*, 58(3):319–335, November 2018.
- [111] Yanming Zhang, Zhen Zhang, Guojun Zhang, and Wenyuan Li. Reduction of energy consumption and thermal deformation in wedm by magnetic field assisted technology. *International Journal of Precision Engineering and Manufacturing-Green Technology*, 7(2):391–404, 2020.
- [112] Zhen Zhang, Yi Zhang, Wuyi Ming, Yanming Zhang, Chen Cao, and Guojun Zhang. A review on magnetic field assisted electrical discharge machining. *Journal of Manufacturing Processes*, 64:694–722, April 2021.

- [113] Greg Poole. Gauss's law for magnetism & law of universal magnetism: Calculate the charge of a monopole. *Journal of High Energy Physics, Gravitation and Cosmology*, 4(4):581–587, 2018.
- [114] Haihui Wu, Tong Wang, and Junqi Wang. Research on discharge state detection of finishing in high-speed wire electrical discharge machine. *The International Journal of Advanced Manufacturing Technology*, 103(5-8):2301–2317, April 2019.
- [115] SH Yeo, E Aligiri, PC Tan, and H Zarepour. An adaptive speed control system for micro electro discharge machining. In *AIP Conference Proceedings*, volume 1181, pages 61–72. American Institute of Physics, 2009.
- [116] Fuzhu Han, Li Chen, Dingwen Yu, and Xiaoguang Zhou. Basic study on pulse generator for micro-edm. *The International Journal of Advanced Manufacturing Technology*, 33(5):474–479, 2007.
- [117] B Bommeli, C Frei, and A Ratajski. On the influence of mechanical perturbation on the breakdown of a liquid dielectric. *Journal of electrostatics*, 7:123–144, 1979.
- [118] Deepak Kumar, Vivek Bajpai, and Nirmal Kumar Singh. Nano electrical discharge machining – the outlook, challenges, and opportunities. *Materials and Manufacturing Processes*, pages 1–35, April 2021.

- [119] Vijay Kumar Meena and Man Singh Azad. Grey relational analysis of micro-EDM machining of ti-6al-4v alloy. *Materials and Manufacturing Processes*, 27(9):973–977, September 2012.
- [120] BB Pradhan, M Masanta, BR Sarkar, and B Bhattacharyya. Investigation of electro-discharge micro-machining of titanium super alloy. *The International Journal of Advanced Manufacturing Technology*, 41(11):1094–1106, 2009.
- [121] B Kuriachen, KP Somashekhar, and Jose Mathew. Multiresponse optimization of micro-wire electrical discharge machining process. *The International Journal of Advanced Manufacturing Technology*, 76(1):91–104, 2015.
- [122] S Rajamanickam and J Prasanna. Effect of conductive, semi-conductive and non-conductive powder-mixed media on micro electric discharge machining performance of ti-6al-4v. *INTERNATIONAL JOURNAL OF ELECTRO-CHEMICAL SCIENCE*, 16(3), 2021.
- [123] AP Tiwary, BB Pradhan, and B Bhattacharyya. Study on the influence of micro-edm process parameters during machining of ti-6al-4v superalloy. *The International Journal of Advanced Manufacturing Technology*, 76(1):151–160, 2015.
- [124] Donato Firrao, Paolo Matteis, Giorgio Scavino, Graziano Ubertalli, Maria Giuseppina Ienco, Maria Rosa Pinasco, Enrica Stagno, Riccardo Gerosa, Barbara Rivolta, Antonio Silvestri, et al. Relationships between

- tensile and fracture mechanics properties and fatigue properties of large plastic mould steel blocks. *Materials Science and Engineering: A*, 468:193–200, 2007.
- [125] Vijay Kumar Meena, Man Singh Azad, Suman Singh, and Narinder Singh. Micro-edm multiple parameter optimization for cp titanium. *The International Journal of Advanced Manufacturing Technology*, 89(1):897–904, 2017.
- [126] Takahisa Masuzawa. State of the art of micromachining. *Cirp Annals*, 49(2):473–488, 2000.
- [127] Chaojiang Li, Xi Xu, Yong Li, Hao Tong, Songlin Ding, Quancun Kong, Lei Zhao, and Jun Ding. Effects of dielectric fluids on surface integrity for the recast layer in high speed edm drilling of nickel alloy. *Journal of Alloys and Compounds*, 783:95–102, 2019.
- [128] SF Hsieh, SL Chen, HC Lin, MH Lin, and SY Chiou. The machining characteristics and shape recovery ability of ti–ni–x (x= zr, cr) ternary shape memory alloys using the wire electro-discharge machining. *International Journal of Machine Tools and Manufacture*, 49(6):509–514, 2009.
- [129] Farnaz Nourbakhsh, Kamlakar P Rajurkar, Ajay P Malshe, and Jian Cao. Wire electro-discharge machining of titanium alloy. *Procedia CirP*, 5:13–18, 2013.

- [130] T Muthuramalingam and B Mohan. Influence of discharge current pulse on machinability in electrical discharge machining. *Materials and Manufacturing Processes*, 28(4):375–380, 2013.
- [131] Neeraj Sharma, Gurpreet Singh, Munish Gupta, Hussien Hegab, and Moza-mmel Mia. Investigations of surface integrity, bio-activity and perfor-mance characteristics during wire-electrical discharge machining of ti-6al-7nb biomedical alloy. *Materials Research Express*, 6(9):096568, 2019.
- [132] Ali Ozgedik and Can Cogun. An experimental investigation of tool wear in electric discharge machining. *The International Journal of Advanced Manufacturing Technology*, 27:488–500, 2006.
- [133] Philipp Steuer, Andreas Rebschläger, Olivier Weber, and Dirk Bähre. The heat-affected zone in edm and its influence on a following pecm process. *Procedia CIRP*, 13:276–281, 2014.
- [134] Naveed Ahmed, Kashif Ishfaq, Khaja Moiduddin, Rafaqat Ali, and Naif Al-Shammary. Machinability of titanium alloy through electric discharge machining. *Materials and Manufacturing Processes*, 34(1):93–102, 2019.
- [135] Linfeng Deng and Rongzhen Zhao. Fault feature extraction of a rotor sys-tem based on local mean decomposition and teager energy kurtosis. *Journal of Mechanical Science and Technology*, 28(4):1161–1169, 2014.
- [136] B Singaravel, K Chandra Shekar, G Gowtham Reddy, and S Deva Prasad. Experimental investigation of vegetable oil as dielectric fluid in electric dis-

- charge machining of ti-6al-4v. *Ain Shams Engineering Journal*, 11(1):143–147, 2020.
- [137] Anshuman Kumar Sahu and Siba Sankar Mahapatra. Surface characteristics of edmed titanium alloy and aisi 1040 steel workpieces using rapid tool electrode. *Arabian Journal for Science and Engineering*, 45(2):699–718, 2020.
- [138] S Oliver Nesa Raj and S Prabhu. Modeling and analysis of titanium alloy in wire-cut edm using grey relation coupled with principle component analysis. *Australian Journal of Mechanical Engineering*, 15(3):198–209, 2017.
- [139] Kun Liu, Dominiek Reynaerts, and Bert Lauwers. Influence of the pulse shape on the edm performance of si<sub>3</sub>n<sub>4</sub>–tin ceramic composite. *CIRP annals*, 58(1):217–220, 2009.
- [140] Deepak Kumar, Mangal Singh Sisodiya, Deepak Kumar Mandal, and Vivek Bajpai. Maglev micro-EDM: Feasibility and performance on inconel 625. *CIRP Journal of Manufacturing Science and Technology*, 40:155–166, February 2023.
- [141] E. Buckingham. On physically similar systems; illustrations of the use of dimensional equations. *Physical Review*, 4(4):345–376, October 1914.
- [142] Y Chen, T Nguyen, and LC Zhang. Polishing of polycrystalline diamond by the technique of dynamic friction—part 5: Quantitative analysis of ma-

- terial removal. *International Journal of Machine Tools and Manufacture*, 49(6):515–520, 2009.
- [143] Biing Hwa Yan, Hsien Chung Tsai, Fuang Yuan Huang, and Long Chorng Lee. Examination of wire electrical discharge machining of al<sub>2</sub>o<sub>3</sub>p/6061al composites. *International Journal of Machine Tools and Manufacture*, 45(3):251–259, 2005.
- [144] MP Jahan, M Rahman, and YS Wong. A review on the conventional and micro-electrodischarge machining of tungsten carbide. *International journal of machine tools and manufacture*, 51(12):837–858, 2011.
- [145] Saman Fattahi and Hamid Baseri. Analysis of dry electrical discharge machining in different dielectric mediums. *Proceedings of the Institution of Mechanical Engineers, Part E: Journal of Process Mechanical Engineering*, 231(3):497–512, 2017.
- [146] Edgar Buckingham. Physically similar systems. *Journal of the Washington Academy of Sciences*, 4(13):347–353, 1914.
- [147] Kuo-Ming Tsai and Pei-Jen Wang. Semi-empirical model of surface finish on electrical discharge machining. *International Journal of Machine Tools and Manufacture*, 41(10):1455–1477, 2001.
- [148] Mangesh R Phate and Shraddha B Toney. Modeling and prediction of wedm performance parameters for al/sicp mmc using dimensional analy-

- sis and artificial neural network. *Engineering Science and Technology, an International Journal*, 22(2):468–476, 2019.
- [149] A Yahya and CD Manning. Determination of material removal rate of an electro-discharge machine using dimensional analysis. *Journal of Physics D: Applied Physics*, 37(10):1467, 2004.
- [150] JY Kao, CC Tsao, SS Wang, and CY Hsu. Optimization of the edm parameters on machining ti-6al-4v with multiple quality characteristics. *The International Journal of Advanced Manufacturing Technology*, 47(1):395–402, 2010.
- [151] L Tang and YT Du. Experimental study on green electrical discharge machining in tap water of ti-6al-4v and parameters optimization. *The International Journal of Advanced Manufacturing Technology*, 70(1):469–475, 2014.
- [152] Dileep Kumar Mishra, Saurav Datta, Manoj Masanta, et al. Effects of tool electrode on edm performance of ti-6al-4v. *Silicon*, 10(5):2263–2277, 2018.
- [153] Murahari Kolli and Adepu Kumar. Assessing the influence of surfactant and b4c powder mixed in dielectric fluid on edm of titanium alloy. *Silicon*, 11(4):1731–1743, 2019.
- [154] Saurabh Nair, Ayushman Dutta, and Abimannan Giridharan. Investigation on edm machining of ti6al4v with negative polarity brass electrode. *Materials and Manufacturing Processes*, 34(16):1824–1831, 2019.



- [155] Anish Kumar, Vinod Kumar, and Jatinder Kumar. Investigation of machining parameters and surface integrity in wire electric discharge machining of pure titanium. *Proceedings of the Institution of mechanical engineers, Part B: Journal of engineering manufacture*, 227(7):972–992, 2013.
- [156] E.S. Gadelmawla, M.M. Koura, T.M.A. Maksoud, I.M. Elewa, and H.H. Soliman. Roughness parameters. *Journal of Materials Processing Technology*, 123(1):133–145, 2002.
- [157] Mangal Singh Sisodiya, Shashank Shukla, and Vivek Bajpai. Feasibility analysis of novel maglev EDM by comparing with conventional micro EDM. *Scientific Reports*, 12(1), February 2022.
- [158] Naotake Mohri, Yasuhiro Fukusima, Yasushi Fukuzawa, Takayuki Tani, and Nagao Saito. Layer generation process on work-piece in electrical discharge machining. *CIRP Annals*, 52(1):157–160, 2003.
- [159] Naotake Mohri, Yasushi Fukuzawa, Takayuki Tani, and Toshio Sata. Some considerations to machining characteristics of insulating ceramics-towards practical use in industry-. *CIRP Annals*, 51(1):161–164, 2002.
- [160] Rajesh Sahoo, Nirmal Kumar Singh, and Vivek Bajpai. A novel approach for modeling MRR in EDM process using utilized discharge energy. *Mechanical Systems and Signal Processing*, 185:109811, February 2023.

- [161] S Dhanabalan, K Sivakumar, and C Sathiya Narayanan. Analysis of form tolerances in electrical discharge machining process for inconel 718 and 625. *Materials and Manufacturing Processes*, 29(3):253–259, 2014.
- [162] Sushil Kumar, Mudimallana Goud, and Narendra Mohan Suri. Experimental investigation of magnetic-field-assisted electric discharge machining by silicon-based dielectric of inconel 706 superalloy. *Sādhanā*, 45(1):1–8, 2020.
- [163] B Jabbaripour, MH Sadeghi, Sh Faridvand, and MR Shabgard. Investigating the effects of edm parameters on surface integrity, mrr and twr in machining of ti-6al-4v. *Machining Science and Technology*, 16(3):419–444, 2012.
- [164] Minh Dang Nguyen, Mustafizur Rahman, and Yoke San Wong. An experimental study on micro-edm in low-resistivity deionized water using short voltage pulses. *The International Journal of Advanced Manufacturing Technology*, 58(5):533–544, 2012.
- [165] Fred L. Amorim and Walter L. Weingaertner. The behavior of graphite and copper electrodes on the finish die-sinking electrical discharge machining (EDM) of AISI p20 tool steel. *Journal of the Brazilian Society of Mechanical Sciences and Engineering*, 29(4):366–371, December 2007.
- [166] Krishna Kumar Saxena, Anand Suman Srivastava, and Sanjay Agarwal. Experimental investigation into the micro-EDM characteristics of conductive SiC. *Ceramics International*, 42(1):1597–1610, January 2016.

- [167] Ghaus Ali, Dipraj Banik, Akshansh Yadav, BC Rautara, Ashok Kumar Sahoo, et al. Analysis and optimization of surface integrity characteristics of edmed work surface inconel 718 super-alloy using grey-based taguchi method. In *Advances in Industrial and Production Engineering*, pages 441–448. Springer, 2019.
- [168] Dileep Kumar Mishra, Saurav Rahul, and Datta, Manoj Masanta, and Siba Sankar Mahapatra. Through hole making by electro-discharge machining on inconel 625 super alloy using hollow copper tool electrode. *Proceedings of the Institution of Mechanical Engineers, Part E: Journal of Process Mechanical Engineering*, 233(2):348–370, 2019.
- [169] Rahul, Saurav Datta, Bibhuti Bhusan Biswal, and Siba Sankar Mahapatra. A novel satisfaction function and distance-based approach for machining performance optimization during electro-discharge machining on super alloy inconel 718. *Arabian Journal for Science and Engineering*, 42(5):1999–2020, February 2017.
- [170] Chandramani Upadhyay, Saurav Datta, Manoj Masanta, and Siba Sankar Mahapatra. An experimental investigation emphasizing surface characteristics of electro-discharge-machined inconel 601. *Journal of the Brazilian Society of Mechanical Sciences and Engineering*, 39(8):3051–3066, 2017.
- [171] Y Chen and SM Mahdavian. Parametric study into erosion wear in a computer numerical controlled electro-discharge machining process. *Wear*, 236(1-2):350–354, 1999.

- [172] Vinod Kumar, Kamal Kumar Jangra, Vikas Kumar, and Neeraj Sharma. Wedm of nickel based aerospace alloy: optimization of process parameters and modelling. *International Journal on Interactive Design and Manufacturing (IJIDeM)*, 11(4):917–929, 2017.
- [173] Amitava Mandal, Amit Rai Dixit, S Chattopadhyaya, A Paramanik, Sergej Hloch, and Grzegorz Królczyk. Improvement of surface integrity of nimonic c 263 super alloy produced by wedm through various post-processing techniques. *The International Journal of Advanced Manufacturing Technology*, 93(1):433–443, 2017.
- [174] CC Kao and Albert J Shih. Sub-nanosecond monitoring of micro-hole electrical discharge machining pulses and modeling of discharge ringing. *International Journal of Machine Tools and Manufacture*, 46(15):1996–2008, 2006.
- [175] YS Liao, TY Chang, and TJ Chuang. An on-line monitoring system for a micro electrical discharge machining (micro-edm) process. *Journal of Micromechanics and Microengineering*, 18(3):035009, 2008.
- [176] M.B. Kiran, B. Ramamoorthy, and V. Radhakrishnan. Evaluation of surface roughness by vision system. *International Journal of Machine Tools and Manufacture*, 38(5-6):685–690, May 1998.
- [177] Hao Huang, Zhen Zhang, Wuyi Ming, Zhong Xu, and Yanming Zhang. A novel numerical predicting method of electric discharge machining process

- based on specific discharge energy. *The International Journal of Advanced Manufacturing Technology*, 88(1):409–424, 2017.
- [178] Sachin Ashok Sonawane and ML Kulkarni. Optimization of machining parameters of wedm for nimonic-75 alloy using principal component analysis integrated with taguchi method. *journal of king saud university-Engineering sciences*, 30(3):250–258, 2018.
- [179] Debashish Sahu, Santosh Kumar Sahu, Thrinadh Jadam, and Saurav Datta. Electro-discharge machining performance of nimonic 80a: an experimental observation. *Arabian Journal for Science and Engineering*, 44(12):10155–10167, 2019.
- [180] Renu K Shastri and Chinmaya P Mohanty. Machinability investigation on nimonic c263 alloy in electric discharge machine. *Materials Today: Proceedings*, 26:529–533, 2020.
- [181] Renu K Shastri and Chinmaya P Mohanty. Sustainable electrical discharge machining of nimonic c263 superalloy. *Arabian Journal for Science and Engineering*, 46(8):7273–7293, 2021.
- [182] Wuyi Ming, Haojie Jia, Hongmei Zhang, Zhen Zhang, Kun Liu, Jinguang Du, Fan Shen, and Guojun Zhang. A comprehensive review of electric discharge machining of advanced ceramics. *Ceramics International*, 46(14):21813–21838, 2020.

- [183] R Gil, Jose A Sánchez, S Plaza, N Ortega, B Izquierdo, and I Pombo. Modeling recast layer and surface finish in the manufacturing of high-aspect ratio micro-tools using the inverse slab electrical discharge milling process. *Proceedings of the Institution of Mechanical Engineers, Part B: Journal of Engineering Manufacture*, 228(4):553–562, September 2013.
- [184] H. Ramasawmy, L. Blunt, and K.P. Rajurkar. Investigation of the relationship between the white layer thickness and 3d surface texture parameters in the die sinking EDM process. *Precision Engineering*, 29(4):479–490, October 2005.
- [185] H Ramasawmy and L Blunt. Effect of edm process parameters on 3d surface topography. *Journal of Materials Processing Technology*, 148(2):155–164, 2004.
- [186] Anish Kumar, Vinod Kumar, and Jatinder Kumar. Surface integrity and material transfer investigation of pure titanium for rough cut surface after wire electro discharge machining. *Proceedings of the Institution of Mechanical Engineers, Part B: Journal of Engineering Manufacture*, 228(8):880–901, December 2013.